Removal of volatile to semi-volatile organic contaminants from water using hollow fiber membrane contactors and catalytic destruction of the contaminants in the gas phase

Dissertation

zur Erlangung des Grades eines Doktors der Naturwissenschaften

der Geowissenschaftlichen Fakultät

der Eberhard-Karls-Universität Tübingen

vorgelegt von

Shamsul Abedin Tarafder

Aus

Bangladesh

2007

Tag der mündlichen Prüfung:	25. Juni 2007
Dekan:	**Prof. Dr. Peter Grathwohl**
1. Berichterstatter:	**Prof. Dr. Christoph Schüth**
2. berichterstatter:	**Prof. Dr. Peter Grathwohl**

Dedicated to my Parents:

Prof. (Rtd.) Zainul Abedin Tarafder

and

Mrs. Hosne Afruza Tarafder

Whose Enthusiastic Inspiration Encouraged me to Persuade a Doctorate Degree

Abstract

Chlorinated organic compounds and ether compounds are frequently found in groundwater and efficient treatment options are needed. In this study, the efficient transferal of the compounds from the water phase to the gas phase was studied followed by the catalytic treatment of the gas phase.

For the removal of the organic contaminants from water, a microporous polypropylene hollow fiber membrane (HFM) module was operated under low strip gas flow to water flow ratios (≤ 5:1). Removal efficiencies were found to be strongly dependent on the Henry's law constants indicating a substantial mass transfer resistance on the gas side. Vacuum can be either used to increase removal efficiencies, or to decrease the amount of strip gas that has to be treated without sacrificing efficiency. Empirical formulations based on the resistance in series model failed to predict the experimental results. Therefore, a hybrid numerical/analytical modelling approach in the finite element simulator RockFlow/GeoSys for hydraulic flow and mass transport was developed. The modelling results were validated against 177 experimental data under different operating conditions (water flow, gas flow, pressure) and 12 organic compounds covering a wide range of Henry's law constants, from Naphthalene at circa 0.017 to 1,1-Dichloroethene at circa 1.19. The combination of analytical solutions and the finite element numerical solution coupled over source terms provided a rapid and efficient solution of the mass balance equations and predicted the experimental results very well. Geometrical considerations, the diffusion coefficients in the various media, and the flow conditions, are enough to describe the operation of the HFM module and the principle processes operating. With this, the model can be used to efficiently design HFM filtration systems and to optimize stripping schemes.

After transferral of the organic compounds from water to the gas-phase, their reductive catalytic destruction under elevated temperatures using a palladium based catalyst with hydrogen as the reductant was studied. Compounds studied included chlorinated alkenes and alkanes (perchloroethylene (PCE), trichloroethylene (TCE), cis-1,2-dichloroethylene (cis-1,2-DCE), 1,1-dichloroethylene (1,1-DCE), 1,2-dichloroethane (1,2-DCA), 1,1,2,2-tetrachlrooethane (1,1,2,2-TeCA)), ethyl chloride, as well as several ether compunds (methyl tert butyl ether (MTBE), ethyl tert butyl ether (ETBE), tert amyl ethyl ether (TAME), diisopropyl ether (DIPE), diethyl ether (DEE), dimethyl ether (DME)). The study demonstrated that the catalyst rapidly destroyed the gas phase chlorinated compounds as well as the ether compounds efficiently, with half-lives on the order of seconds or less. Reaction kinetics were pseudo first order with respect to the concentration of the compounds and reaction rates were found to be temperature dependent. Therefore, the Arrhenius

equation was applied to determine the activation energies of the reactions. Hydrogenolysis and hydrogenation were the main observed reaction pathways for the chlorinated aliphatic compounds and chlorinated ethenes reacted much faster than the chlorinated ethanes. For the study with chlorinated aliphatic compounds, the reaction rate decreased towards 1,1-DCE > cis-1,2-DCE > TCE > PCE > 1,1,2,2-TeCA > 1,2-DCA > ethyl chloride. Ethane and ethene were the primary end products. Partially dechlorinated intermediates were observed in low concentrations during degradation, however, they were transitory. The reaction rates for the ether compounds decreased towards TAME > ETBE > MTBE > DIPE > DEE > DME. The primary reaction products for MTBE are isobutane and methanol, for ETBE isobutane and ethanol, for TAME isopentane and methanol, for DIPE propane and 2-propanol, for DEE ethane and ethanol, for DME methane and methanol. In addition, the catalytic oxidation of gas phase selected ether compounds (MTBE, ETBE, TAME and DIPE) at different temperatures was studied. Reaction rates were also pseudo-first order with carbondioxide and water as the main products.

Kurzfassung

Organische Schadstoffe und insbesondere chlorierte organische Verbindungen sowie Ether die als Zusätze in Vergaserkraftstoffen eingesetzt werden, können verbreitet im Grundwasser nachgewiesen werden. Zur Behandlung von derart kontaminierten Grundwässern werden effiziente Technologien benötigt. In dieser Arbeit wurde ein Verfahren untersucht, welches eine effektiver Strippung der Schadstoffe aus der wässrigen Phase in die Gasphase mittels Hohlfasermembranmodulen mit einer anschließenden Gasphasenkatalyse kombiniert.

Zur Strippung wurde ein Modul mit mikroporösen Polypropylen-Hohlfasermembranen eingesetzt und mit geringen Gasfluss/Wasserfluss-Verhältnissen betrieben. Die Strippeffizienzen waren dabei stark von den Henry-Konstanten der Verbindungen abhängig, was auf signifikante Massentransferlimitierungen in der Gasphase hinweist.

Vakuum kann einerseits zur Erhöhung der Strippeffizienzen verwendet werden und andererseits um bei gleicher Strippeffizienz die Menge an Strip-Gas zu verringern. Eine Modellierung der experimentellen Daten mittels konventioneller Ansätze (‚Resistance in Series' model) brachte nur unbefriedigende Ergebnisse. Deshalb wurde ein prozessbasiertes hybrid numerisch/analytisches Modell auf Basis des finite Elemente Simulators RockFlow/GeoSys entwickelt. Die Modellergebnisse wurden gegen 177 experimentell bestimmte Daten die unter unterschiedlichen Bedingungen (Wasserfluss, Gasfluss, Druck) ermittelt wurden, validiert. In den Experimenten wurden 12 organische Verbindungen eingesetzt , die eine große Breite von Henry Konstanten abdeckten (von Naphthalin mit ca. 0,017 bis 1,1-Dichlorethan mit ca. 1,19).

Die Kombination von analytischen und numerischen Lösungen, gekoppelt über Quellterme, lieferte schnelle und aussagekräftige Lösungen für die Massenbilanzgleichungen und konnte die experimentellen Ergebnisse gut vorhersagen. Geometrische Betrachtungen, die Diffusionskoeffizienten der Verbindungen in den verschiedenen Medien, sowie die experimentellen Bedingungen waren als Eingabeparameter in das Modell ausreichend. Damit kann das Modell eingesetzt werden um Strippeffizienzen vorrauszusagen und um die Betriebsbedingungen von Hohfasermembranmodulen zu optimieren.

Nach der Überführung der organischen Verbindungen vom Wasser in die Gasphase, wurde deren reduktiver katalytischer Abbau bei erhöhten Temperaturen unter Verwendung eines auf Palladium basierenden Katalysators mit Wasserstoff als Reduktionsmittel untersucht. Die untersuchten Verbindungen schlossen chlorierte Alkene und Alkane (Perchlorethylen (PCE), Trichlorethylen (TCE), cis-1,2-Dichlorethylen (cis-1,2-DCE), 1,1-Dichlorethylen (1,1-DCE),

1,2-Dichlorethan (1,2-DCA), 1,1,2,2-Tetrachlorethan (1,1,2,2-TeCA)) und Chloroethan sowie mehrere Ether-Verbindungen (Methylentertbutylether (MTBE), Ethylentertiärbutylether (ETBE), Teritäramylethylenether (TAME), Diisopropylether (DIPE), Diethylether (DEE), Dimethylether (DME)) ein. Es konnte gezeigt werden, dass in der Gasphase ein schneller und effizienter Abbau sowohl der chlorierten Verbindungen als auch der Ether-Verbindungen mit Halbwertszeiten im Bereich von Sekunden oder kürzer erreicht werden kann. Die Reaktionskinetiken waren in der Regel pseudo-erster Ordnung hinsichtlich der Konzentration der Verbindungen wobei die Reaktionsraten eine deutliche Temperaturabhängigkeit zeigten. Damit konnten für die einzelnen Reaktionen Aktivierungsenergien bestimmt werden.

Hydrogenolyse und Hydrierung waren die am häufigsten beobachteten Reaktionsmechanismen für die chlorierten aliphatische Verbindungen, wobei chlorierte Ethene viel schneller als chlorierte Ethane reagierten. Die Reaktionsraten nahmen dabei wie folgt ab: 1,1-DCE > cis-1,2-DCE > TCE > PCE > 1,1,2,2-TeCA > 1,2-DCA > Chloroethan . Ethan und Ethen waren die primären Endprodukte. Teilweise wurden dechlorierte Zwischenprodukte während des Abbaus in niedrigen Konzentrationen beobachtet, diese waren jedoch nicht stabil. Die Reaktionsraten für Ether-Verbindungen nahmen in der Reihenfolge TAME > ETBE > MTBE > DIPE > DEE > DME ab. Die primären Reaktionsprodukte waren für MTBE Isobutan und Methanol, für ETBE Isobutan und Ethanol, für TAME Isopentan und Methanol, für DIPE Methan und Methanol. Zusätzlich wurde die katalytische Oxidation in der Gasphase von ausgewählten Ether-Verbindungen (MTBE, ETBE, TAME und DIPE) bei unterschiedlichen Temperaturen untersucht. Die Reaktionsraten waren wiederum pseudo-erster Ordnung mit Kohlendioxid und Wasser als Hauptprodukte.

Acknowledgment

Funding was provided by the German Federal Ministry for Education and Research (BMBF) through Grant 02WT0412.

The author expresses his sincere most and deepest sense of gratitude to supervisors: to Prof. Dr. Christoph Schüth for his constant supervision, guidance and advice throughout this research which has made it possible to accomplish the task properly; to Prof. Dr. Peter Grathwohl for his all sort of help especially, to allow me to work in his research laboratory. The author is indebted to Prof. Dr. Rudolf Liedl for his helpful suggestions and discussions in many aspects. The author is indebted to Dr. Christopher Ian McDermott for developing a numerical-analytical model for predicting theoretical removal efficiencies of extra flow hollow fiber membrane contactors.

The author is very much indebted to Dr. Nikolai Alexeji Kumer for his very detail and specific suggestions regarding many aspects of the experimental work. The author would like to thank Kerstin Ruopp for her help especially in organizing the kurzfassung (abstract), to Dr. Thomas Wendel for his help whenever necessary, especially during GC or GC-MS operation in the laboratory. The author is grateful to Bernice Nisch, Renate Seelig, Renate Reley, Annegrate Walz for their assistances within a pleasant working environment in the hydrogeochemistry laboratory of Applied Geology Group.

The author would like to express his gratitude to Prof. Md. Sazzad Hossain, Prof. Dr. Md. Hussain Monsur and Prof. Dr. A.S.M. Woobaidullah, Dhaka University, Nehal Uddin, Md. Khurshid Alam, and Md. Khairul Islam, Geological Survey of Bangladesh for their help and encouragement.

The author is very much thankful to Md. Muhit Razzaque for his help during the formatting and submission of the thesis. Thanks are extended to friends and colleagues Md. Nurul Hoque, Md. Rezaul Halim, H.A.G. Jayathisa, Dr. Ludwig Biermanns, Mr. Uwe Schmidt, Mr. Matthias Flegr, Dr. Arifur Rahman and Dr. Md. Mokhlesur Rahman for their help and companionship during leisure activities.

Special thanks to Rajendra Joshi, PhD researcher, Department of Chemistry, University of Tuebingen, for his help and valuable suggestions.

The author would like to express his gratitude to parents, brothers and sisters for their encouragement to persuade a higher study abroad.

Lastly, the author would like to thank his wife Dr. Naima Zahir for her constant support, understanding and encouragement throughout the work.

Table of content

Abbreviations and notations

VOCs	volatile organic contaminants
HFM	hollow fiber membrane
GFT	stripe gas flow tubes
SFT	solute flow tubes
GC	gas chromatography
GC-MS	gas chromatography-mass spectrometry
CHCs	chlorinated hydrocarbon compounds
GAC	granular activated carbon

a	surface to volume ratio (m^2/m^3)
A_n	cross sectional area represented by a node (n) (m^2)
C	general concentration (kg/m^3)
C_g	concentration of contaminants in gas phase (mg/l)
C_{in}	VOC concentration in the membrane module inlet (mg/l)
C_{out}	VOC concentration in the membrane module outlet (mg/l)
C_i	VOC aqueous concentration at node (i) (kg/m^3)
C_{gw}	VOC gaseous concentration at membrane wall, gas side (kg/m^3)
C_{shw}	VOC gaseous equilibrium concentration at membrane wall, aqueous side (kg/m^3)
C_{sw}	VOC aqueous concentration at membrane wall (kg/m^3)
C_s	Source terms, ($kg/m^3/s$)
C_w	concentration of contaminants in aqueous phase (mg/l)
d	diameter of pores in membrane (cm)
d_a	diameter of a fiber bundle (m)
d_d	diameter of the distribution/collection tube (m)
d_h	hydraulic diameter of a hollow fiber (m)
d_i	inner diameter of a hollow fiber (m)
d_o	outer diameter of a hollow fiber (m)
D	diffusion coefficient (m^2/s)
D^*	effective diffusion coefficient of a compound (m^2/s)
D_{eff}	effective diffusion coefficient of a compound in the gas phase (m^2/s)
D_c	continuum diffusion coefficient of a compound (m^2/s)
D_m	membrane diffusion coefficient of a compound (m^2/s)
D_{kn}	knudson diffusion coefficient of a compound (m^2/s)
D_w	aqueous diffusion coefficient of a compound (m^2/s)
E_a	reaction activation energy (kJ/mol)

F	mass flux, (kg/s)
Fg	flow of gas (ml/min)
F_i	mass flux at a node (i) (kg/m³)
F_w	mass flux from one node to another (kg/s)
F_{2D}	2D flux defined by model assumptions (kg/m³/s)
F_{3D}	3D flux in membrane (kg/m³)
g	acceleration due to gravity (m/s²)
Gz	Graetz number (-)
H	Henry's law constant (-)
k	permeability (m²)
K	overall mass transfer coefficient (m/s)
k_a	local air phase mass transfer coefficient (m/s)
k_L	local liquid phase mass transfer coefficient (m/s)
k_m	membrane mass transfer coefficient (m/s)
k_r	reaction rate constant (1/s)
L	hollow fiber length (m)
L_D	ratio between the diffusive path length in the model and the HFM (-)
M	molecular weight of a compound (g/mol)
M_D	shortening of the average diffusive path length due to lateral movement in the solute tube (-)
M_n	molecular weight of nitrogen (g/mol)
n	number of hollow fibers (-)
n_c	porosity in the catalyst column (-)
nn	number of nodes (-)
P	pressure (atm)
Q	flow rate for a unit volume (1/s).
Q_a	gas flow rate (m³/s)
Q_w	liquid flow rate (m³/s)
R	gas constant (j/mol/K)
$R_{a/w}$	normalized strip gas to water ratio (-)
Re	Reynolds number (-)
R_a, R_f, R_p, R_v	geometrical ratios (-)
S	storage (Pa^{-1})
Sc	Schmidt number (-)
Sh	Sherwood number (-)
T	temperature (K)

Δt	time step (s)
t	detention/contact time (s)
V	velocity (m/s)
v_f	void fraction (-)
v_{av}	average velocity across a pipe opening (m/s)
V_a	velocity in gas tube (m/s)
V_c	volume of the catalyst (ml)
V_g	velocity in the gas tube (m/s)
V_{gas}	volume of the gas flow (l/min)
V_s	velocity in the solute tube (m/s)
V_w	liquid phase / solute flow tube velocity (m/s)
V'	molar volume of a compound (cm^3/mol)
V'_n	molar volume of nitrogen (cm^3/mol)
VR	volume flow ratio, SFT : GFT
w_i	weighting function (-)
x	distance (m)
x_i	location in the x direction of node (i)
x_w	location in the x direction of the membrane wall
x_t	membrane thickness (m)
z	reference datum (m)

Greek letters

μ	dynamic viscosity of fluid (Pa)
δ	pore length (m)
ε	fiber porosity (-)
υ_w	kinematic viscosity of water (m^2/s)
ρ	density (cm^3/g)
τ	pore tortuosity (-)

Chapter 1

1 General introduction

1.1 Contaminants in the environment

Contamination of both ground water and air by organic contaminants, especially by chlorinated hydrocarbons and gasoline constituents such as fuel oxygenates is becoming a widespread problem in the industrialized countries. Contamination of water supplies by volatile organic compounds (VOCs) is an established problem (Clark et al., 1984). An estimated 1.6 to 5.0 million tons of volatile organic chemicals (VOCs) enters the environment each year (Shen and Sewell, 1988), which cause a significant pollution burden. Sources of these contaminants may be one or more of the followings: hazardous waste disposal sites, improper disposal of common industrial solvents, leaking storage tanks, municipal or industrial landfills, septic tanks, use of highly toxic pesticides and fertilizers and accidental spills etc.

1.2 Motivation

The presence of organic pollutants is toxic and harmful for human consumption even though the contaminated ground water may contain very low concentrations of those. Therefore, it is very important to treat water before its use, especially for drinking purpose. However, the cleaning up of contaminated aquifers is very difficult, expensive and time consuming. Moreover, the conventional water treatment technique becomes challenged with the identification of increasing numbers of contaminants.

The evaluation and selection of an appropriate VOCs treatment technology depends on several factors like the contaminants chemical-physical properties, their concentrations, and the amount of water to be treated. Also, the water quality in terms of other organic and inorganic constituents has to be considered. No single method meets every need. The familiar conventional methods for the treatment of water contaminated with VOCs include activated carbon adsorption and air stripping. In addition to this, advance oxidation, biological treatment, and distillation are also in use. All these methods have some limitations.

In conventional air stripping, the surface area can be reduced by the precipitation of Iron and Manganese, which may cause decreasing efficiency. Moreover, pretreatment to remove suspended matter or oil is essential. As adsorption decreases with increasing volatility, it is effective and economic only for VOCs with low concentration to remove contaminants after air stripping. Also the disposal or regeneration of adsorbents is troublesome and costly.

The effectiveness of advanced oxidation is compound-dependent, and it can also form new products, which are more harmful than the original ones (Brewer, 1991). Their high cost is the primary disadvantage of most advanced oxidation processes. Biological treatment (biodegradation) is an environmental friendly and natural process but not all compounds can be rapidly and completely degraded, toxic by-products can sometimes be formed in the treatment process, performance is difficult to verify and proper airflow into the soil must be maintained to provide oxygen if using aerobic bacteria.

The limitations of the existing conventional removal processes of VOCs led to a search for alternative methods in order to find out comparatively better ones. In this context membrane air stripping can be considered as an alternative for VOCs removal from liquid phase. Removal of contaminants by microporous polypropylene hollow fiber membranes is a promising technique and has been successfully used to strip various compounds from aqueous phase such as hydrogen sulfides (Wang et al., 2002), VOCs (Semmens et al., 1989, Keller and Bierwagen, 2001, and Mahmud et al., 2000, 2002, 2004), oxygen (Yang and Crussler, 1986), carbondioxide, sulfur dioxide, bromine (Qi and Cussler, 1985) and ammonia. Liquid liquid extraction of aroma compounds from tomato industry effluent (Souchon et al., 2002) and from sunflower oil (Baudot et al., 2001) have also been successfully studied.

Hollow fiber membrane filtration has proved several significant advantages in comparison to the conventional methods: (1) hollow fibers have large surface area per unit volume, allowing greater contact between phases that provides relatively fast removal of the contaminants, (2) to maximize mass transfer, water and gas flow rates can be controlled independently as they are separated from each other by the membrane, (3) in conventional strip towers large treatment systems for the gaseous phase are essentially needed as water to gas flow ratio can be as high as 1:50 whereas in membrane contactors with large surface areas higher flow ratios are possible by applying vacuum on the gas side, (4) no aqueous flow channeling because of the hollow fiber configuration, (5) due to the hydrophobic nature of the membrane the air stream contains little water, (6) by using nitrogen as strip gas instead of ambient air fouling problems can be controlled.

The main disadvantage is that the overall mass transfer coefficient of membrane based air stripping is usually lower than that of conventional processes due to the mass transfer resistance created by the membrane itself. However, steps can be taken to overcome this problem (Gabelman and Hwang, 1999).

This study presents the evaluation of a polypropylene microporous hollow fiber membrane (HFM) to remove selected aliphatic, aromatic and ether compounds (volatile to semi-volatile) of a wide range of Henry's law constants (0.017 - 1.19). Since some of the compounds have very low Henry's law constants a treatment concept with individual parameter settings (water flow rates, gas flow rates and vacuum) needs to be optimized in order to get high removal efficiency using this HFM.

The organic contaminants in the stripping gas can be subjected to further treatment prior to release. Using photooxidation, studies were conducted to treat VOCs contaminated stripped air (Bhowmick and semmens, 1994, Bhowmick 1992). In those studies, VOCs were irradiated with ultraviolet light in a photooxidation chamber. The main problem of the study was the production of more toxic byproducts e.g. phosgene gas (Bhowmick and semmens, 1994). Though phosgene gas can be hydrolyzed to HCl and CO_2, restripping should be considered and the effect must be investigated in detail (Greenwood and earnshaw, 1984). A promising alternative of the photooxidation may be the catalytic hydrogenation (Schüth 2003, Kopinke et al., 2003) or decomposition of VOCs at elevated temperatures.

1.3 Research objectives

The main objective of this study is to optimize a treatment concept to treat water contaminated with volatile to semi-volatile organic contaminants. Therefore, for the study the following steps have been followed:

- the transfer of volatile to semi-volatile organic contaminants from water to gas phase using air stripping with the help of a polypropylene microporous hollow fiber membrane module.
- the modification of resistance in series model and the application of a hybrid numerical-analytical modeling approach to estimate the theoretical removal of the contaminants and validation of model results against experimental results.
- the catalytic hydrogenation of the gas phase aliphatic contaminants.
- the catalytic hydrogenation of the gas phase ether compounds.
- the catalytic oxidation of gas phase ether compounds.

The research presented in this dissertation has been organized into 8 chapters:

Chapter 2 illustrates the theory of hollow fiber membrane filtration and the gas phase catalytic treatment of contaminants. Resistance in series model for the overall mass transfer coefficients and the individual mass transfer coefficient equations like Lévéque equation and dimensionless correlation between the Sherwood (Sh), Reynolds (Re), and Schmidt (Sc)

numbers are discussed to find out the local liquid phase, gas phase and membrane mass transfer coefficients. Moreover, this chapter illustrates a hybrid numerical and analytical modeling approach to predict the theoretical removal efficiencies of contaminants from aqueous solution to the gaseous phase using hollow fiber membrane module. The input parameters for the model are defined by the geometry of the HFM module and the experimental operating conditions. The solution procedure of the modeling is discussed in this chapter.

Chapter 3 illustrates the materials and methods used for the removal of volatile to semi-volatile organic contaminants from water to gas phase and the catalytic degradation of gas phase contaminants. A detail experimental set up is illustrated here. Also, the measurement parameters for the contaminants in both aqueous and gas phase using GC/FID and GC-MS are listed in this chapter.

Chapter 4 contains the detail study of contaminants transfer from water to gas phase using air stripping with the help of hollow fiber membrane contactor. A total of 12 aliphatic, aromatic, polycyclic aromatic and ether compounds of a wide range of Henry's law constants (0.017-1.19) were chosen. The adjustments of different parameters (water flow, gas flow and vacuum pressure) are studied to optimize the strip efficiencies. The dependencies of removal efficiency as well as mass transfer coefficient on the Henry's law constants are discussed. Moreover, the failure of the resistance in series model in the prediction of overall mass transfer coefficient and the necessity of the alternative modeling approach is discussed. The validation of modeling results against experimental results is discussed in this chapter.

Chapter 5 discusses the catalytic destruction of gas phase saturated and unsaturated aliphatic contaminants. The catalytic degradation was carried out using palladium catalyst in the presence of hydrogen at different elevated temperatures. Reaction kinetics including reaction order, rate constants and thermodynamics of reaction is discussed. Reaction products were identified and mass balances for the individual compounds were established.

Chapter 6 describes the destruction of gas phase ether compounds, normally used as fuel oxygenates, such as methyl tert butyl ether (MTBE), ethyl tert butyl ether (ETBE), tert amyl methyl ether (TAME) diisopropyl ether (DIPE), diethyl ether and dimethyl ether in the presence of hydrogen and palladium catalyst at elevated temperatures. Reaction kinetics thermodynamics and products are discussed.

Chapter 7 discusses the possible catalytic oxidation of ether compounds (MTBE, ETBE, TAME and DIPE). The reaction products, kinetics and thermodynamics are discussed in this chapter.

Chapter 8 summarizes the presented research.

Chapter 2

2. Fundamentals

2.1 Removal of volatile to semi-volatile organic contaminants from water to gas phase using hollow fiber membrane contactors

2.1.1 Membrane filtration

A hollow fiber membrane contactor contains thousands of microporous polypropylene hollow fibers knitted into an array that is wound around a distribution tube and a central baffle (figure 2.1). The baffle provides a component of velocity normal to the membrane surface, which results in higher mass transfer coefficient than that achieved with strictly parallel flow (Gabelman and Hwang, 1999).

The membrane contactors allow direct contact between two phases (liquid/gas liquid/liquid, gas/gas) without dispersing one phase into the other, and finally serve the purpose of mass transfer from one phase to the other phase. To remove VOCs, membrane contactors are operated with the contaminated water on one side of a hydrophobic membrane (shell side) and sweep gas and vacuum are applied on the other side (lumen side) of the membrane (figure 2.2). The membrane does not allow water to pass through the pores into the gas side because of the hydrophobic nature of the microporous membrane.

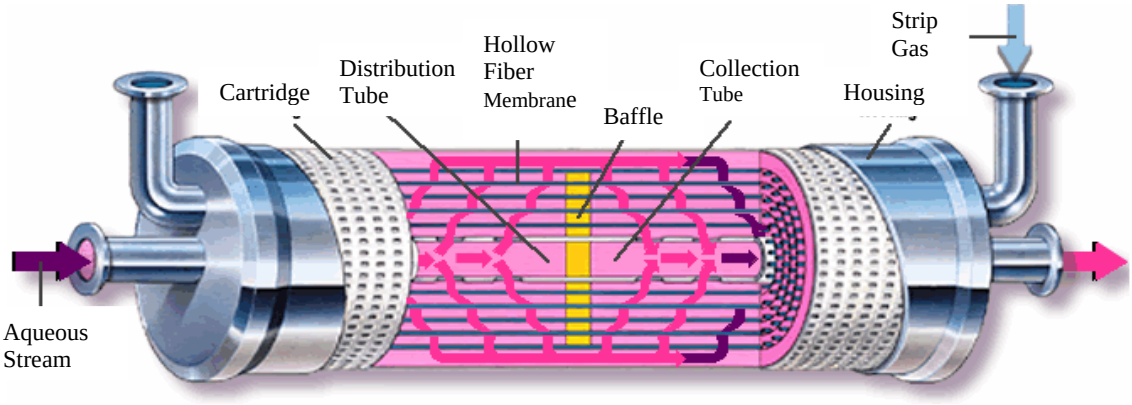

Fig. 2.1: Cross section of a Celgard© membrane contactor. Celgard© Inc.

The main concept of such a treatment technique is to transfer the contaminants from aqueous phase to the gaseous phase. Therefore, the compounds of interest should be volatile to semi volatile and a measure of the volatility of a compound is the Henry's constant, *H* (-). Henry's constant, a dimensionless constant, can be explained as the ratio of the

concentration of a compound in the gaseous phase (C_g) to the concentration in the aqueous phase (C_w) under equilibrium conditions, which can be expressed as:

$$H = \frac{C_g}{C_w} \tag{1}$$

The higher the Henry's constant is, the higher the transfer of organic contaminants from aqueous phase to the gaseous phase will be, as well as the higher will be the removal of the contaminants. That means in order to achieve high removal efficiencies for the compounds with low Henry's constants a large volume of strip gas has to be brought into contact with a small volume of water. However, by using membrane contactor with large contact area maintaining water and gas flow rates and moreover applying a vacuum on the gas side, this limitation can potentially be overcome.

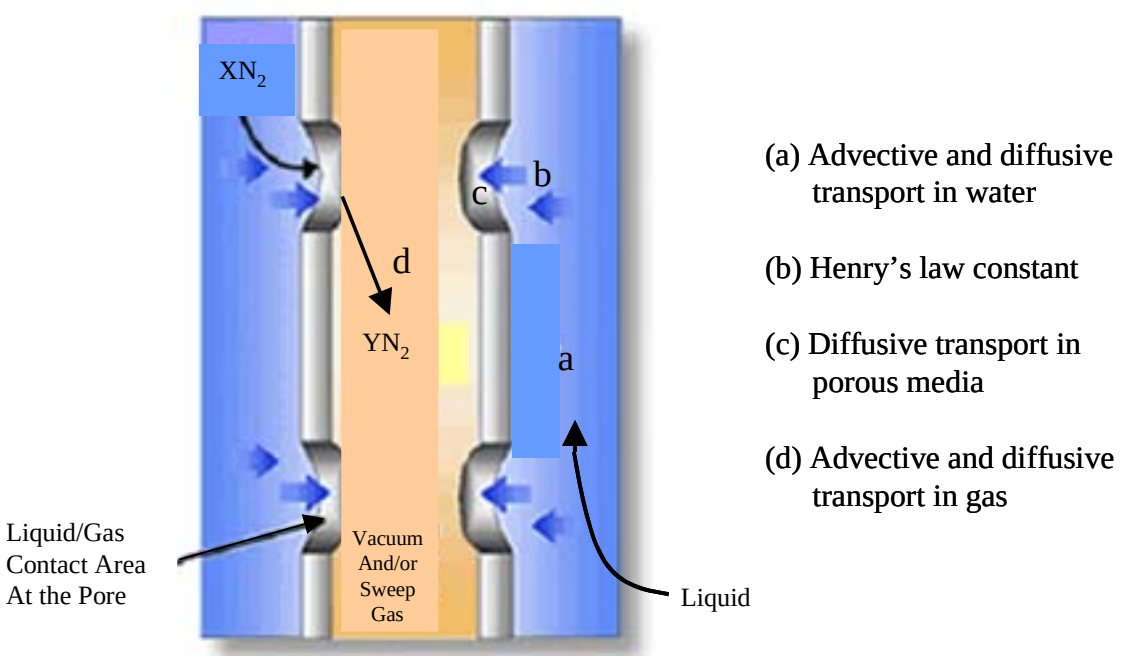

Fig. 2.2: Pathway of contaminants transfer from aqueous to gaseous phase. Modified after Celgard© Inc.

2.1.2 Resistance in series model

Driving force for the mass transfer in HFM modules from the water phase to the gas phase is a concentration gradient between the two phases. Theoretically, the mass transfer is limited by three resistances: (1) diffusion from the bulk aqueous solution through a liquid boundary layer to the membrane surface, (2) diffusion through the air filled pores of the membrane, and, (3) diffusion through the gas boundary layer outside the membrane pore into the

stripping gas. As the mass transfer resistance is the reciprocal of the mass transfer coefficient K (m/s), the overall mass transfer resistance ($1/K$) is typically expressed in a series model as follows (Yang and Cussler, 1986):

$$\frac{1}{K} = \frac{1}{k_L} + \frac{1}{k_m H} + \frac{1}{k_a H} \tag{2}$$

where k_L is the local liquid phase mass transfer coefficient (m/s), k_m the membrane mass transfer coefficient (m/s) and k_a the local gas phase mass transfer coefficient (m/s). In the gas phase, also the Henry's law coefficient H (-) of the stripped compound has to be taken into account.

To calculate the individual mass transfer coefficients, a series of empirically based formulations are available in the literature. Assuming water flow on the lumen side (inside) of the hollow fibers, the local liquid phase mass transfer coefficient, k_L can be predicted based on the correlation of Lévéque (1928) for laminar flow in a cylindrical tube, that is widely used in the literature (Semmens et al.,1989, Gabelman and Hwang, 1999):

$$\frac{1}{k_L} = 0.617 \left(\frac{L\, d_i}{V_w\, D_w^2} \right)^{0.33} \tag{3}$$

where L is the hollow fiber length (m), d_i the inner diameter of the hollow fiber (m), V_w the velocity of the aqueous solution (m/s), and D_w the diffusion coefficient of the contaminants in water (m²/s). In Liquicel extra flow modules, however, water flows on the shell side of the hollow fibers. Specifically for extra flow modules, Schöner et al. (1998) considered the fiber bundle as a densely packed bed and based the mass transfer correlation on the hydraulic diameter d_h (m) of a single fiber:

$$d_h = \frac{d_a^2 - d_d^2 - n\, d_o^2}{n\, d_o} \tag{4}$$

where d_a is the diameter of the fiber bundle (m), d_d the diameter of the distribution/collection tube in the extra flow module (m), d_o the outer diameter of a single fiber (m), and n the number of hollow fibers in the module. To apply eq. 3 for extra flow modules, d_i can therefore be substituted by d_h. Also, the velocity of the aqueous solution (V_w) flowing on the shell side is diameter dependent because of its radial component, due to the extra flow design. Therefore, the mean superficial velocity can be obtained by integrating the local velocity from the axis to the wall of the module (Schöner et al., 1998), and finally, accounting for the void fraction (Mahmud et al., 2000), the effective velocity of the water in the module can be defined:

$$V_w = \frac{2\,Q_w}{\pi\,L}\,\frac{ln(d_a / d_d)}{d_a - d_d}\,\frac{1}{v_f} \tag{5}$$

where Q_w is the aqueous feed flow (m³/s) and v_f the void fraction (-).

In a dimensionless form, k_L can be defined as a correlation between the Sherwood (*Sh*), Reynolds (*Re*), and Schmidt (*Sc*) numbers with the general form of $Sh = a\,Re^b\,Sc^{0.33}$, where *a* and *b* are being fitted from experimental results. Published correlations depend strongly on the experimental system, e.g. the geometry of the experimental setup and the compounds used. For cross flow in closely packed tube bank heat exchangers, Kreith and Black (1980) developed the following correlation:

$$Sh = 0.39\,Re^{0.59}\,Sc^{0.33} \tag{6}$$

where the individual numbers are defined as:

$$Sh = \frac{k_L\,d_o}{D_w} \qquad Re = \frac{V_w\,d_o}{\upsilon_w} \qquad Sc = \frac{\upsilon_w}{D_w} \tag{7}$$

with V_w being the kinematic viscosity of water (m²/s). Note, that also in this set of equations, d_h has to be used instead of d_0 for extra flow modules. Applying this set of equations for the gas flow on the lumen side, d_o is substituted by d_i and the gas phase coefficients have to be used. An excellent summary on these type of mass transfer correlations is given by Gabelman and Hwang (1999).

The membrane mass transfer coefficient k_m and the local gas phase mass transfer coefficient k_a can be defined by the correlations of Qi and Cussler (1985) and Lévéque (1928), respectively:

$$\frac{1}{k_m H} = \frac{\delta\,\tau}{D_{eff}\,\varepsilon\,H} \tag{8}$$

and,

$$\frac{1}{k_a H} = \frac{0.617}{H}\left(\frac{L d_i}{V_a D_c^{\,2}}\right)^{0.33} \tag{9}$$

where L is the hollow fiber length (m), δ the pore length/membrane thickness (m), τ the pore tortuosity (-), D_{eff} the effective diffusion coefficient of the compound in air (m²/s), ε the fiber porosity, V_a the strip gas velocity inside the hollow fiber (m/s), and D_c the continuum (ordinary) diffusion coefficient of the compound in the strip gas (m²/s). For membranes with pore diameters less than 0.1 µm, continuum diffusion as well as Knudsen diffusion have to

be taken into account, and an effective diffusion coefficient D_{eff} has to be defined (Polland and Present, 1948).

In experiments with an extra flow module and chloroform as the compound of interest the Lévéque equation (eq. 9) was found to be inapplicable especially for low strip gas flows, as it overestimated the local gas phase mass transfer coefficient (Mahmud et al., 2004). This was attributed to the low Graetz numbers in these experiments (0.0031 to 0.0069) where the Lévéque equation is no longer valid. The Graetz number can be defined as (Wickramasinghe et al., 1991):

$$Gz = \frac{d_i^2 V_a}{D_c L} \tag{10}$$

To apply the Lévéque equation, Graetz numbers should at least be > 4 (-) (Lévéque, 1928, Gabelman and Hwang, 1999, Wickramasinghe et al., 1991). To account for the low flow velocities, equation 9 was modified by Mahmud et al. (2004):

$$\frac{1}{K_a H} = \frac{0.617}{H}\left(\frac{L d_i}{D_c^2}\right)^{0.33}\left(\frac{1}{V_a}\right)^{2.19} \tag{11}$$

resulting in a much better data fit.

2.1.3 A hybrid numerical-analytical modeling approach

The development of hybrid numerical-analytical model has been discussed in detail by McDermott et al. (2007). However, the very important considerations of the model are discussed below:

2.1.3.1 Model concept

In HFM modules, the water enters the module at one side and flows either over the shell side (outside) or the lumen side (inside) of the hollow fibers to the outlet on the other side. The strip gas is applied on the respective opposite side of the membrane in counterflow. The mass transfer of an organic contaminant from the water phase into the gas stripping phase takes place across the membrane walls forming the hollow fibers. The membrane is porous, does not allow water to move across it, but does allow the diffusion of organic compounds in the gaseous phase. To model these processes, the overall mass transfer is broken down into the different steps, i.e. advective flow as a result of the pressure gradient and mass transport due to flow and diffusive gradients. Figure 2.2 illustrates the path of a typical organic molecule through a HFM module, and the processes taken into account during modeling. After entering the HFM system (a), the molecule is transported some distance inside the

solute tube as a result of advective and diffusive transport. At some point the molecule reaches the edge of the solute tube, and the interface between the water in the solute tube with the gas in the membrane. The organic molecule then leaves the water phase, and enters the pore space of the membrane (b). The relationship between the concentration of the organic molecules in the water and in the gas is governed at the boundary by Henry's law. Once in the pore space of the membrane, concentration driven diffusion occurs across the membrane following Fick's first law of diffusion (c). After leaving the membrane the molecule is again transported by advective and diffusive transport out of the system in the gas phase in counterflow (d).

The strip gas flow tubes (GFT) are assumed to be almost perfectly hexagonally packed. The spaces between the GFT form the solute flow tubes (SFT), carrying the dissolved organic contaminant in counterflow. In HFM modules, flow in the SFT is conventionally along the length of the GFT. For the model development, a Liqui-Cel© 2.5" x 8" extra flow hollow fiber module was taken as a reference for a HFM module geometry. The main characteristics of the module are summarized in the table 4.1. In Liqui-Cel© extra flow modules with a central baffle, flow has a radial component transverse to the GFT (figure 2.1).

On considering the geometry of the HFM module, it becomes clear that there is a consistent relationship between the volume and surface area ratio of both the water phase and the gas phase. This fact allows the construction of a simplified 2D geometrical model, where the flow and transport equations can be solved using the finite element method. The simplification is possible by applying constant geometrical factors maintaining the volume and area ratios and consideration of the length of diffusion paths in the system. To ensure representative transport characteristics the flow velocities in the SFT and GFT tubes are held identical to the experimental flow velocities in the HFM. The SFT dimensions in 2D section are reproduced in the model, the GFT flow parameters are accounted for by including geometrical factors in the modeling discussed later. For the modeling it was found that 3 elements in the cross section provided sufficient accuracy.

2.1.3.2 Solution procedure

The solution procedure adopted during modeling mass transfer in the HFM module included:

- Flow simulation
- Mass transport simulation
- Diffusion path lengths
- Aqueous diffusion limitation

In overview, two major processes were solved, the hydraulic and the transport mass balance equations. In terms of the hydraulic solution the membrane was simulated as a hydraulic

barrier and the flow tubes were simulated as high permeable areas. For the mass transport, both a numerical and an analytical solution were applied, providing a hybrid approach. The advective diffusive transport in the flow tubes was simulated numerically. The mass transfer across the membrane was modeled analytically by the inclusion of linked source and sink terms.

The mass balance equations describing hydraulic flow can be expressed as (Freeze and Cherry, 1979):

$$S\frac{\partial p}{\partial t} - \nabla\left(\frac{k}{\mu}\left(\nabla p + \rho g \nabla z\right)\right) = Q \tag{12}$$

where S is the storage (Pa^{-1}), p the pressure (Pa), k the intrinsic permeability (m^2), μ the dynamic viscosity (Ns/m^2), ρ the density (kg/m^3), g the gravity constant (m/s^2), z the height above a datum (m), and Q the flow rate for a unit volume (1/s). The discretisation and solution of Eq. (12) using the finite element method is illustrated by Istok (1989) or Kolditz (2002). Solving Eq. (12) provides the fluid pressure at each discrete node in the finite element model which then can be interpolated for the elements and converted into flow velocities (m/s) in the elements. The flow velocities are then used to derive the solution of the 2D mass transport equation (Carslaw and Jaeger, 1959):

$$\frac{\partial C}{\partial t} = D\nabla^2 C - \nabla\cdot\left(vC\right) - C_s \tag{13}$$

Here, C is the concentration of the organic compound (kg/m^3) under investigation and D represents the effective diffusion coefficient (m^2/s), depending on the media. The term C_s refers to a source term, given as a rate (kg/m^3 s). Again, this is solved using the finite element method as described by Istok (1989), or Kolditz (2002).

The concentrations on either side of the membrane determine the amount of mass transfer in the system. To maintain the realistic concentrations in the model in comparison to the HFM, the three dimensional geometry of the HFM once transferred to a two dimensional model needs to be approximated using geometrically defined ratios. These ratios can be identified by addressing the simplest geometrical unit in the HFM and modeling situation (McDermott et al., 2007). Four ratios can be identified, described as (1) cross sectional area ratio available to flow, R_f, (2) surface area available to mass exchange, R_a, (3) volume to surface area ratio, R_v, (4) packing ratio, R_p.

2.1.3.2.1 Flow simulation

The coupling between the hydraulic mass balance equation (Eq. 12) and the transport equation (Eq. 13) is facilitated by the flow velocities. For linear flow conditions the flow velocity can be described by Darcy's law:

$$v = \frac{k}{\mu}\nabla\left(p + \rho g z\right) \tag{14}$$

The flow velocity can be matched to the HFM flow velocity by altering the boundary pressure conditions but maintaining a constant permeability. The boundary pressure conditions can be used to adjust the model to the experimental system in such a way as to match the HFM velocities.

Examining the formulation of the transport equation (Eq. 13) the type of carrying fluid actually transporting the organic contaminant is not important. Important for the transport equation is the velocity of the carrying fluid and the diffusion coefficient of the organic contaminant in the carrying fluid. Therefore as a further simplification for the whole system both the solute and gas flow tubes are represented by the same fluid mathematically, with very different velocities and diffusion coefficients. This removes the need to consider multiphase flow (Rutqvist et al., 2002; Miller et al., 1998; Helmig, 1997).

For the approximation of the system, the velocity of the flow in the solute tube is critical as the volume ratio of the gas flow to the water flow is represented over the flow velocity ratio. For example, assuming the volume of the water side to be the same as the gas side, to simulate a volume flow ratio (*VR*) of 1:25 (solute : stripping gas), the flow velocity in the gas tubes is 25 x that in the solute tubes. In the model the ratio R_f (McDermott, 2007) needs to be taken into account, so that

$$v_s = \frac{v_g}{R_f VR} \tag{15}$$

This means in the model $1/R_f$ of the actual gas volume is used to match the flow conditions, and therefore to maintain a realistic concentration in the model gas tubes the mass flux calculated as flowing into the gas tubes due to diffusion needs to be reduced by the same factor.

The velocity differences were practically implemented by setting the boundary pressure conditions for the solution of Eq. (13) such that the pressure gradient in the GFT was appropriately larger (or smaller) than that in the SFT. To ensure that the membrane separating the SFT and GFT was hydraulically impermeable it was assigned a minimal

permeability, of the order of 5^{-19} m². In comparison the SFT were assigned a permeability 10 orders of magnitude larger, 5^{-9} m². The tremendous contrast in material properties proved problematic for a standard iterative linear equation solver. A direct solver rather than the standard iterative solver had to be applied to achieve accurate solutions.

Examining Eq. (12), it can be seen that in the hydraulic equation the only time dependent parameter is the storage *S* in the system. The storage represents the elastic uptake of fluid in a unit volume dependent on pressure changes. Assuming that the pressure in the system was steady state and not altering during operation, and that the elastic response of the HFM was negligible, enables the initial solution of the hydraulic equation system to be valid at all times during the simulation. This means that the hydraulic equations need only be solved once at the start of the simulation, whereas the transport equations were solved successively according to the time step.

2.1.3.2.2 Mass transfer simulation

Numerical stability criteria, time step limitation: Using the finite element method to numerically solve the balance equations for mass transport requires the solution procedure to satisfy certain numerical stability criteria. Advective flow and transport are the dominant processes along the length of the flow tubes, whereas across the membrane the diffusive transport dominates. Consequently both the criteria for advective dominated transport (Courant Criteria) and diffusive transport (Neumann Criteria) have to be satisfied. Additionally, the solutions are time progressive, and it was found that the transport solution reached steady state conditions after 2.5 pore volumes of the SFT had (mathematically) been exchanged, providing a minimum simulated real time length for the model runs.

To ensure numerical stability under advective dominated transport conditions, the Courant Criteria is given as

$$\frac{v\Delta t}{x} \leq 1 \tag{16}$$

Likewise under diffusive dominated transport the Neumann Criteria is given as

$$\frac{D\Delta t}{x^2} \leq 0.5 \tag{17}$$

In both, Eq. (16) and Eq. (17), the term Δt refers to the size of the time step (s), and *x* refers to the size of the element in the direction of mass transport (m), v is the velocity in the *x* direction (m/s), and *D* is the diffusion coefficient (m²/s).

Remaining within both the stability criteria proved to be a significant problem for the numerical solution techniques due to the extreme gradients. On hand of real modeling and experimental data this can be illustrated as follows.

Courant Criteria for the GFT: Typically the HFM would be represented in its length by circa 20 elements, i.e. the element length (*x* in Eq. (16)) is 0.0075m (length of the module 0.15 m). Experimental operation would involve a flow velocity of circa 0.00183 m/s in the solute tubes, and for a volume ratio (VR) of 1:25 solute to gas a corresponding velocity of 0.0074 m/s in the GFT. According to Eq. (16) the maximum time step for stable calculation would be circa 1 second, requiring a minimum of 50 time steps to satisfy the pore volume criteria.

Neumann Criteria for the SFT and Membrane: The aqueous diffusion coefficients of common organic contaminants are of the order of 10^{-9} m²/s. Solving Eq. (17) for diffusion in the direction of flow in the SFT suggests a time step of no larger than 28125s. However, for diffusion across the membrane, the effective diffusion coefficients of organic molecules in the gas filled porous membrane are on the order of 10^{-6} m²/s. The length x of the membrane elements in the direction of mass transfer are of the order of 10 µm, therefore the largest time step possible to match the diffusive flow in the system across the membrane would be of the order of 0.00005s. To achieve an exchange of circa 2.5 pore volumes would require circa 1 million time steps.

Satisfying only the Courant criteria allows a model run to be completed in less than 2 minutes real time, however satisfying both Courant and Neumann criteria required a model run of circa 5 days real time.

Due to this time limitation, an analytical solution for the diffusive dominated mass transport across the porous membrane was developed. The coupling of the analytical and numerical solutions occurred via source terms. This resulted in a numerically stable solution with only the Courant criteria being taken into account. Additionally this approach allowed the easy inclusion of Henry's law for the behaviour of the organic contaminants at the water gas interface (Fetter, 1993), avoiding multiphase flow simulation.

Pressure and temperature dependent diffusion coefficients: Examining equation 13 it can be seen that the diffusion coefficient is a dominant factor in determining the rate of mass transfer from one phase into another. Three diffusion coefficients are required to model the system, (1) the diffusion coefficient of the organic compound in gas (GFT), (2) the diffusion coefficient of the organic compound in the membrane (gaseous phase) and (3) the aqueous diffusion coefficient of the organic compound (SFT).

Including the pressure and temperature dependency of these diffusion coefficients in the model rather than assuming standardized table results at constant temperature and pressure (say 20°C and 1 atm pressure), increased the reliability of the results.

The diffusion coefficient of the organic compound in free space, D_c, can be calculated using the correlation given by Fuller et al. (1966):

$$D_c = 10^{-7} \frac{T^{1.75}\left(1/M_n + 1/M\right)^{\frac{1}{2}}}{P\left(V_n'^{\frac{1}{3}} + V'^{\frac{1}{3}}\right)^2} \tag{18}$$

where M_n is the molecular weight of the strip gas (g/mol), M the molecular weight of the stripped contaminant (g/mol), P the gas phase pressure (atm), V'_n the molar volume of the strip gas (e.g. for nitrogen 17.9 cm³/mol), and V' is the molar volume of the contaminant (cm³/mol).

For membranes with pore diameters less than 0.1 μm, continuum diffusion as well as Knudsen diffusion have to be taken into account, and the diffusion coefficient in the membrane D_m can be defined as (Polland and Present, 1948):

$$D_m = \left(\frac{1}{D_c} + \frac{1}{D_{Kn}}\right)^{-1} \tag{19}$$

where D_{Kn} is the Knudsen diffusion coefficient (m²/s). For dilute gases, D_{Kn} can be calculated using (Evans et al., 1961):

$$D_{Kn} = 4850\, d \sqrt{\frac{T}{M}}\ 10^{-4} \tag{20}$$

where d is the pore diameter (cm), T the temperature in Kelvin (k), and M the molecular weight of the compound (g/mol).

The aqueous diffusion coefficient D_w can be calculated using the correlation given by Wilke and Chang (Wilke and Chang, 1955), which was modified by Hayduk and Laudie [1974]:

$$D_w = \frac{13.26\ x\ 10^{-9}}{\mu_w^{1.14}\ V'^{0.589}} \tag{21}$$

where μ_w is the dynamic viscosity of water (1.0 cP at 20°C), and V' the molar volume of the compound (cm³/mol).

Analytical solution of the diffusion across the membrane: The diffusive flux across the membrane from the SFT to the GFT is calculated for each time step during the simulation. The time step is assumed to be small enough so that changes in the concentration on one side of the membrane with respect to the other side can be ignored. This means that Ficks first law of diffusion (Fetter, 1993) can be used to calculate the flux across the membrane:

$$F = -D\frac{dC}{dx} \tag{22}$$

where F is the mass flux of solute (kg/m²s), C is the solute concentration, and dC/dx is the concentration gradient. Here the concentration gradient in a time step is considered to be constant. Figure 2.3 (left) illustrates the distribution of the source terms on the nodes of the membrane / flow tube interfaces, and figure 2.3 (right) illustrates a close up view of the linked source terms. Here C_{sw} refers to the concentration of the dissolved organic compound at the boundary of the membrane at the node in question, but still in the solute pipe, C_{shw} refers to the concentration of the organic compound at the boundary of the membrane at the node in question but in the membrane, that is in the gas phase, and C_{gw} refers to the concentration of the organic compound at the boundary of the membrane to the gas flow tube for the linked node.

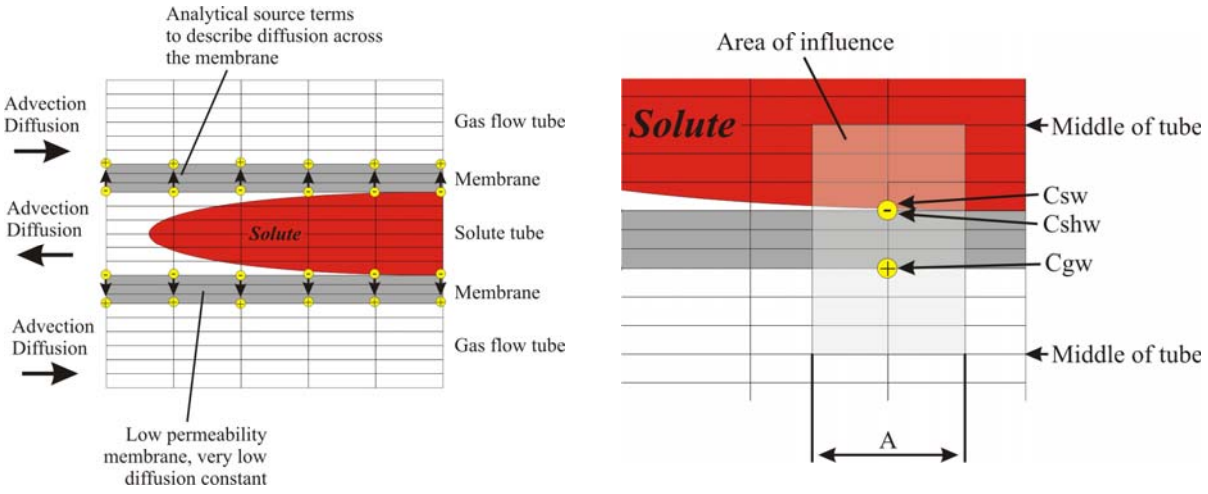

Fig. 2.3: Concept of analytical mass transfer model (left) and mass transfer by source/sink linking (right).

From Fick's first law, the diffusive flux across the membrane wall F_w (mass/s) for one pair of nodes is then

$$F_w = D^* \frac{C_{shw} - C_{gw}}{x_t} A_n R_a \tag{23}$$

where A_n is the cross sectional area represented by the node *n* across which diffusion is occurring (discussed below), R_a is a geometrical ratio factor (McDermott, 2007), x_t is the membrane thickness given as 30 µm, and D^* is the effective gas diffusion coefficient of the organic compound in the membrane, after Grathwohl (Grathwohl, 1998) given by:

$$D^* = D_m \varepsilon^2 \tag{24}$$

where ε is the porosity of the membrane and D_m (m²/s) the continuum gaseous diffusion coefficient in the membrane.

The term C_{shw} is given by including Henry's law Eq. (25), where *H* is Henry's constant.

$$C_{shw} = C_{sw}.H \tag{25}$$

The nodal concentrations C_{gw} and C_{sw} are given by the solution to the previous time steps transport equations in the finite element calculations, or by the initial conditions for the first time step.

Calculation of source term C_s contribution: The flux F_w represents the flux across the membrane around the node *n* during a time step Δt. The flux comprises contributions from all points within the SFT where a concentration gradient towards the wall (node) exists. Assuming the concentration gradient to be normal to the wall, there is a contribution from all points normal to the wall. Representing this in terms of finite element approximation, nodes normal to the wall all provide part of the flux F_w. This is illustrated in figure 2.4. Ignoring this factor and applying the entire flux to the nodes adjacent to the membrane causes numerical instability due to the well criteria, i.e., more mass could be removed from a node than is actually present numerically in a time step.

Following Fick's first law of diffusion, the contribution from a point at node (i) to the flux across the wall is

$$F_i = \frac{C_i - C_{sw}}{x_i - x_w} D_w A_n \tag{26}$$

where C_{sw} is assumed to remain constant for the time step Δt. The sum of the diffusion flux is

$$\sum_0^{nn} F_i = \sum_0^{nn} \frac{C_i - C_{sw}}{x_i - x_w} D_w A_n \tag{27}$$

where *nn* is the number of nodes over which the diffusion flux is distributed. However, the total diffusion flux across the membrane is controlled by the concentration at the edge of the membrane, not the distribution of concentrations within the solute tube.

A weighting, w_i, needs to be included due to the discritisation of the finite element approach to include the fact that boundary nodes represent the flux from two elements, other nodes the flux from 4 elements. This can be understood by considering a node in the flow channel where four elements are contributing to the flux at the node, and a node at the edge where only two elements contribute to the flux. The value w_i can be calculated from the volume of the elements connected to the node. The contribution according to Eq. (26) of each node is normalised and multiplied by F_w to give the actual contribution of each node. The contribution per node to the diffusive flux is then:

$$F_i = \frac{\frac{C_i - C_w}{x_i - x_w} w_i}{\sum_0^n \frac{C_i - C_w}{x_i - x_w} w_i} D_w A_n F_w \tag{28}$$

Note that F_i is always negative as it represents the removal of organic compound from the solute tube. We assume complete mixing in the GFT, and the source term is then distributed evenly on the GFT side (figure 2.4), dividing the source term by the number of nodes in the GFT to be effected.

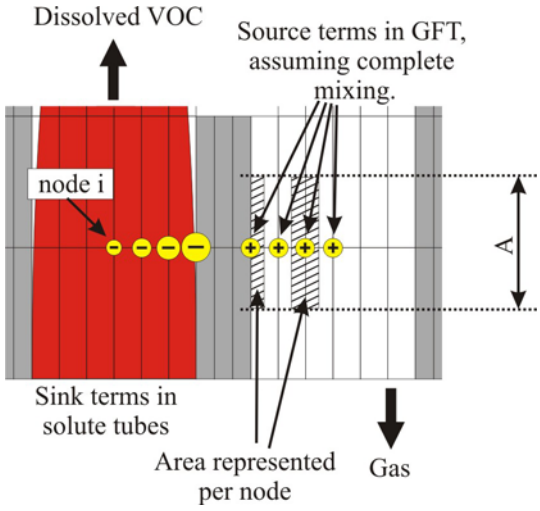

Fig. 2.4: Distribution of flux across the SFT and GFT.

Finally on the gas side to maintain realistic concentrations the source term needs to be corrected by the geometrical factors and the volume flow ratio *VR* (2.1.2.2.1) needs to be taken into account Eq. (30). The volume flow ratio accounts for the difference in velocities in the SFT and the GFT, and the fact that the source term is given as a rate per unit volume.

$$C_s = F_w \frac{R_a R_p}{nnR_f VR} \tag{29}$$

On the fluid side the source term is given by

$$C_s = F_i \tag{30}$$

2.1.3.3 Diffusion path lengths

Ficks first law of diffusion Eq. (23) shows that the diffusion path length is significant in determining the amount of flux to occur as a result of the concentrations. In the 2D approximation the flow tubes are represented by rectangular channels with two surfaces available for diffusive exchange (figure 3.3). In reality due to the geometry of the 3D system the length of the diffusive paths are much shorter than predicted by the 2D approximation. Given in Eq. (23) that ΔC and D remain constant, then in the 3D situation

$$F_{3D} \propto \frac{1}{x} \tag{31}$$

therefore to correct for the diffusive path length difference:

$$F_{2D} L_D = F_{3D} \tag{32}$$

where L_D is the ratio between the diffusive path length in the model and the HFM. If the flow is purely longitudinal by integration and weighting with the area available to flow, L_D can be shown to be circa 2.2. However the HFM are designed to allow transverse flow, which would then remove the weighting due to the cross sectional area due to flow, and L_D becomes circa 4.1.

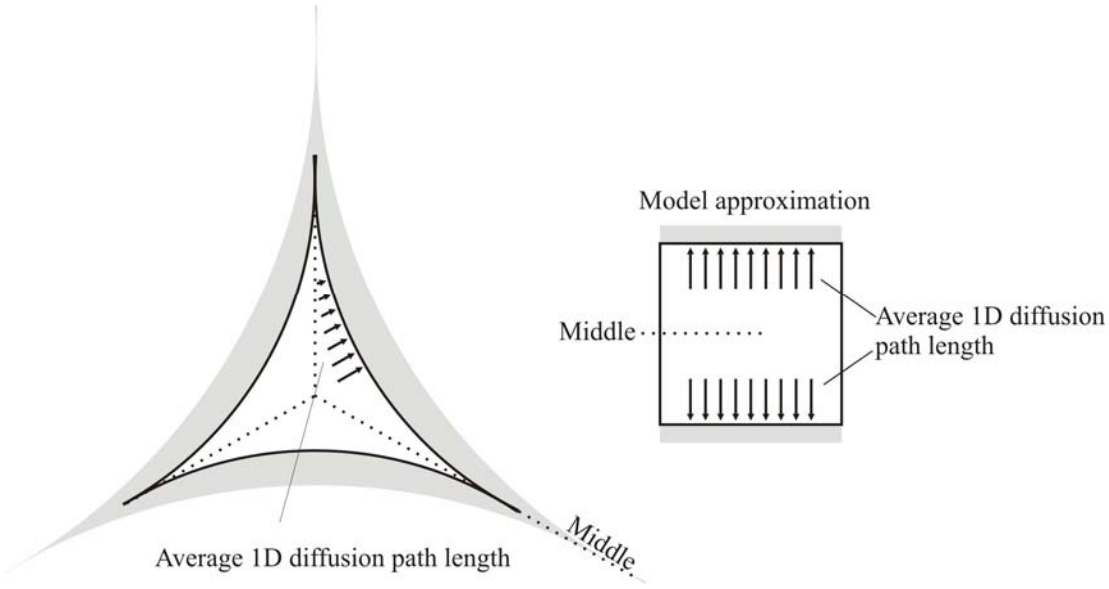

Fig. 2.5: Diffusive path length approximation.

2.1.3.4 Aqueous diffusion limitation

The size of the source term per node in the solute tubes is dependent on concentrations at the membrane surface and the discretisation in the model. The flux predicted by the model

as possible across the membrane, is physically larger than actually available by diffusive flux in the aqueous solute. In other words the sink term is trying to remove more organic molecules in a given time step than is available through delivery from the adjacent elements where aqueous diffusion provides the diffusive flux. This problem occurs particularly with compounds with high Henry's law coefficients, where high potential fluxes into the gas phase across the membrane are possible. In such cases the system is limited by the rate at which the organic molecules can reach the membrane due to the aqueous diffusion coefficient.

The maximum aqueous diffusive flux can be estimated by Eq. (27) and can then be introduced as an upper value during calculation of F_w. From comparison with the experimental results it was clear that there was more aqueous diffusion taking place than predicted by Eq. (27). This is considered to be due to the simplification of the modeling approach and the fact that there is likely to be mixing in the HFM due to radial flow which has not been taken into account in the 2D modeling approach. This mixing would lead to a shortening of the average diffusive path length due to lateral movement in the solute tube. To account for this, the upper limit on aqueous diffusion was set by geometrical considerations and by introducing a factor to represent mixing in the solute tubes. The maximum diffusive flux is then given by

$$F_w = F_{2D} L_D M_D \tag{33}$$

where M is the factor representing the further shortening of the average diffusive path length due to lateral movement in the solute tube. Although M_D can be viewed as a fitting factor, it was held constant for all simulations at a value of 1.35. For ease of modeling L_D and M_D were combined to give the "Diffusive path length multiplier" with a resulting value of 5.5. This simply represents a shortening of the diffusive path length as a consequence of the HFM module geometry and a mixing factor due to the non-linear flow conditions.

2.2 Catalytic degradation of contaminated off-gas

Catalytic hydrogenation of organic compounds using noble metals is a widely used technique (Rylander, 1979). Catalysts are of enormous importance to the chemical industry, because they allow a reaction to occur with a reasonable rate and decreasing the reaction activation energy, E_a.

Catalytic hydrogenation is potentially applicable for the conversion of contaminants present in water or air to non-toxic compounds. Hydrodechlorination reaction: R-Cl + H_2 = R-H + HCl is one important synthetic technique and has many applications. Hydrodechlorination reaction is usually performed under the presence of noble metals and numbers of studies

have been performed using different metal catalysts including palladium (Schüth and Reinhard, 1998, Schüth et al., 2004, Moon et al., 1998, Ribeiro et al., 1997 and 1998, Early et al., 1999, Karpinski et al., 1996, Rupprechter and Somorjai, 1997), platinum (Wiersma et al., 1998, Choi et al., 1996, Fung and Sinfelt, 1987) and rohdium (Wiersma et al., 1998, Fung and Sinfelt, 1987, Bodnariuk et al., 1989, Coq et al., 1986). It is found that Pd has the highest hydrodecloriation reaction activity and this is the most selective metal catalyst for this reaction (Rylander, 1979). Hydrogenation of ether compound: R-O-R´ + H_2 = RH + R´OH might also be potentially used for the conversion of ether compounds to non-toxic substances.

The contact time, t (s) for reaction in the catalytic reactor bed was calculated multiplying the volume of the catalyst by the porosity and dividing by the flow of gas as:

$$t = \frac{V_c n_c}{F_g} \tag{34}$$

Where, t is the detention/contact time (S), V_c is the volume of the catalysts (ml), n_c is the porosity (-), considered here as 50%, and F_g is the flow of gas (ml/s).

2.2.1 Reaction type

Among the VOCs, chlorinated aliphatic hydrocarbons (CAHs) belong to the most frequently found contaminants in the environment. Dechlorination of CAHs under anaerobic conditions may occur in several ways, these reactions are discussed in detail. The first are **hydrogenolysis** where the halogen substituent is replaced by hydrogen, probably according to a nucleophilic substitution mechanism. This type of reaction is one, which occurs most frequently. **Dihaloelimination** of CAHs is a reductive elimination of two chlorine substituents to form an alkene and is only found with chlorinated alkanes. The third important reaction which occurs under anaerobic conditions, dehydrohalogenation, does not involve the transfer of electrons and therefore does not directly depend on the presence of either an electron donor or electron acceptor. **Dehydrohalogenation** involves the elimination of halogen from carbon atom followed by the elimination of a hydrogen atom from an adjacent carbon. This results in the formation of an additional bond between the two carbon atoms. The fourth type of reaction, **hydrogenation**, involves the addition of hydrogen in the carbon atom to form alkane from alkene.

2.2.2 Reaction kinetics

2.2.2.1 First order rate law

A general unimolecular reaction can be written as:

$$C \rightarrow P$$

where, *C* is the reactant and *P* is a product is called a first-order reaction. The rate is proportional to the concentration of a single reactant raised to the first power. The decrease in the concentration of *C* over time can be written as:

$$-\frac{d[C]}{dt} = k_r[C] \tag{35}$$

$$-\frac{d[C]}{[C]} = k_r dt \tag{36}$$

Equation 36 represents the differential form of the rate law. Integrating equation 36 leads to:

$$ln[C] = -k_r t + A \tag{37}$$

The integration constant *A* can be evaluated using boundary conditions. When *t=0*, $[C]=[C]_0$, $[C]_0$ is the original concentration of *C*. Substituting into equation 37 gives:

$$ln[A]_0 = -k_r(0) + C \tag{38}$$

Therefore the value of the constant of the integration is:

$$A = \ln[C]_0 \tag{39}$$

Substituting equation 39 into equation 37 yields:

$$ln\frac{[C]}{[C]_0} = -k_r t \tag{40}$$

Plotting ln *[C]* or ln $[C] / [C]_0$ against contact time creates a straight line with slope *–k*. The equation 40 can also be written in the form:

$$[C] = [C]_0 e^{-k_r t} \tag{41}$$

This means that the concentration of *C* decreases exponentially as a function of time.

The rate constant k_r can also be determined from the half life $t_{1/2}$. Half life is the time it takes for the concentration to fall from $[C]_0$ to $[C]_0/2$. According to equation 41 is obtained:

$$k_r t_{1/2} = ln \frac{[C]_0}{[C]_0 / 2} \quad \text{or,} \quad k_r = \frac{ln\, 2}{t_{1/2}} \tag{42}$$

2.2.2.2 Pseudo first order reaction

C and D react to produce P: C+D → P

If the initial concentration of the reactant D is much higher than the concentration of organic contaminant C, the concentration D will not change appreciably during the course of the reaction, thus the rate dependence of organic contaminants can be isolated and the rate law can be written as equation 35 and the solution of this equation will be like the first order reaction as equation 40.

2.2.3 Thermodynamics of reaction

The dependency of chemical reaction rates can be quantified by activation energies, which essentially describes how rate constants of chemical reaction vary with temperatures.

2.2.3.1 Arrhenius equation

The rate of thermodynamically feasible reaction is controlled by the activation energy (E_a) according to Arrhenius equation:

$$k_r = Ae^{-Ea/R} \tag{43}$$

Where k_r is the rate constant (S^{-1}), A is the absolute rate constant (S^{-1}) which equals the rate at which all transition states proceed to products, R is the gas constant (8.314 J/mol/K) and T is the absolute temperature (K). The symbol A in the Arrhenius equation does have a slight dependence on temperature and usually it can be ignored. The Arrhenius equation can be rearranged in the form of y = c + mx like:

$$ln\, k_r = ln\, A + \left(\frac{-Ea}{R}\right)\left(\frac{1}{T}\right) \tag{44}$$

This means that a plot of ln k_r against $1/T$ should give a straight line, the slope of which is $-E_a/R$ and that can be used to calculate the activation energy, E_a (Ebbing and Gammon, 2003-2004).

2.2.4 Catalyst activity

The catalyst activity for the gas phase reaction in the fixed bed reactor can be calculated after Kopinke et al. (2003) as:

$$A_{pd} = \frac{V_{gas} \ln(C_0 / C)}{m_{pd} \ln 2} \text{ (l/(g-min))} \quad (45)$$

Where, V is the volume of the gas flows (l/min), m_{pd} is the mass of palladium, C_0 and C the inflow and out flow contaminated gas concentrations respectively of the catalytic reactor.

Chapter 3

3. Materials and methods

3.1 Experimental set up

The instrumental set up to study the contaminant transfer from the aqueous phase to the gaseous phase followed by catalytic conversion of gas phase contaminants is shown in figure 3.1. Central part is a hollow fiber membrane module (4) manufactured by Celgard© Inc., which is shown in detail in figure 2.1.

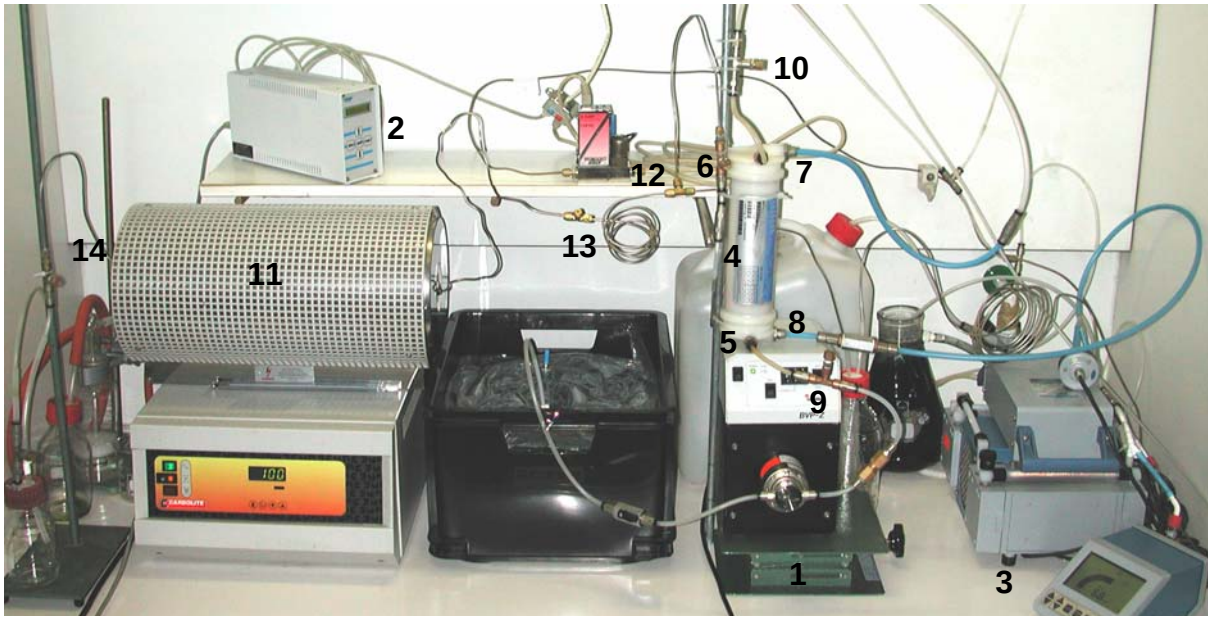

Fig. 3.1: Experimental set up for the treatment of contaminated water. 1 - Water pump, 2 - Gas-flow controller, 3 - Vacuum pump and controller, 4 - Hollow fiber membrane module, 5 - Water inflow, 6 - Water outflow, 7- Gas inflow, 8- Gas outflow, 9- Sampling port water inflow, 10- Sampling port water outflow, 11- Furnace having isothermal zone, 12 - place of hydrogen gas addition, 13 - Sampling port contaminated gas inflow, 14 - Sampling port gas outflow.

During operation, the contaminated water was pumped (1) and allowed to enter the module at the bottom (5) that flowed over the shell side (outside) of the hollow fibers to the outlet (6). Nitrogen was used as an inert strip gas and was applied on the lumen side (inside) of the hollow fibers in counter flow, gas in at (7), gas out at (8). In addition, a vacuum was applied on the lumen side (inside the hollow fibers) to increase strip efficiencies. Nitrogen flow can be adjusted independently through a gas flow controller (2) and vacuum pump with controller (3) respectively. Inflow and outflow samples for the water phase analyses can be collected at sampling ports (9) and (10) respectively. The contaminated gases were collected through

stainless tubing and allowed to pass through the catalytic column reactor placed inside a tube furnace (11) having 45 cm long and 3.5 cm diameter isothermal zone, (model: MTF 12/38/400) equipped with temperature controller type 201 and manufactured by Carbolite® for the catalytic degradation in the presence of hydrogen / oxygen added at (12). The contaminated gas inflow and outflow sampling ports are located at 13 and 14 respectively.

3.2 Materials used

The compounds of interest were the chlorinated aliphatic, aromatic and polycyclic aromatic and ether compounds. Details of the compounds are given in the chapter 4 to chapter 6.

For the catalytic destruction of the gas phase chlorinated aliphatic and ether compounds, 2.5 g of palladium catalyst coated on spherical sized alumina (3 mm diameter) with a bulk density of about 0.5 kg/l and palladium loading of 0.5% was packed on a stainless steel column (figure 3.2).

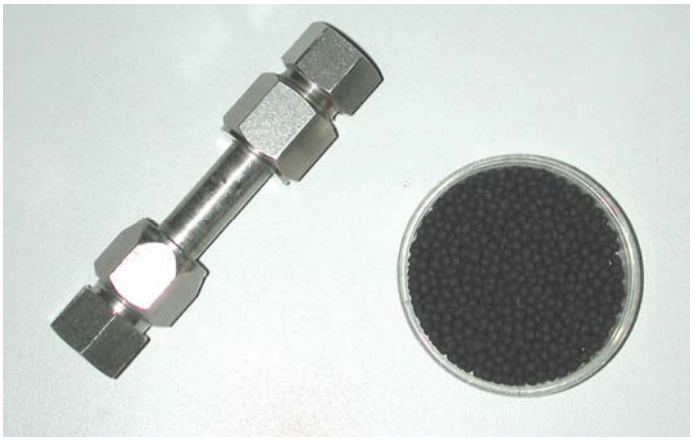

Fig. 3.2: Palladium on alumina catalysts and the column used for the catalytic degradation of the chlorinated aliphatic and the ether compounds.

3.3 Standard solutions

Concentrated standards, stock solution of 10 g/l in methanol, of 1,1-DCE, PCE, TCE, cis-1,2-DCE, 1,2-DCA and 1,1,2,2-TCA were prepared taking 1 gram of each aliphatic compound. For aromatic compounds standard solutions of 10 g/l for MTBE, Toluene and Chlorobenzene, 5 g/l for 1,2-DCB and 1,4-DCB, and 1 g/l for Naphthalene were also prepared in 100 ml vials. In case of aromatic compounds internal standards were used to correct variations of the injection volume and fluctuations in the ionization efficiency of the mass spectrometer. Toluene d8 (100 µg/ml in methanol) was added with MTBE, Toluene and Chlorobenzene, and 1,2-DCB d4 (240 µg/ml in methanol) was added with 1,2-DCB, 1,4-DCB

and Naphthalene. Both the standards and internal standards were preserved in the fridge at 4^{o}C temperature.

3.4 Sample preparation

For aliphatic compounds about 25 to 30 liters of water were taken in a teflon bag and then the necessary amount of standard of chlorinated aliphatic compounds was added to achieve a concentration of 10 mg/l. Then the sample was placed on a shaker for about 12 hours before starting experiments. For aromatic and ether compounds, a similar procedure was followed but concentrations of 10 mg/l for MTBE, Toluene and Chlorobenzene, 5 mg/l for 1,2-DCB and 1,4-DCB, and 1 mg/l for Naphthalene were selected.

3.5 Analytical techniques

3.5.1 Sampling

The instrumental set up was previously described (section 3.1). During operation contaminated water was pumped and allowed to pass through the shell side (outside) of the hollow fibers. The strip gas was applied on the lumen side (inside) of the hollow fibers in counter flow. In the most of the cases, nitrogen was used as the strip gas, instead of ambient air, to prevent oxygen from entering into the system and thus minimizing the risk of precipitations of e.g. iron or manganese oxides, as contaminated aquifer systems are in general anoxic. However, during the catalytic oxidation of the gas phase ether compounds air was used as striping gas.

Different settings for gas flow, water flow and vacuum were used in different experiments in order to show the performance of the membrane module under those conditions.

Before collecting the first sample, the instrument was run for 30 minutes in the case of aliphatic and around 1 hour 30 minutes in the case of aromatic and polycyclic aromatic hydrocarbons in order to avoid the effect of sorption of some compounds in the system. Then for the following each sample a ten-minute run interval was chosen, except in some cases where a thirty-minute interval was taken into consideration to minimize the sorption effect of Naphthalene specifically.

For every set up, 2.5 ml of inflowing and outflowing water samples were collected in a 5 ml glass syringe. Moreover, in the case of aromatic and polycyclic aromatic hydrocarbons, 2.5 μl of Toluene d8 and 2.5 μl of 1,2-Dichlorobenzene internal standard were added. Before analysing in GC-FID, GC-Varian or GC-MS, a headspace of 2.5 ml was created in the syringe. To achieve equilibrium conditions between the water phase and the gas phase, the

syringe was shaken for 10 minutes in the case of aliphatic compounds and for 25 minutes in the case of aromatic and polycyclic aromatic compounds.

The contaminated strip gas was collected through stainless steel tubing and was allowed to pass through catalytic reactor bed for gas phase degradation of the contaminants. For the analysis of the gas phase contaminants the gas samples were directly collected from the ports shown on the figure 3.1.

3.5.2 GC analyses

During the removal of contaminants from water to gas phase, for the detection of the aliphatic compounds, gas chromatographic analyses using a flame ionisation detector (FID) and for aromatic compounds gas chromatography coupled with mass spectrometric detector were used. During the catalytic degradation study, for the detection of chlorinated aliphatic and ether compounds, GC-Varian 3800 coupled with both FID and TCD was also used.

In all the cases, samples from headspace (gas phase) were taken using a 250 μl gas-tight, valve-locking micro-syringe (VICI, A-2, 250 μl, RN). Parameters for analysing the different compounds by GC-FID and GC-MS are listed in the table 3.1 to 3.4.

Table 3.1: Parameters for analyses of aliphatic compounds by GC-FID.

GC/FID (Carlo Erba HRGC 5160)				
Injector temperature:	180°C	**Oven (temperature program)**		
FID temperature:	220°C		T_0 = 45°C	t_0 = 3 min
Column		R1 = 2.5°C/min	T_1 = 55°C	t_1 = 4 min
Type:	CP-SIL-13CB	R2 = 30°C/min	T_2 = 160°C	t_2 = 2 min
Film thickness:	1.2			
Inner diameter:	0.32mm	**Carrier gas:**	Nitrogen	
Length:	50m	**Fuel gas:**	Hydrogen	

Table 3.2: Parameters for analyses of aliphatic chlorinated hydrocarbons, C1-C6 hydrocarbons and ether compounds by GC-Varian (FID).

GC-Varian (3800)-FID				
Injector temperature:	200°C	**Oven (temperature program)**		
FID temperature:	220°C		T_0 = 100°C	t_0 = 2 min
Column		R1 = 20°C/min	T_1 = 200°C	t_1 = 2 min
Type:	Alltech AT-Q™			
Film thickness:	50 μm			
Inner diameter:	0.53 mm	**Carrier gas:**	Nitrogen	
Length:	30 m	**Fuel gas:**	Hydrogen	

Table 3.3: Parameters for analyses of aromatic and polycyclic aromatic hydrocarbons by GC-MS.

GC-MS (HP 6890-MSD 5973)				
Detector (MSD 5973 Hewlett Packard**)**		**Column**		
Temperature:	315^{o}C	Type:	DB-5MS (J&W Scientific)	
Injector		Film thickness:	0.25µm	
Temperature:	320^{o}C	Inner diameter:	0.25mm	
Mode:	Pulsed splitless	Length:	30 m	
Pressure:	6.70 psi	**Compound information**		
Pulse pressure:	25 psi	Compound	Target mass(m/z)	Qualifier(m/z)
Gas type:	Helium	Toluene d8	98	100
Oven (temperature program)		MTBE	73	57
Initial Temperature:	50^{o}C	Toluene	91	92
Initial time:	2 min	Chlorobenzene	112	77
Final Temperature:	240^{o}C	1,4-DCB	145	147
Final time:	2 min	1,2-DCB d4	152	115
Increment rate:	30^{o}C	1,2-DCB	145	147
Mode:	SIM	Naphthalene	128	127

Table 3.4: Parameters for analyses of carbondioxide, carbonmonoxide and hydrogen by GC-Varian (TCD).

GC-Varian (3800)-TCD			
Injector temperature:	150^{o}C	**Oven (temperature program)**	
TCD temperature:	220^{o}C	For CO_2 35^{o}C	2 min
Column		For CO 125^{o}c	2 min
Type:	GS-Carbon PLOT	For H_2 50^{o}C	2 min
Film thickness:	3 µm		
Inner diameter:	0.32 mm	**Carrier gas:**	Nitrogen
Length:	30 m	**Fuel gas:**	Hydrogen

Chapter 4

Vacuum assisted removal of volatile to semi volatile organic contaminants from water using hollow fiber membrane contactors- Experimental results and model application

4.1. Introduction

Contamination of groundwater with organic contaminants, especially chlorinated hydrocarbon compounds (CHCs) and petroleum hydrocarbons as constituents of gasoline, has become a widespread problem in industrialized countries. The treatment of the contaminated groundwater is in most cases achieved by pumping it through an adsorbent on-site, e.g. granular activated carbon (GAC). The efficiency of such a system can be further increased by air stripping the contaminants, as the sorption capacities of these compounds on GAC are increased out of the gas-phase, due to the minimization or absence of competitive effects of the groundwater itself or other groundwater solutes (Crittenden et al., 1988). Furthermore, alternative destructive treatment options for the gas phase exist, e.g. catalytic oxidation, or reductive catalysis especially for chlorinated compounds (Kopinke et al., 2003)

Packed tower aeration is the most common stripping method, although it has several disadvantages. In general, the method is limited to compounds with dimensionless Henry's law constants larger than 0.01. However, for the low Henry's law constants compounds, high strip-gas to water ratios (> 100:1) are necessary to achieve reasonable stripping efficiencies. This requires large strip-towers and the high gas flow makes any off gas treatment expensive.

An alternative approach is the use of polypropylene hollow fiber membrane modules (HFM), that are routinely used for the degassing of process waters e.g. in the electronics industry or for the deaeration of bottled beverages. These units provide a large surface area for mass transfer and enable an independent control of gas and liquid flow rates without the risk of flooding. Volume specific overall mass transfer coefficients for HFM stripping have been reported to be an order of magnitude higher compared to packed tower stripping, and therefore much lower strip-gas to water flow ratios are needed for an effective stripping (Zander et al., 1989).

Since an early study by Semmens et al. (1989), several studies investigated the potential of HFM modules to remove volatile organic contaminants (VOCs) from water. HFM modules have been applied on a laboratory scale to remove e.g. chlorinated and brominated

hydrocarbons (Zander et al., 1989) chloroform and toluene (Mahmud et al., 2000; Mahmud et al., 2002; Mahmud et al., 2004) or MTBE (Keller and Bierwagen, 2001) from water.

The use of vacuum on the gas side of the modules to assist the stripping process has not been considered in most of these studies. The reason is, that for volatile to semi-volatile compounds and the normal operating range of gas and water flow rates it was found, that the overall mass transfer is in general dominated by the liquid side, as the diffusivities of the compounds in the water phase are about 4 orders of magnitude lower compared to the gas phase diffusivities (Semmens et al., 1989). A normal operating range is hereby considered when gas flow rates are at least ten times or several tenth of the water flow rates. Bierwagen and Keller (2001) e.g. applied gas flow to water flow ratios between about 10 and 100 to remove MTBE from water and found no significant effect in applying a moderate vacuum on the gas side of 0.8 atm and 0.5 atm, respectively. In their study, however, vacuum and gas flow could not be regulated independently and the lower vacuum corresponded to a lower gas flow.

However, especially for low gas flow to water flow ratios and compounds with low Henry's law constants, vacuum can potentially be used to enhance stripping efficiencies or to decrease the volume of strip gas that has to be treated. In this study, a Liqui-Cel© extra flow (gas on lumen side, water on shell side, central baffle) polypropylene hollow fiber membrane module was operated in laboratory experiments under various water flow, gas flow, and pressure conditions to demonstrate its effectiveness for the removal of 12 different organic contaminants from the aqueous phase under low gas flow to water flow ratios. The contaminants used were chlorinated and non-chlorinated aromatic as well as aliphatic compounds representing a range of Henry's law constants of two orders of magnitude.

4.2. Materials and methods

4.2.1 Membrane module

For all experiments, a Liqui-Cel© 2.5" x 8" extra flow hollow fiber membrane module with X-50 type fibers was used. The module contains thousands of microporous polypropylene hollow fibers knitted into an array that is wound around a distribution tube and a central baffle. This extra flow design is used in most of Liqui-Cel's bigger modules relevant for water treatment.

During operation, the contaminated water enters the module at one side and flows over the shell side (outside of the hollow fibers) to the outlet on the other side. The strip gas is applied

on the lumen side (inside of the hollow fibers) in counter flow. The main characteristics of the module are summarized in Table 4.1.

Table 4.1: Characteristics of the Liqui-Cel© extra flow hollow fiber membrane module

Module type[#]	2.5" x 8"	Fiber lengths*	15 cm
Membrane material[#]	Polypropylene	Outer fiber diameter[#]	300 µm
Shell diameter*	6.3 cm	Inner fiber diameter[#]	240 µm
Fiber bundle diameter*	4.7 cm	Fiber wall thickness[#]	30 µm
Distribution tube diameter*	2.2 cm	Fiber porosity[#]	40 %
Void fraction*	0.47 (-)	Pore diameter[#]	0.03 µm
Membrane surface area (outer)[#]	1.4 m^2	Pore tortuosity[§]	2.5 (-)
Effective surface to volume ratio[§]	2930 $m^2\ m^{-3}$	Shell side volume[#]	~ 330 ml
Number of fibers*	9,950	Lumen side volume[#]	~ 90 ml

[#] Supplied by manufacturer; * Schöner et al. (1998); [§] Mahmud et al. (2000)

4.2.2 Chemicals

Module performance was analyzed using a total of 11 different aromatic and aliphatic organic contaminants and methyl *tert*-butyl ether (MTBE). The Henry's law constants of these compounds cover two orders of magnitude. The relevant chemical/physical properties of the compounds are summarized in Table 4.2. All compounds were obtained from Aldrich Co and used as received.

Table 4.2: Chemical/physical properties of the organic compounds used

Compound	***M*** **[g/mol]**	ρ **[g/cm³]**	***V'***[#] **[cm³/mol]**	***H**** **[-]**	D_w[§] **[m²/s]**	D_c[$] **[m²/s]**
1,1-Dichloroethene (1,1-DCE)	97.0	1.21	79.9	1.195	1.15E-09	9.57E-06
Tetrachloroethene (PCE)	165.8	1.62	102.2	0.687	9.92E-10	8.22E-06
Trichloroethene (TCE)	131.5	1.46	90.1	0.397	1.07E-09	8.83E-06
cis-1,2-Dichloroethene (cis-DCE)	97.0	1.28	75.5	0.172	1.19E-09	9.79E-06
1,2-Dichloroethane (1,2-DCA)	99.0	1.26	78.8	0.052	1.16E-09	9.60E-06
1,1,2,2-Tetrachloroethane (TCA)	167.9	1.60	104.9	0.021	9.77E-10	8.12E-06
Toluene (TOL)	92.1	0.87	105.9	0.262	9.72E-10	8.55E-06
Chlorobenzene (CB)	112.6	1.11	101.4	0.148	9.97E-10	8.52E-06
1,4-Dichlorobenzene (1,4-DCB)	147.0	1.24	118.5	0.130	9.10E-10	7.78E-06
1,2-Dichlorobenzene (1,2-DCB)	147.0	1.31	112.2	0.075	9.39E-10	7.97E-06
Naphthalene (NAP)	128.2	1.15	111.4	0.017	9.43E-10	8.08E-06
Methyl *tert*-butyl ether (MTBE)	88.1	0.74	119.1	0.026	9.07E-10	8.16E-06

* at 25°C, Staudinger and Roberts (2001); [§] at 25°C, Hayduk and Laudie (1974); [$] at 25°C, Fuller et al. (1966); [#] Satterfeld (1970).

The aqueous contaminant solutions were prepared by injecting a concentrated methanol stock solution of a single contaminant, or a mixture of contaminants, into deionized and

degassed water stored in 30 liter Teflon© bags. Aqueous concentrations were in general 10 mg/l for MTBE, Toluene (TOL), Chlorobenzene (CB) and the aliphatic compounds, 5mg/l for 1,2-dichlorobenzene (1,2-DCB) and 1,4-dichlorobenzene (1,4-DCB), and 1 mg/l for naphthalene (NAP).

Concentrations in the mg/l range can be frequently found for these compounds in contaminated groundwaters. Also, these concentrations allowed to measure removal efficiencies of at least 99% (C_{out}/C_{in} < 0.01) without reaching the detection limit of the analytical method.

4.2.3 Experimental setup

The experimental set up is shown in figure 4.1. During an experiment, contaminated water was pumped through the membrane module from the bottom while nitrogen as the strip gas was swept through the module from the top. The set up allowed to adjust the three key operation parameters (water flow rate, gas flow rate, pressure), that all influence the stripping efficiency, independently.

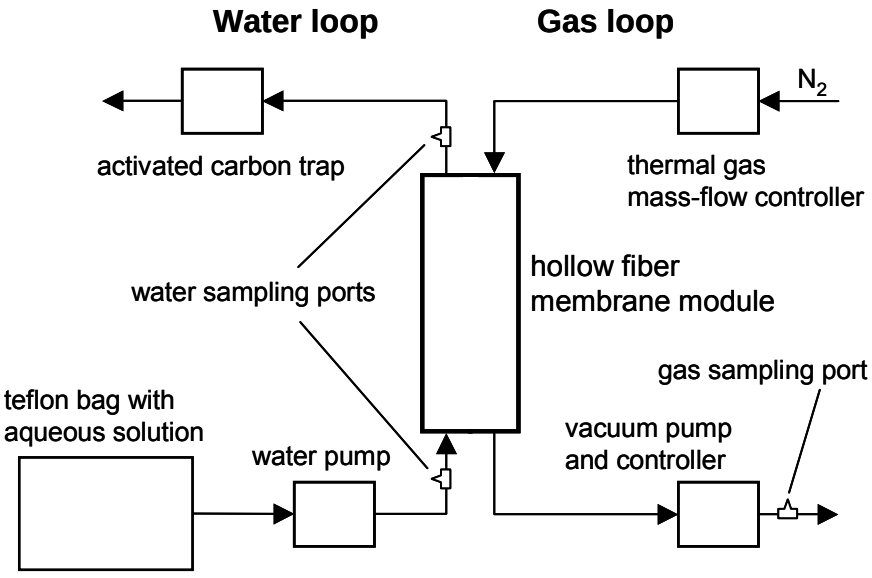

Fig.4.1: Experimental set up.

This was achieved for the water loop by using an Ismatec© BVP-Z gear pump, and for the gas loop by using a Bronkhorst© F-201C thermal gas mass-flow controller and a Vaccubrand© MD4 VARIO diaphragm pump with vacuum controller. Water flow rates were varied between 0.2 l/min and 1.3 l/min and gas flow rates between 0.4 l/min and 6.5 l/min. The pressure was varied between ambient conditions and 0.035 atm. In general, the module

was operated for several hours at a time. No dependency of the removal efficiencies on the operation time and no water breakthrough was observed during this time periods even at the lowest pressure setting.

For performance monitoring during an experiment, 2.5 ml of aqueous samples were collected from the inflow and the outflow of the membrane module using 5 ml glass syringes with septum locks. An internal standard was injected through the septum and 2.5 ml of additional headspace was created by temporarily loosening the septum and withdrawing the plunger. For the analysis of concentrations of the organic compounds, the headspace of the 5 ml syringes was sampled after equilibration using gas-tight syringes (Schüth et al., 2000). For the detection of the aliphatic compounds, the gas phase was injected into a Carlo Erba HR-GC (Model 5160) equipped with a CP-SIL-13CB capillary column and an electron capture detector (ECD) in series with a flame ionization detector (FID). Aromatic compounds were analyzed using a GC-MS (HP 6890 with MSD 5973) with a DB-5MS capillary column.

For mass balance considerations, the strip gas was sampled at a sampling port at the outlet of the vacuum pump using gas-tight syringes. The sampled gas phase was analyzed as described above.

4.3. Results and discussion

As the removal efficiencies for a total of 12 compounds under various operation conditions were studied, in general experiments were performed using a mixture of several compounds. In figure 4.2 the removal efficiencies for 1,1-DCE, cis-DCE and TCA, covering the range of Henry's law constants of all 12 compounds (Table 4.2), out of a mixture of the six aliphatic compounds and as the single compounds, are compared. Over the range of water flow rates studied (0.2 l/min – 1.3 l/min), removal efficiencies are identical within reproducibility limits. That indicates, that at least for the concentrations used (10 mg/l for each compound), the mixture does not influence the removal of a single compound. Therefore, results of the experiments using contaminant mixtures represent also the efficiency of the HFM module for a single compound. Changes in the water flow rate influence directly the residence time of the water in the HFM module, leading to better removal efficiencies for lower flow rates. This can be seen in figure 4.3, where the removal efficiencies for all compounds are shown for different water flow rates, and are plotted against the Henry's law constants. In these experiments, the strip gas flow was also increased to keep a constant ratio between the water flow and the strip gas flow, while the pressure was kept constant at 0.2 atm. It can also be seen, that removal efficiencies are a function of the Henry's law constants of the compounds, with increasing efficiencies with an increase in the Henry's law constants.

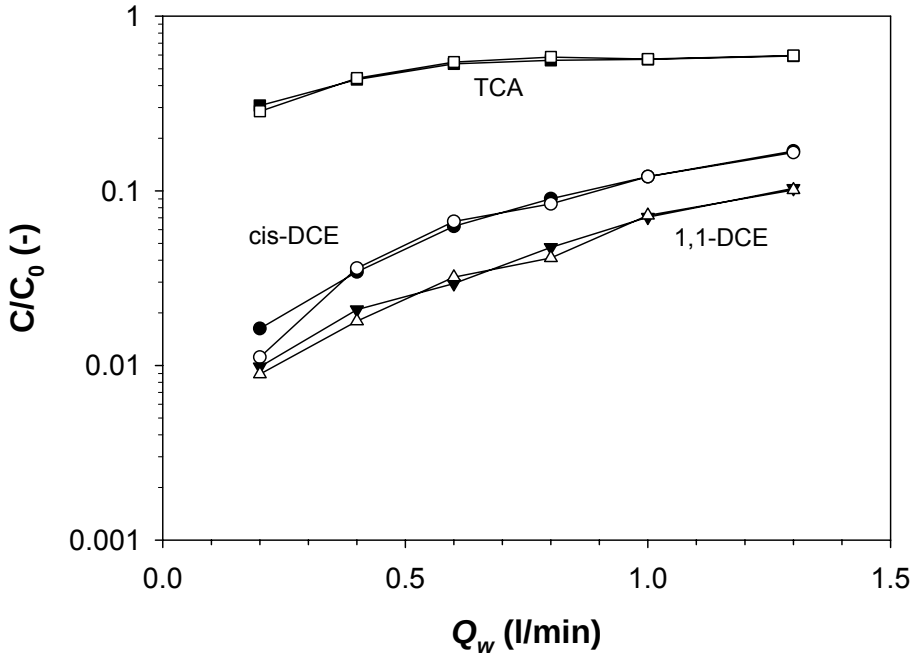

Fig.4.2: Removal efficiencies for aqueous solutions of a single aliphatic compound (open symbols), and for the compound out of a mixture of 6 aliphatic compounds (solid symbols). Concentration for each compound 10 mg/l. Strip gas flow 5x water flow, pressure 0.2 atm.

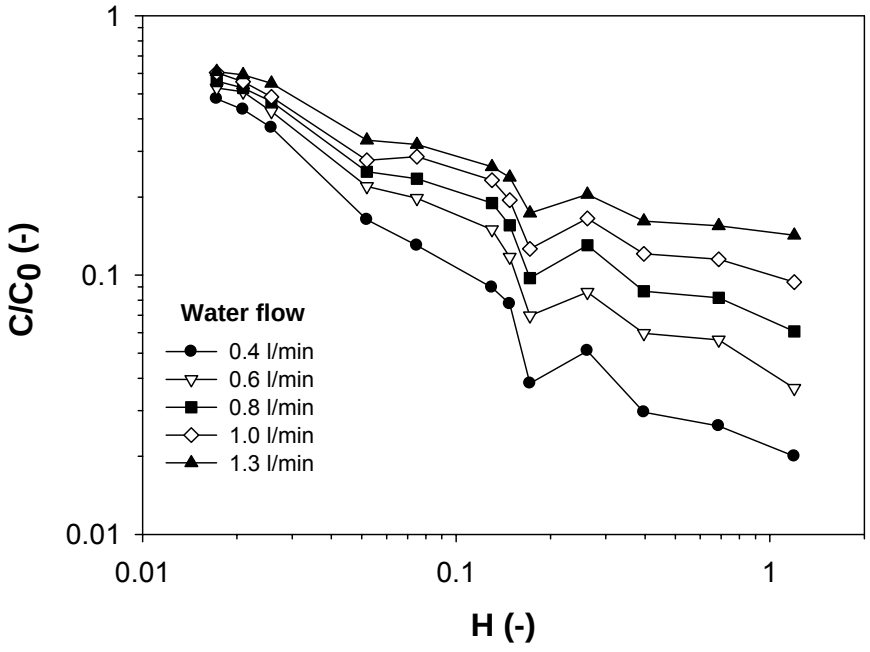

Fig.4.3: Dependency of removal efficiencies on the water flow rate. Strip gas flow 5x water flow, pressure 0.2 atm.

One major advantage of HFM modules is the fact, that vacuum can be used to either enhance the stripping efficiencies, or to decrease the volume of contaminated strip gas that has to be treated. Normalized to the pressure P (atm), the strip gas to water ratio $R_{a/w}$ (-) can be defined as:

$$R_{a/w} = \frac{Q_a}{P\,Q_w} \tag{46}$$

where Q_a and Q_w are the feed flows (m³/s) for strip gas and water, respectively. In the first set of experiments, the pressure was gradually decreased from ambient pressure to 0.035 bar while leaving Q_a and Q_w constant at 0.5 l/min, each. That results in $R_{a/w}$ values from 1 to 28.6. In figure 4.4 the removal efficiencies for six selected compounds for the various $R_{a/w}$ settings are shown. By applying vacuum (increasing $R_{a/w}$), the removal efficiencies can be greatly increased without increasing the volume of strip gas that has to be treated.

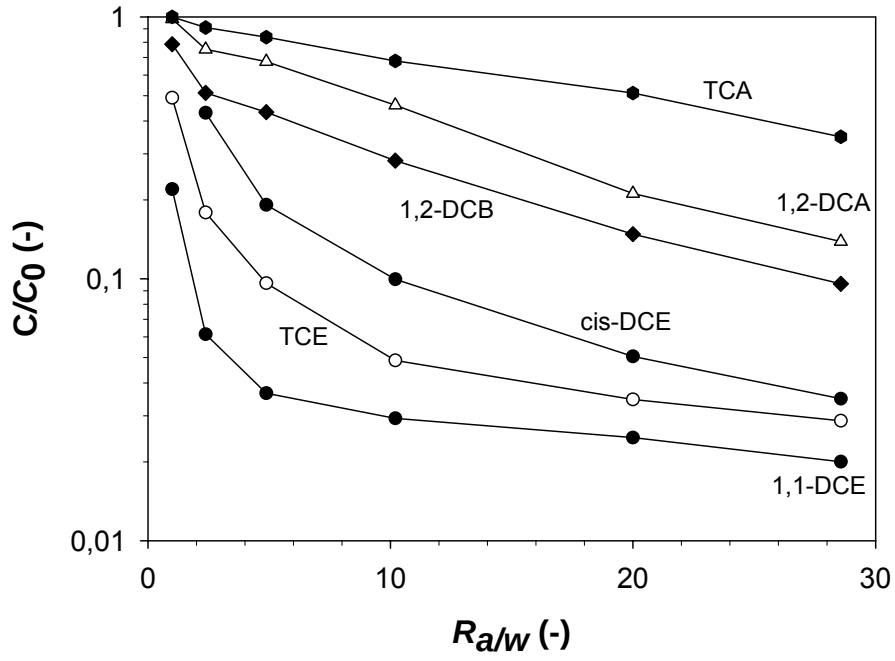

Fig.4.4: Dependency of removal efficiencies on the pressure. In all cases water flow rates and gas flow rates 0.5 l/min. The pressure was gradually decreased from ambient conditions to 0.035 atm, resulting in $R_{a/w}$ ratios from 1 to 28.5.

It is also evident from eq. 46, that by decreasing the pressure *(P)* on the gas side of the module, the gas flow Q_a can be decreased without changing $R_{a/w}$. To show this effect, a series of experiments was conducted, where the pressure was gradually decreased but $R_{a/w}$ was maintained constant at a value of 20 by decreasing the strip gas flow, Q_a, accordingly. The water flow was kept constant at 0.4 l/min. Figure 4.5 shows the results for gas flows of 2.0, 0.8, and 0.4 l/min with pressure settings of 0.25, 0.1, and 0.05 atm, respectively. For all

compounds investigated, the removal efficiencies were constant within reproducibility limits for the three different settings. This indicates the importance of the strip gas to water ratio $R_{a/w}$ while, at least for the setting used here, the absolute values for Q_a and P have no significant influence on the removal efficiencies. At the lowest pressure setting (0.05 atm), a ratio of 1 between the feed flows of strip gas and water is sufficient to achieve an about 50 % contaminant removal even for NAP and TCA with Henry's law constants of 0.017 and 0.021, respectively. Vacuum can therefore be also effectively used to decrease the volume of contaminated off gas that has to be treated, without sacrificing efficiency. At least for the pressure settings used here, no negative effects of low pressures, e.g. decreasing efficiencies due to a partial or complete wetting of the membrane pores (Malek et al., 1997) were observed.

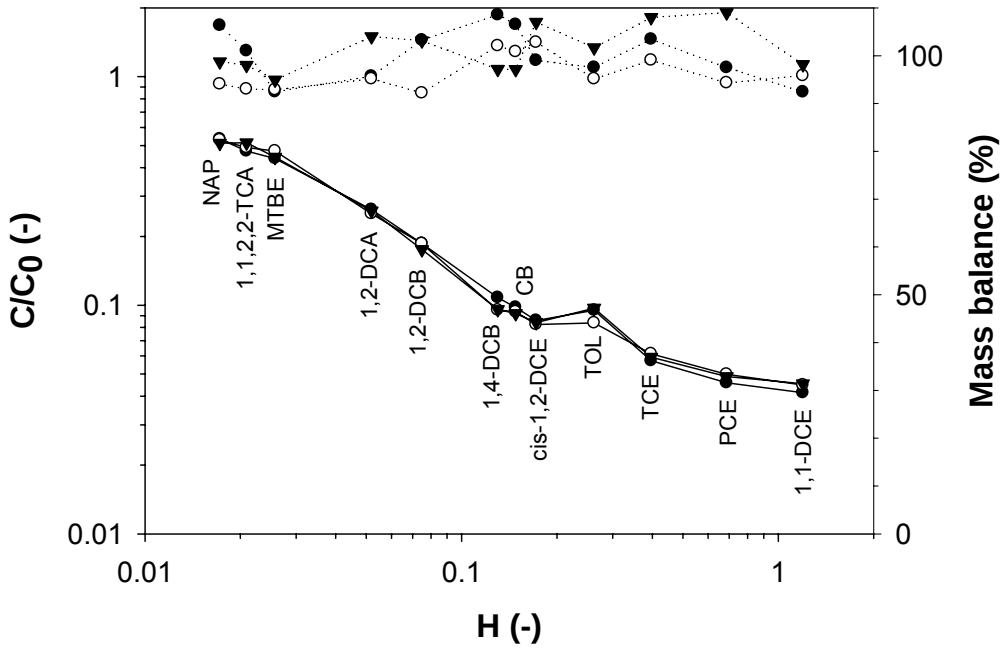

Fig.4.5: Removal efficiencies for the 12 compounds using three different experimental conditions (water flow rate constant at 0.4 l/min, gas flow and pressure combinations of 2.0 l/min and 0.25 atm (open circles), 0.8 l/min and 0.1 atm (solid circles), 0.4 l/min and 0.05 atm (solid triangles) respectively, resembling constant $R_{a/w}$ ratios of 20, and corresponding mass balances (symbols with dotted lines).

Again, figure 4.5 shows also very clearly the dependency of the removal efficiencies on the Henry's law constant. Compared to H, the molecular structure (aromatic or aliphatic) and the polarity of the molecule seem to not significantly influence the efficiencies. This is most obvious when comparing the results for NAP and MTBE. Having similar Henry's law constants (0.017 and 0.026, resp.) the removal efficiencies are also very similar, despite having very different polarities, as can be deduced from their water solubilities (30 mg/l for

NAP; 48 g/l for MTBE). This indicates that the membrane has no selectivity and has no impact on the partition coefficients, and the differences in the removal efficiencies for the different compounds are solely dependant on their Henry's law constants. Figure 4.5 also shows the mass balances based on the analysis of the inflowing water, the outflowing water and the strip gas. Mass balances were in general between 92 % and 109 %.

4.3.1 Theoretical vs. experimental overall mass transfer coefficient *K*

The strong dependency of the removal efficiencies on the Henry's law constants indicates that for most operation conditions used here there is a substantial mass transfer resistance in the membrane or in the gas phase. Therefore, the overall mass transfer coefficient *K* varies along the length of the module as the gas phase concentrations of the stripped compounds approach equilibrium. In most studies where high gas-flow rates are used, however, a negligible gas phase concentration is assumed to calculate *K* from the experimental results, based on a simple exponential function (Keller and Bierwagen, 2001; Aptel and Semmens, 1996; Reed et al., 1995):

$$\frac{C_{out}}{C_{in}} = e^{-K\frac{a\,L}{V_W}} \tag{47}$$

where C_{in} (mg/l) is the inflow aqueous concentration of the compound of interest, C_{out} (mg/l) is the outflow aqueous concentration, *L* the length of the fiber (m) and *a* the effective surface to volume ratio of the membrane module (m^2/m^3). Using eq. 47 to calculate *K* for our experiments would therefore lead to an averaged mass transfer coefficient *K* along the module length.

Theoretically, *K* can also be predicted based on the resistances in series model (eq. 3) by calculating the individual mass transfer coefficients k_L, k_m and k_a using the properties of the HFM module (Table 4.1) and considering the experimental conditions. However, using either eqs. 3, 8 and 9, or a dimensionless expression for k_L (eq. 6) together with eqs. 8, and 9, the calculated *K* values substantially deviate from the experimental values (figure 4.6).

As the Graetz numbers (eq. 10) in our experiments for gas flow on the lumen side were between 0.00044 and 0.206 (-) and therefore well below the applicability range of the Lévéque equation, the modified Lévéque equation (eq. 11) developed by Mahmud et al. (2004) was also used instead of eq. 9 to calculate the lumen side mass transfer coefficient k_a. Although the modified Lévéque equation produces slightly higher *K* values in the range of low mass transfer coefficients, this does not significantly improve the correlation between calculated and experimental mass transfer coefficients. Specifically, as can be seen in figure

4.6, calculated *K* values are very similar for all experiments, while the *K* values observed in the experiments showed a strong and positive dependence on the Henry's law constants.

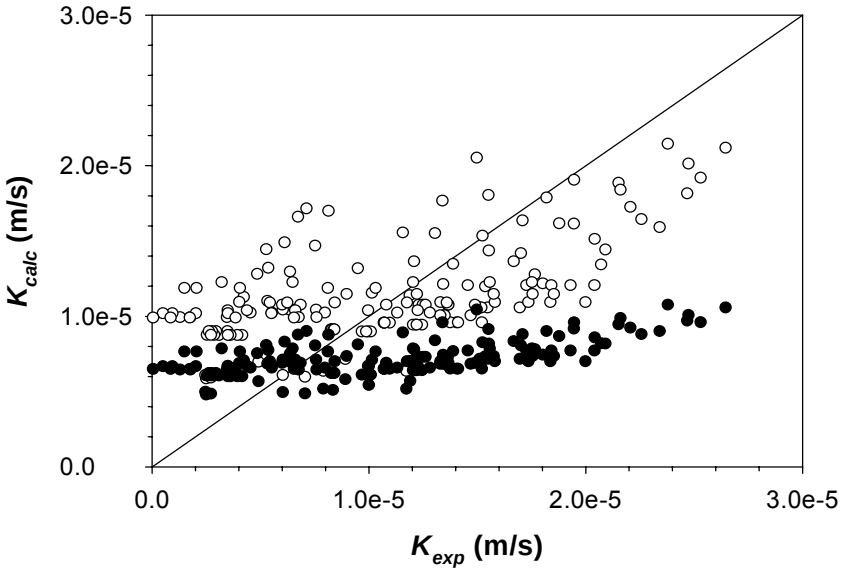

Fig.4.6: Calculated overall mass transfer coefficients *K vs*. experimental *K*. Calculations based on eqs. 3, 8, and 9 (open symbols), and eqs. 6, 8 and 9 (solid symbols).

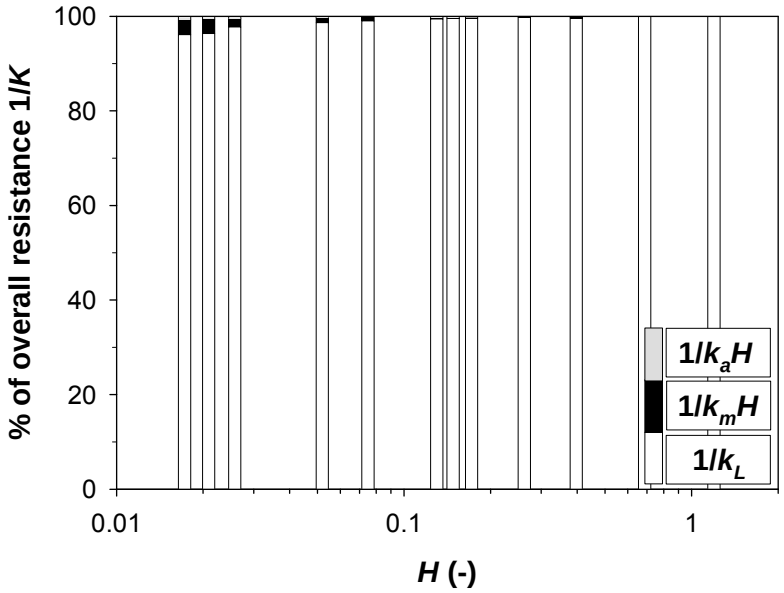

Fig.4.7: Theoretical normalized contributions of the liquid phase ($1/k_L$), membrane ($1/k_mH$), and gas phase ($1/k_aH$) resistances on the overall resistance using eqs. 3, 8, and 9, and settings of 0.4 l/min, 2.0 l/min, and 0.25 atm for the water flow, gas flow and pressure, respectively.

The reason for the poor agreement between experimental K and theoretical K is evident when comparing the theoretical contributions of the liquid phase ($1/k_L$), membrane ($1/k_M H$), and gas phase resistances ($1/k_a H$) on the overall mass transfer resistance ($1/K$). Using again eqs. 3, 8, and 9, and the previously used settings of 0.4 l/min, 2.0 l/min, and 0.25 atm for the water flow, gas flow and pressure, respectively (figure 4.5), the theoretical contributions of the liquid phase, membrane, and gas phase resistances can be calculated. In figure 4.7 the normalized individual contributions of the three resistances on the overall resistance are shown. It is evident, that using this set of equations, for all compounds the liquid phase mass transfer resistance is by far the most important resistance while the other two resistances are negligible. As the aqueous diffusivities, the only variable in eq. 3, are very similar for all compounds, $1/k_L$ values, and consequently also $1/K$ values, for all compounds are very similar. Therefore, the dependency of the observed removal efficiencies and mass transfer coefficients on the Henry's law constants can not be explained using the set of equations, as changes in H have only a minor effect on the calculated K values.

The reason for the failure of the resistance in series model to match the experimental results is unclear. It might stem from the extra flow design of the module that may cause an enhanced mixing in the water phase resulting in less resistance on the water side.

Due to the failure of the resistance in series model to describe mass transfer in HFM modules the following two different modeling approaches are proposed:

(i) Modification of the resistance in series model
(ii) A hybrid numerical-analytical modeling approach

4.3.1.1. Modification of the resistance in series model

As the liquid phase mass transfer resistance seemed to be overestimated using eq. 3, and the experimental results showed the significant influence of H on the removal efficiencies, equation 3 and 9 were modified to achieve a better correlation between the experimental and calculated mass transfer coefficients. Eq. 8 for the membrane mass transfer was unchanged as it contains no variables besides the effective diffusion coefficient.

For fitting, first the contribution of the liquid phase mass transfer resistance was decreased by lowering the multiplier in eq. 3. Then, the equation for the mass transfer resistance for the gas phase (eq. 9) was modified. Fitting of the modified equations to the data was done by trial and error minimizing the sum of weighted squared errors between calculated and experimental mass transfer coefficients. The resulting modified equations were:

$$\frac{1}{k_L} = 0.213 \left(\frac{L\, d_h}{V_w\, D_w^2} \right)^{0.33} \tag{48}$$

for the liquid phase mass transfer resistance, and:

$$\frac{1}{K_a H} = \frac{0.617}{H} \left(L\, d_i \right)^{0.33} \left(\frac{1}{V_a\, D_c^2} \right)^{0.56} \tag{49}$$

for the gas phase mass transfer resistance. With this two modified equations and equation 9, a good correlation between experimental and calculated mass transfer coefficients was obtained (figure 4.8). It has to be noted, that figure 4.8 contains all experimental data obtained in this study, i.e. a total of 177 data points. That includes experiments with 12 different compounds, water flow rates ranging from 0.2 l/min to 1.3 l/min, gas flow rates ranging from 0.4 l/min to 6.5 l/min, and pressures ranging from 0.035 atm. to ambient pressure.

Using eqs. 48 and 49, again the normalized individual contributions of the three resistances on the overall resistance can be calculated (figure 4.9). Especially for the compounds with low Henry's law constants, about 80 % of the overall resistance is now on the gas side and the gas side resistance decreases, as expected, with an increase in Henry's law constants. This behavior is well reflected by the experimental results, were from cis-DCE (H = 0.172) to 1,1-DCE (H = 1.195), removal efficiencies are increasing from 95 % to 97.5 % only (figure 4.3), indicating the decreasing importance of the gas phase resistance.

For eqs. 48 and 49, the shell side and the lumen side mass transfer, also dimensionless correlations between the Sherwood, Reynolds, and Schmidt numbers can be given. For the shellside the correlation can be written as:

$$Sh = 0.63\, Re^{0.33} Sc^{0.33} \tag{50}$$

In the case of the lumen side, the Henry's constant was incorporated into the correlation in order to account for the dependency of the removal efficiencies on this parameter:

$$Sh = 0.0006\, H\, Re^{0.92} Sc^{0.33} \tag{51}$$

Using eqs. 50 and 51 instead of eqs. 48 and 49 results virtually in an identical plot as presented in figure 4.8.

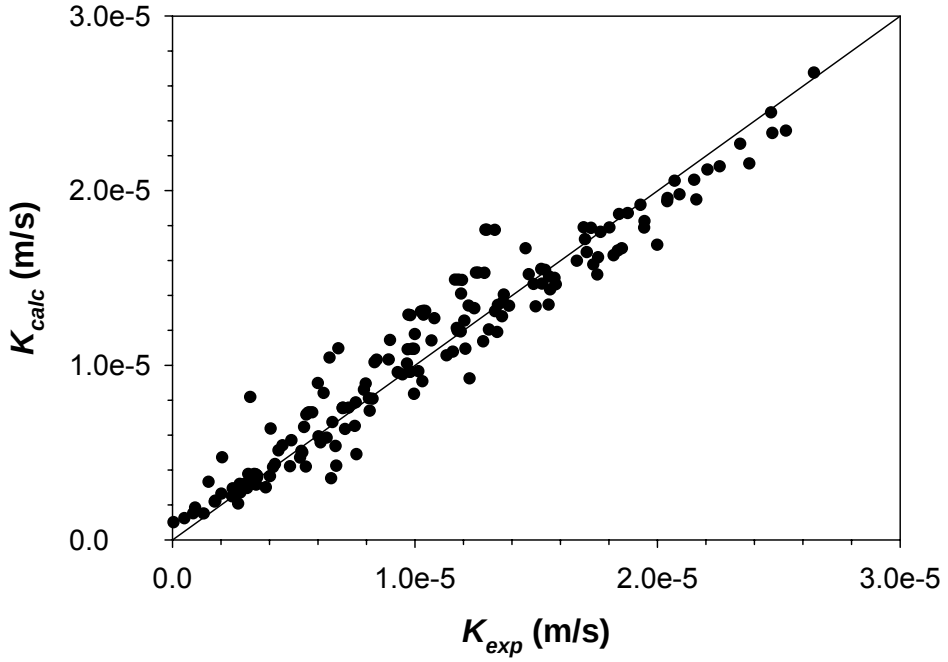

Fig.4.8: Calculated overall mass transfer coefficients *K vs*. experimental *K*. Calculations based on eqs. 8, 48, and 49.

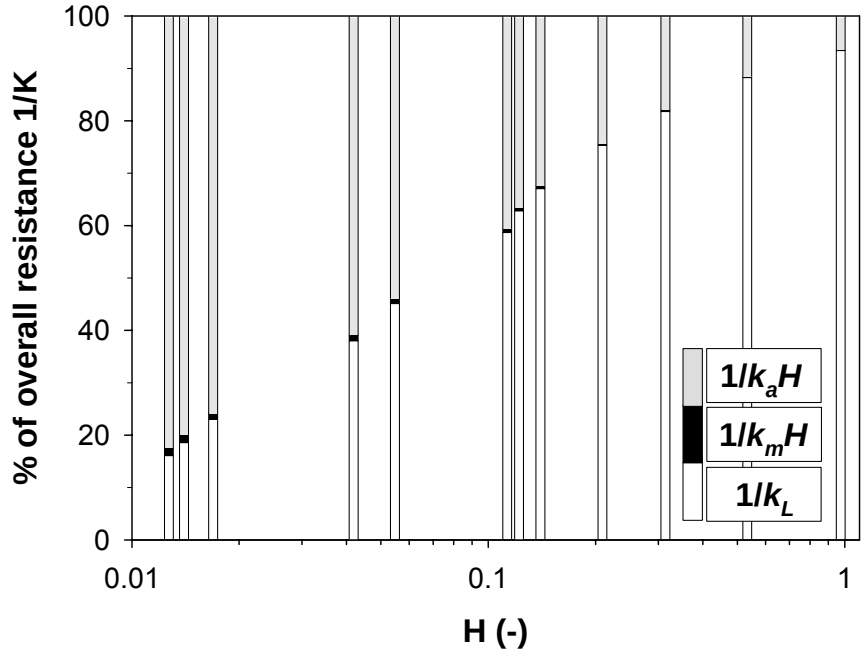

Fig.4.9: Theoretical normalized contributions of the liquid phase ($1/k_L$), membrane ($1/k_mH$), and gas phase ($1/k_aH$) resistances on the overall resistance using eqs. 8, 48 and 49, and settings of 0.4 l/min, 2.0 l/min, and 0.25 atm for the water flow, gas flow and pressure respectively.

4.3.1.2. A hybrid numerical-analytical modeling approach

Typically, high strip gas flow to water flow conditions are chosen to operate HFM modules and under these conditions, mass transfer is in general limited by the liquid phase. However, for a set of recently performed laboratory experiments, the empirically based formulations failed to predict removal efficiencies for a large variety of organic compounds under low strip gas flow to water flow conditions.

To accurately predict removal efficiencies for low strip gas to water ratios, the resistance in series model was modified (4.3.1.1). However, the resistance in series model includes empirical correlations that are lacking a process based background. Therefore, a process based hybrid model was developed in cooperation with the Geohydrology/Geoinformatics group at the Center for Applied Gescience in Tübingen to describe mass transfer in HFM modules. The model applies finite element techniques and analytical source term solutions to define the flow and transport problem (Helmig and Huber, 1998; Helmig and Zielke, 1996; Istok, 1989; Kolditz, 2002). Modeling involved a geometrical simplification of the flow system, the application of the finite element model RockFlow/GeoSys (Kolditz et al., 2005) to solve the hydraulic and mass transport equations mathematically and the inclusion of analytical source terms to describe diffusive flux across the membrane. Input parameters for the model are the geometry of the HFM module (Table 4.1), the diffusion coefficients of the stripped compounds in air and water dependent on temperature and pressure, the tabulated Henry's law coefficients (Table 4.2), and the operation conditions. Details on the model can be found in McDermott et al., (2007).

The model is verified using the data set for the removal of organic contaminants from water by HFM filtration presented in this chapter.

The experimental study showed clearly the dominating influence of the Henry's law constants and the strip gas to water ratios ($R_{a/w}$) on the removal efficiencies (figure 4.3). Therefore, in particular the model responses to variations in these two parameters were compared to the experimental results. Figure 4.10 shows the comparison of the simulations for the dependency of the removal efficiencies on the Henry's law constants with the experimental data for two water flow rates (0.4 l/min and 1.0 l/min).

Although some deviations between simulations and experimental data can be observed, the model captures the general trend of the data very well. Also the simulation results for the dependency of removal efficiencies on the strip gas to water ratios ($R_{a/w}$) are in good agreement with the experimental results (figure 4.11). At low strip gas to water flow ratios the

concentration on the gas side can limit the diffusive flux from the water phase into the gas phase. At high flow ratios the limiting factor is the rate of diffusion from the aqueous side.

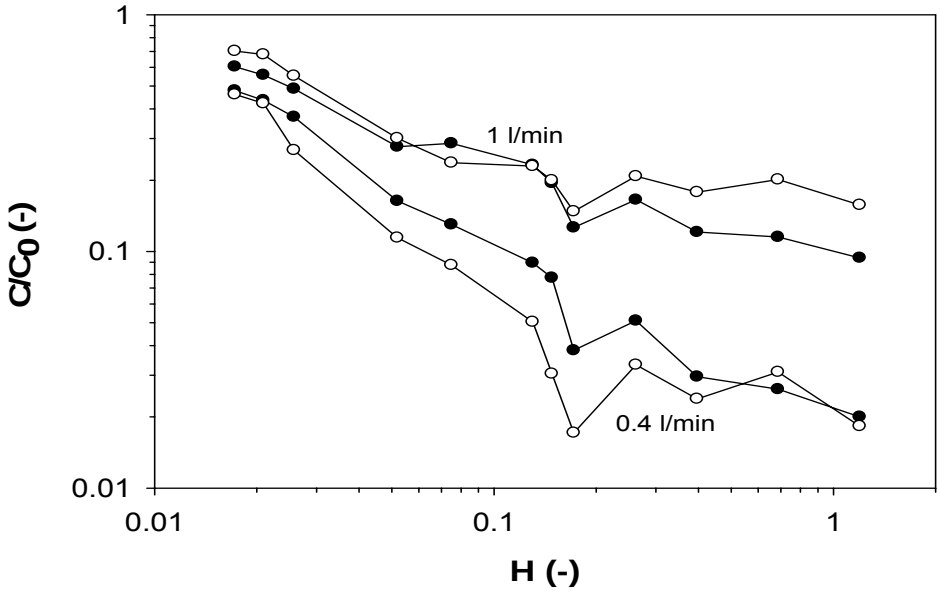

Fig.4.10: Dependency of removal efficiencies on the Henry's law constants and water flow rates. Experimental data - solid symbols, modeling results - open symbols. Strip gas flow 5x water flow, pressure 0.2 atm.

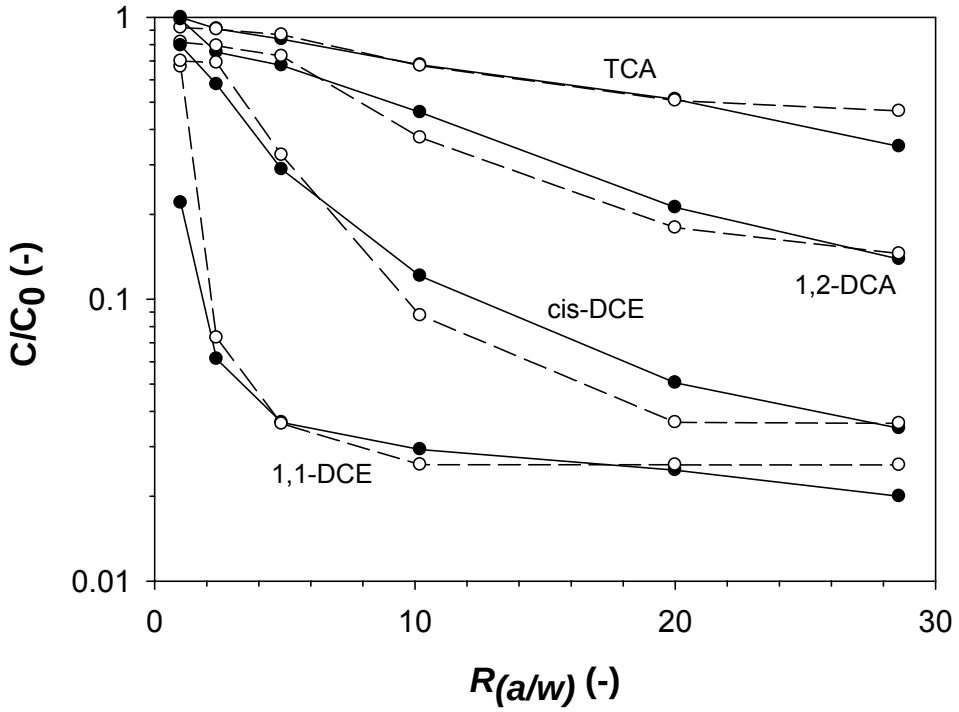

Fig.4.11: Dependency of removal efficiencies on the strip gas to water ratio ($R_{(a/w)}$). Experimental data - solid symbols, modeling results - open symbols. Water flow and gas flow constant at 0.5 l/min. Pressures were decreased from ambient pressure to 0.035 atm.

Once the aqueous phase diffusion limitation has been reached, increasing the flow ratio further has little effect on the rate of removal of the organic compound. The transition from gas-phase limitation to a water phase limitation is dependent on the compounds Henry's law constants with a transition at lower $R_{a/w}$ values for high Henry's law constant compounds (figure 4.11). For the four selected compounds (TCA, 1,2-DCA, cis-DCE, 1,1-DCE), this behaviour is reflected by the experimental data as well as by the modeling results.

Finally all data from the experimental study were modeled using the hybrid numerical-analytical model and the removal efficiencies were compared. In total, 177 simulations were performed and the results are presented in figure 4.12. In general, a very good agreement between model results and experimental data was achieved. The comparative study on the model results calculated using hybrid numerical-analytical model and experimental results under different experimental conditions are presented in appendix 1.1 to 1.2.

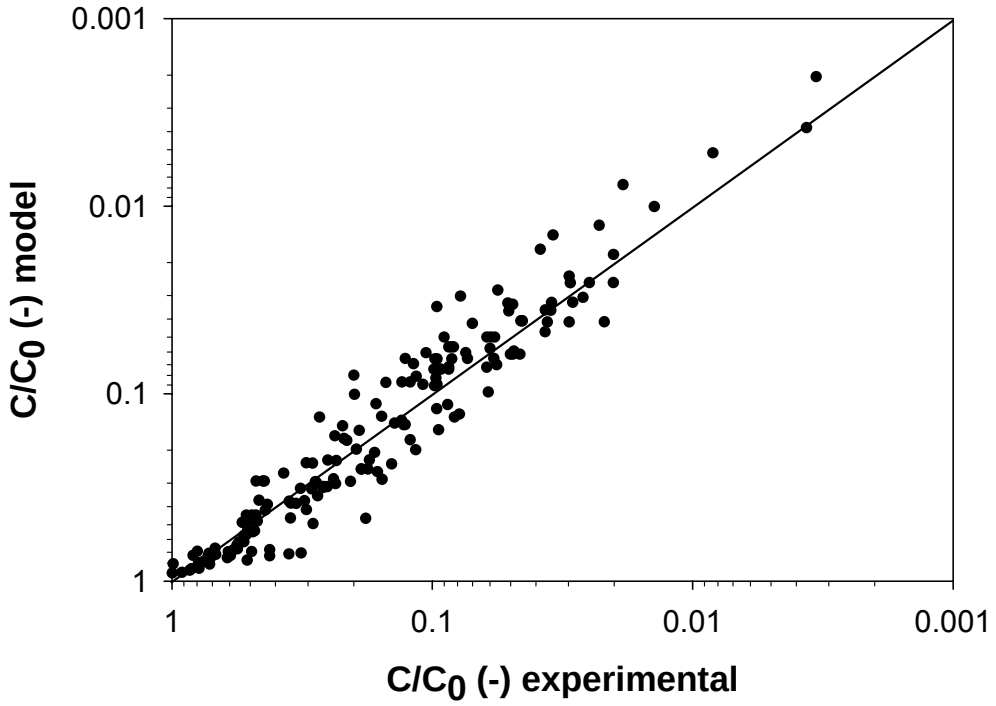

Fig.4.12: Comparison of the experimental removal efficiencies (C/C_0) with the removal efficiencies calculated by the proposed hybrid numerical-analytical model.

4.4. Conclusions

It was shown, that hollow fiber membrane modules could be efficiently used to remove volatile to semi volatile hydrocarbons from aqueous solutions. For the typical operation conditions used here it was found, that removal efficiencies are strongly dependent on the Henry's law constants, indicating a substantial mass transfer resistance on the gas side.

Vacuum can either be used to enhance the stripping efficiencies, or to decrease the volume of contaminated strip gas that has to be treated. In the latter case, contaminant concentrations in the gas phase will be much higher compared to ambient pressure conditions, however, the contaminant fluxes will be the same. This is especially favorable when using e.g. a catalytic conversion of the contaminants in the gas phase, as a catalytic conversion typically follows a first order behavior that is especially efficient at high contaminant concentrations (Kopinke et al., 2003). Also, a sorptive removal, using e.g. activated carbon, of the contaminants from the strip gas is more efficient for high concentrations as in general the contaminant loading on carbonaceous sorbents at breakthrough increases with increasing contaminant concentrations (Kleineidam et al., 2002).

Due to the failure of the resistance in series model to describe mass transfer in HFM modules in the experiments, two alternative modeling approaches are proposed: (i) modifications of the Lévéque equation by finding new dimensionless correlations between the Sherwood, Reynolds, and Schmidt numbers, (ii) development of a hybrid model, applying both numerical and analytical source term solutions to define the flow and transport problem (McDermott et al., 2007).

The modified resistance in series model allowed to predict mass transfer coefficients for a large variety of compounds under various flow and pressure conditions.

The conceptual model of the hybrid approach and the simplified 2D approach is shown to be a valid method to modeling flow and mass transfer where extreme gradients exist. The combination of analytical solutions and the finite element numerical solution coupled over source terms provided a rapid and efficient solution of the mass balance equations. Geometrical considerations, the diffusion coefficients in the various media, and the flow conditions, are enough to describe the operation of the HFM module and the principle processes operating.

Three factors were found to be of particular importance in describing the performance of the HFM module, (i) the Henry's law coefficient, (ii) gaseous diffusion limitations, and, (iii) aqueous diffusion limitations. The Henry's law coefficient controls the size of the concentration gradient across the membrane (Eq. (22) & Eq. (24)). The concentration gradient in turn defines via Fick's law the flux of the organic compound from the water phase into the gas stripping phase.

The model simulated experimental data for a wide range of Henry's coefficients and flow rates well. With this, the model can be used to efficiently design HFM filtration systems and to optimize stripping schemes.

Chapter 5

Catalytic destruction of chlorinated aliphatic contaminants in the gas phase using palladium catalyst

5.1. Introduction

Chlorinated organic compounds (COCs) are considered very dangerous environmental pollutants because of their toxicity and carcinogenic character (Ordóñez et al., 2000). As they are widely used in industry (solvents, extractants, dry-cleaning agents, degreasing agents, etc.) COCs are released into the environment in large quantities (USEPA, 1991).

Catalytic hydrodechlorination via palladium catalysts is an efficient way to destroy COCs in aqueous solution (Schüth et al., 2004; Kopinke, et al., 2003; Schüth and Reinhard, 1998; McNab Jr. and Ruiz, 1998; Schlimm and Heitz, 1996; Schreier abd Reinhard, 1995; Kovenklioglu et al., 1992). However, its application in ground water suffers rapid catalyst deactivation, e.g., by sulfur poisoning and interference with biological processes, such as growth of sulfate-reducing bacteria (Schüth et al., 2004). A promising alternative technique may be the transfer of the organic compounds from the water phase to the gas phase followed by catalytic hydrodechlorination at high temperatures. To transfer the contaminants from aqueous phase to the gas phase, air stripping with the aid of hollow fiber membrane modules can efficiently be used (Zander et al., 1989; Semmens et al, 1989; Mahmud et al., 2000; Mahmud et al., 2002) even for compounds with very low Henry's law constants (Keller and Bierwagen, 2001; Tarafder, 2003; Tarafder et al., 2007).

The gas-phase reaction has several advantages (Kopinke et al., 2003). At higher temperatures (100-350^{o}C), the reaction rate is significantly increased, with the consequence that the fixed-bed reactor is very compact. Even those chlorinated organic compounds (COCs) which are particularly inaccessible to reductive dechlorination in the water phase (e.g. 1,2-dichloroethane) react with adequate rates. Transport limitations in porous catalysts can be avoided due to the high diffusion rates in the gas phase. Finally, it is believed that in the gas phase operation at high temperatures noble metal catalysts are less susceptible to deactivation, especially from biological activities (Hughes, 1984).

The aim of the present study was to dechlorinate gas phase chlorinated aliphatic compounds using commercial palladium catalysts at elevated temperatures. Palladium was selected as the catalyst for the present work because of its broad reactivity for dehalogenation and hydrogenation reactions (Rylander, 1979; Balko et al., 1993; Schüth and Reinhard, 1998). The treatment system utilized H_2 gas as an electron donor in the presence of palladium which

acted as an electron transfer mediator. The overall reaction of hydrodechlorination of COCs can be expressed as follows (Kovenklioglu et al., 1992; Pirkanniemi and Sillanpää 2002):

$$C_xH_yCl_z + zH_2 \rightarrow C_xH_{y+z} + zHCl$$

The catalyst activity was studied at different contact times and temperatures.

5.2. Materials and method

5.2.1 Materials

Catalytic degradation was studied using a total of 7 aliphatic (alkenes and alkanes) chlorinated organic compounds – PCE, TCE, cis-1,2-DCE, 1,1-DCE, 1,1,2,2-TCA, 1,2-DCA and chloroethane. All targeted compounds were obtained from Aldrich Co, methanol, cyclohexane and n-hexane from Merck KgaA, ethane, ethene, methane and acetylene from Matheson Tri-Gas Inc., methane and vinyl chloride (VC) from Scott Specialty Gases, chloromethane from Dr. Ehrenstorfer GmbH and were used as received.

To prepare contaminant solutions, concentrated methanol stock solutions were injected into deionized and degassed water stored in 20 liter Teflon© bags. Aqueous concentrations were in general 10 mg/l which corresponds to 60.3 µmol/l for PCE, 76 µmol/l for TCE, 103.2 µmol/l for cis-1,2-DCE and 1,1-DCE, 59.6 µmol/l for 1,1,2,2-TCA, 101 µmol/l for 1,2-DCA and 155 µmol/l for chloroethane. Air stripping with the help of a hollow fiber membrane module (Liqui-cel extra flow contactors-2.5″ x 8″) was used to transfer the contaminants from aqueous phase to the gaseous phase. Gas phase concentrations after air stripping were measured between 3.66-3.95 µmol/l for 1,1-DCE, 3.47-3.81 µmol/l for cis-1,2-DCE, 2.49-2.51 µmol/l for TCE, 1.59-1.85 µmol/l for PCE, 1.68-1.71 µmol/l for 1,1,2,2-TCA, 1.73-2.16 µmol/l for 1,2-DCA. For all compounds except 1,2-DCA, n-Hexane was used as internal standard. Due to peak overlapping, cyclohexane was used as an internal standard for the experiments with 1,2-DCA.

A spherical (3mm) palladium on alumina catalyst with a palladium loading of 0.5% and a bulk density of 0.5 kg/l was used for all experiments.

5.2.2 Experimental setup and procedure

The experimental setup is illustrated in figure 5.1. During the experiment, contaminated water was pumped through the shell side of the membrane module using an Ismatec© BVP-Z gear pump, whereas the sweep gas nitrogen was flowed in counterflow through the lumen side where a Vaccubrand© MD4 VARIO diaphragm pump with vacuum controller were added to enhance the strip efficiencies. Water flow was varied from 0.05 to 0.055 l/min, gas flow

varied from 0.25 l/min to 2.0 l/min and vacuum pressure was kept constant at 0.2 atm through out the experiments. These combinations allowed water to gas flow ratios ranging between 1:25 to 1:180. Under such circumstances, the transferal of contaminants from water to gas phase was 50-90% for low Henry's law constant compound like 1,1,2,2-TCA (H-0.014) and 95-99% for high Henry's law constant compound such as 1,1-DCE (H-1.0) (Tarafder, 2003; Tarafder et al., 2007).

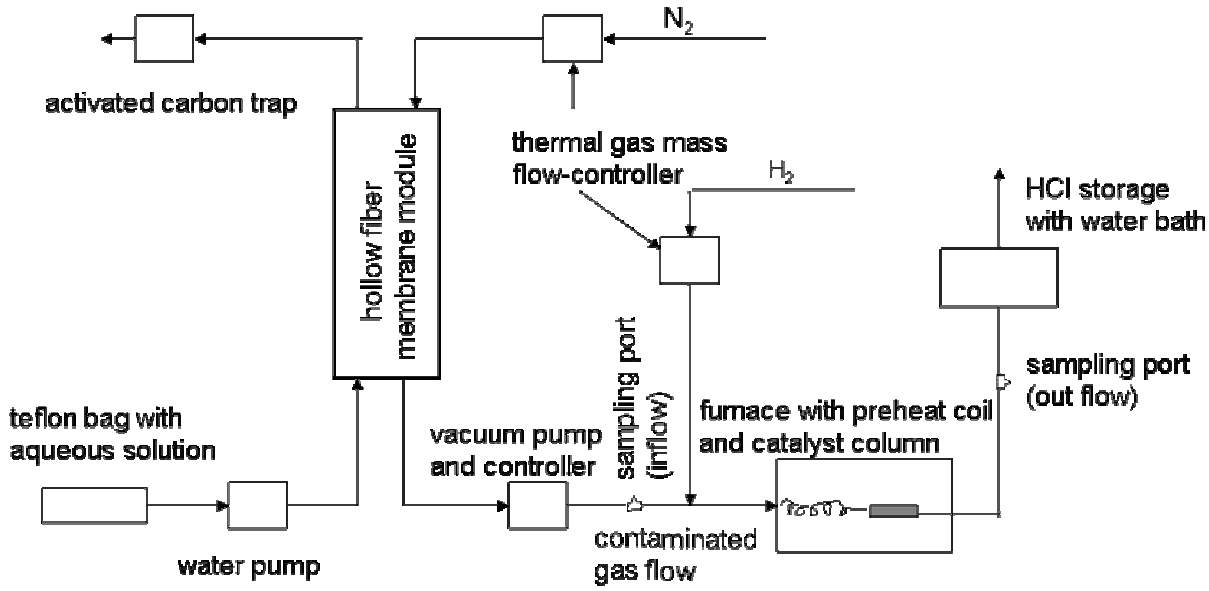

Fig. 5.1: Experimental setup

The contaminants carried by the sweep gas nitrogen were allowed to pass through a catalytic column reactor. The column was made of stainless steel tubing (length 4.7 cm, diameter 1 cm) and was filled with 2.5 g of catalyst. It was placed inside a tube furnace having a 45 cm long and 3.5 cm diameter isothermal zone, (model: MTF 12/38/400) equipped with temperature controller type 201 and manufactured by Carbolite®. Moreover, a preheat coil was added inside the furnace just before the column in order to avoid the sudden cooling down of catalytic bed by the sweep gas at the entrance of the catalytic column, especially during the experiment with high temperatures.

From the vacuum pump to the outflow port, a stainless steel pipe was used to minimize the sorption of the contaminants and to protect itself form heat. Hydrogen gas was added to the contaminated gas before entering into the furnace as well as the catalytic column. Both nitrogen and hydrogen flows were controlled by thermal gas mass-flow controllers (Bronkhorst©, F-201C) and the ratio between hydrogen to nitrogen gas flow varied between 1:25 and 1:200.

5.2.3 Chemical analysis

Gas phase samples were collected from the ports located before and after the catalytic reactor column using gas tight syringes. For the experiments with PCE, TCE, cis-1,2-DCA, 1,1-DCE, 1,2-DCA and chloroethane gas phase samples were injected in a Varian 3800 GC equipped with an Alltech AT-Q^{TM} capillary column (30 m x 0.53 mm i.d) and a FID. For the experiments with 1,1,2,2-TCA, a Carlo Erba HR-GC (Model 5160) equipped with a CP-SIL-13CB capillary column and an electron capture detector (ECD) in series with a flame ionization detector (FID) was used. Products were identified initially by a GC (Hewlett Packard 6890) coupled with a MSD (Hewlett Packard 5972A) and a capillary column DB-624 (length 60 m, ID 0.25 mm, film 1.4 µm) based upon comparison of the full scan spectra with library spectra. For the GC-ECD/FID analyses, standards were injected and identification and quantification of the educts and products was done based on retention times and peak areas.

5.2.4 Data analysis

During data analysis, from the kinetic data overall reaction rate laws were developed by fitting the data of the reaction models. The data were fitted to a first order rate law like equation 40 (Schüth and Reinhard, 1998).

Moreover, the reaction activation energies were calculated. Arrhenius plot, that is a log-linear plot of reaction rate constant (ln k_r) versus $1/T$ (T, temperature in Kelvin), was used to predict the reaction activation energies, which is explained in equations 43 and 44.

Furthermore, the catalyst activities (l/g-min) for the gas phase reaction in the fixed bed reactor at different temperatures and gas flow conditions were calculated after Kopinke et al. (2003) (eqn 45).

5.3. Results and discussion

5.3.1 Decomposition of contaminants over palladium catalysts

The catalytic degradation experiments were conducted at temperatures generally ranging between 50^{o}C to 250^{o}C, for saturated compounds temperatures were increased up to 400^{o}C. The temperatures were increased, in the most cases, with an increment of 50^{o}C.

In the experiments, it was observed that the complete degradation of the targeted compounds was possible**.** As an example, degradation of one chlorinated ethene (TCE) and one chlorinated ethane (1,1,2,2-TCA) are shown in figure 5.2 (A) and figure 5.2 (B) respectively. Data for other compounds are used only to predict the reaction rate constants. The results were within reproducibility limit. A strong dependency of the conversion on both temperatures and contact times was observed. That means that the higher the temperatures and contact times were, the higher the conversion of the chlorinated compounds were.

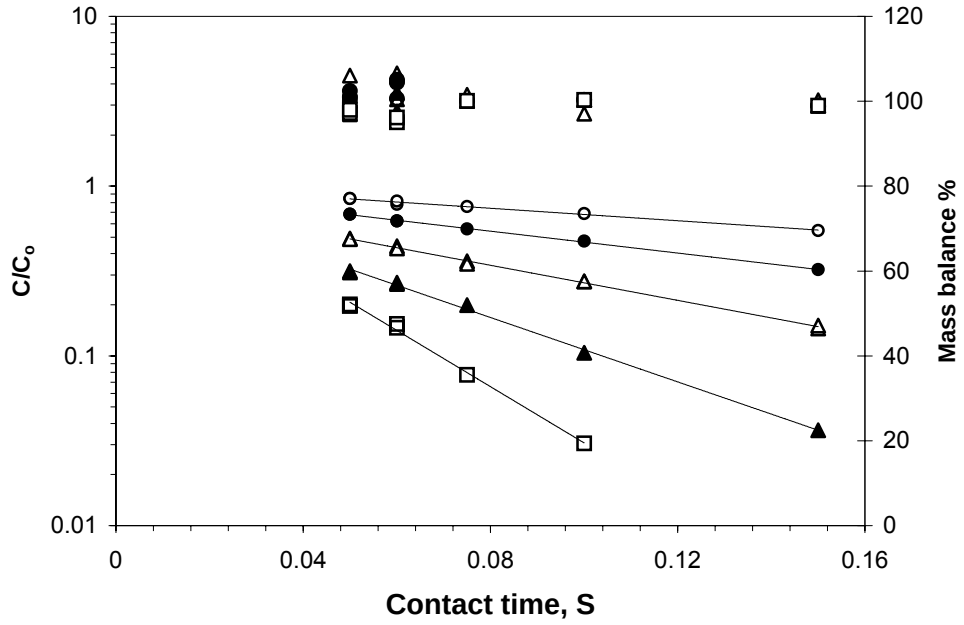

Fig. 5.2 (A): Conversion for TCE under different temperatures and contact times over palladium catalysts. Lines of best fit to the log-transformed normalized concentration versus time (linear regression analysis) were used to estimate compound dependent k_r values (see Table 5.1). Temperature 50^{o}C (open circles), temperature 75^{o}C (solid circles), temperature 100^{o}C (open triangles), temperature 150^{o}C (solid triangles), temperature 200^{o}C (open squares). Mass balances are added on the figure following the right side scale.

The conversion data for 1,1-DCE, PCE, cis-1,2-DCE and 1,2-DCA are presented in Appendix 2.1 and 2.2. The reaction products were ethane and hydrogen chloride (Table 5.3). The product hydrochloric acid is the more likely product, which is not quantified. It is identified from the gas stream passed through water stored in a bottle by measuring the pH of the acidic water. Mass balances were made based on ethane and ethene and were varied between 95% and 107% with an average of 100.36% for 1,1-DCE, 99.22% for cis-1,2-DCE, 100.19% for TCE, 98.89% for PCE, 99.62% for 1,1,2,2-TCA, 98.99% for 1,2-DCA and 99.08% for chloroethane.

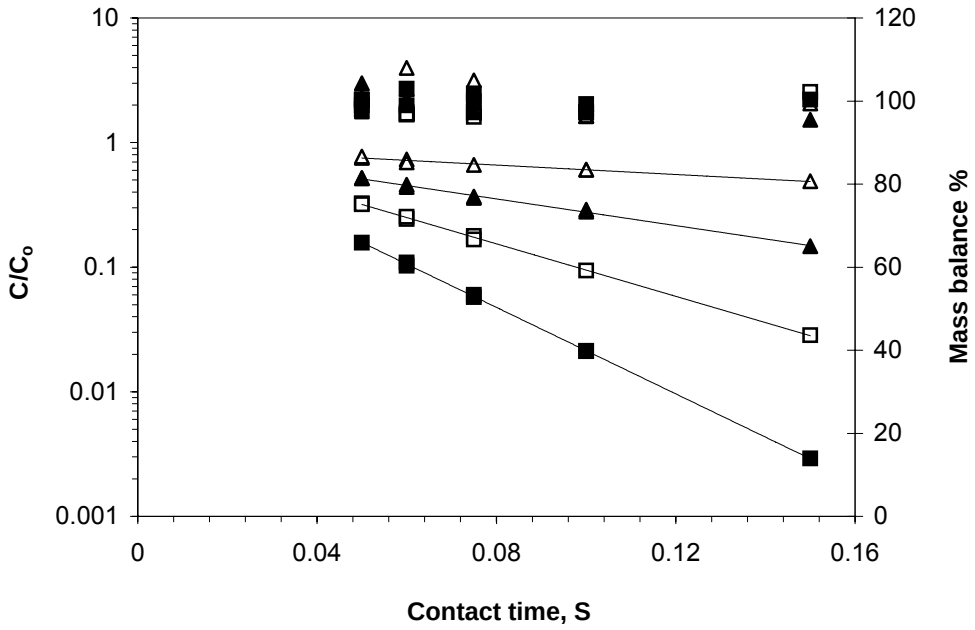

Fig. 5.2 (B): Conversion for 1,1,2,2-TCA under different temperatures and contact times over palladium catalysts. Lines of best fit to the log-transformed normalized concentration versus time (linear regression analysis) were used to estimate compound dependent k_r values (see Table 5.1). Temperature 100°C (open triangles), temperature 150°C (solid triangles), temperature 200°C (open squares) and 250°C (solid squares). Mass balances are added on the figure following the right side scale.

A log-linear plot of normalized concentration C/C_o, where C and C_o are effluent and influent concentrations, versus detention time indicated that the disappearance of the halogenated target compounds were typically first order with respect to the normalized gas phase concentration. The detention time calculated using equation 34 were 0.3, 0.15, 0.1, 0.075, 0.06, 0.05 seconds, which corresponded to the gas flows of 0.5 l/min, 1.0 l/min, 1.5 l/min and 2.0 l/min, 2.5 l/min and 3.0 l/min respectively.

Pseudo-first order reaction rate constants were calculated using a linear regression of the log-transferred data. The rate constants are presented in the Table 5.1. A temperature dependant increase of the rate constants was observed. As expected, if the temperature is increased, the number of collisions in the system will also increase which leads to the more likely combinations of molecules. The reaction will go faster and the rate of the reaction will be higher. Half lives were on the order of second to fraction of a second (0.017 to 0.46 sec).

The catalyst activities (l/(g min)) for the gas phase reaction in the fixed bed reactor were calculated after Kopinke et al. (2003) (Eq. 45) and are presented in the figure 5.3. In the figure 5.3, the catalyst activities at different temperatures and at gas flow of 1.5 l/min (contact time 0.1 second) for 7 studied compounds are presented. As no changes in catalyst activity due to the changes of gas flows was seen, data of only one flow condition was selected. As

expected, from the figure it can be observed that catalyst activity increases with the increase of temperature. It is important to mention here that the catalyst activities of 1,1,2,2-TCA are comparable to the results of Kopinke et al. (2003). However, due to unavailability of data the catalyst activities of the rest of the studied compounds could not be compared.

Table 5.1: Rate constants for different compounds at different temperatures

	Rate constant, S^{-1}						
Tempera-ture, ^{o}C	1,1-DCE	c-1,2-DCE	TCE	PCE	1,1,2,2-PCA	1,2-DCA	Chloroethane
50	9.42±0.09	7.91±0.18	4.23±0.18	3.2±0.04	n.a.	n.a.	n.a.
75	13.39±0.25	11.75±0.40	7.42±0.12	5.82±0.11	n.a.	n.a.	n.a.
100	18.89±0.46	18.22±0.25	11.89±0.18	9.83±0.10	4.35±0.09	n.a.	n.a.
150	29.43±0.54	28.89±0.63	21.84±0.48	19.34±0.25	12.32±0.12	n.a.	n.a.
200	n.a.	n.a.	38.15±1.35	36.77±0.69	24.25±0.27	1.50±0.05	n.a.
250	n.a.	n.a.	n.a.	n.a.	39.95±0.25	3.14±0.04	2.55±0.06
300	n.a.	n.a.	n.a.	n.a.	n.a.	6.13±0.06	5.26±0.15
350	n.a.	n.a.	n.a.	n.a.	n.a.	9.48±0.13	9.05±0.11
400	n.a.	n.a.	n.a.	n.a.	n.a.	n.a.	15.51±0.26

n.a.: not analyzed

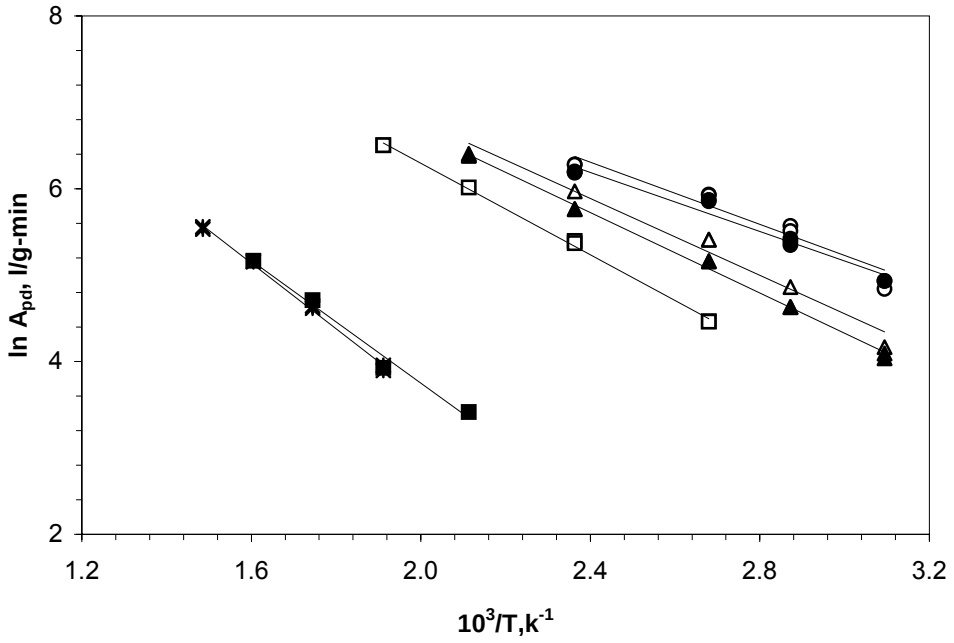

Fig. 5.3: Temperature and gas flow dependencies of the catalyst activity, A_{pd} (l/g-min) in the gas phase reductive dechlorination reaction for 1,1-DCE (open circles), cis-1,2-DCE (solid circles), TCE (open triangles), PCE (solid triangles), 1,1,2,2-TCA (open square), 1,2-DCA (solid square) and chloroethane (star marks) using palladium catalyst. Gas flow 1.5 l/min, different temperatures (Table 5.1).

5.3.2 Reaction rate and activation energy

The rate of a thermodynamically feasible reaction is controlled by the activation energy (E_a) that can be predicted by the Arrhenius equation (Eq. 43) and the rearranged form of the Arrhenius equation (Eq. 44).

The Arrhenius equation predicts, that a plot of ln k_r against 1/T should give a straight line, the slope of which is $-E_a/R$. This slope can be used to calculate the activation energy, E_a (Ebbing and Gammon, 2003-2004).

Figure 5.4 shows such log-linear plot of reaction rate constant (ln k_r) versus 1/T from that the reaction activation energies have been calculated (Table 5.2). From the figure, it can be seen that the rate constant remained sensitive to the temperature throughout the experimental range.

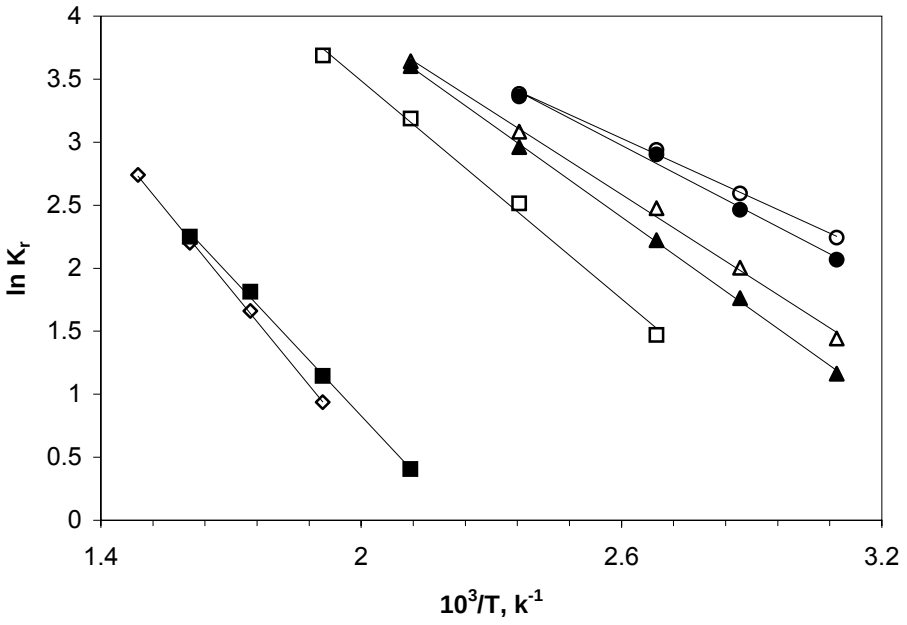

Fig. 5.4: Arrhenius plot. Dependence of first order rate constants (k_r) for 1,1-DCE (open circles), cis-1,2-DCE (solid circles), TCE (open triangles), PCE (solid triangles), 1,1,2,2-TCA (open squares), 1,2-DCA (solid squares) and chloroethane (open diamonds) reductions on temperatures using palladium catalysts.

Because the relationship between k_r and the E_a (kJ mol^{-1}) is exponential, a reaction with a lower E_a will occur much faster than a reaction with higher one. For the present experiments the reactivity of COCs decreased towards 1,1-DCE > c-DCE > TCE > PCE > 1,1,2,2-TCA > 1,2-DCA > chloroethane. Other authors, especially in the case of aqueous phase degradation, have also reported that the reaction rate for unsaturated chlorinated compounds

increased with decreasing number of halogens (Kopinke et al., 2003**;** O'Loughin and Burris 2004).

Table 5.2: Activation energy (E_a) calculated using Arrhenius equation.

Compound name	Activation energy, kJ/mole
1,1-DCE	13.02±0.45
cis-1,2-DCE	14.92±0.93
TCE	18.34±0.56
PCE	20.43±0.28
1,1,2,2-TCA	23.99±1.14
1,2-DCA	30.50±0.89
Chloroethane	34.93±1.08

The formation of a *di-σ* bonded intermediate at the catalyst surface (followed by a hydride transfer and /or abstraction of a sorbed hydrogen atom), which would favor the less halogenated ethenes (Arnold and Roberts, 2000; Schwarzenbach et al., 2003) is a likely explanation for this behaviour. This can also be explained by the electronegativity of elements, such as for 1,1-DCE more polarity is created by two halogen atoms in the same carbon atom, for cis-1,2-DCE polarity is created but on two different carbon atoms. TCE has partially symmetrical structure, so not fully polarized like 1,1-DCE and cis-1,2-DCE. Among all the studied unsaturated compounds, PCE has totally symmetrical structure, so least polarity exists and activation energy is the highest.

For saturated compounds (chlorinated ethanes) the case was opposite that is the reaction was more rapid for compound having more halogen group than for ethanes having less halogen group. Similar results were observed by other authors in the case of aqueous phase catalytic degradation (O'Loughin and Burris 2004). More halogen means more electronegative elements present in the saturated compounds. That means more shifting of electronic clouds occur towards halogen creating δ- towards halogens and δ+ towards carbon.

5.3.3 Reaction pathways

PCE and TCE: The major products of PCE reduction were ethane (~ 90 % of observable products). Major intermediates for PCE detected were TCE (~1-2%), cis-1,2-DCE (~1%),1,1-DCE (<1%), chloroethane and ethene (~1-4%) within temperatures 50^{o}C to 75^{o}C. Above 150^{o}C only ethane (>95%) was observed as product and no intermediates were detected.

The presence and existence of intermediates and end products at different temperatures are shown in Table 5.3.

During the reduction of TCE, similar end products and intermediates were detected as in the PCE reduction experiments. In addition, vinyl chloride (<1%) was observed between 50°C and 75°C as an intermediate product. From the observed products and intermediates it can be speculated that for both the PCE and TCE hydrogenolysis and hydrogenation were the main reaction pathways. The proposed reaction pathways are shown in figure 5.5.

Table 5.3: List of products and the intermediate products formed during the catalytic dechlorination reaction

Compounds	Major products	Intermediate products
PCE	Ethane, HCl[#]	c-DCE[1], TCE[2], Chloroethane[3], 1,1-DCE[1], Ethene
TCE	Ethane, HCl[#]	c-DCE[1], Chloroethane[3], VC[4], Ethene
c-DCE	Ethane, HCl[#]	Chloroethane[3], VC[4], Ethene
1,1-DCE	Ethane, HCl[#]	Chloroethane[3], VC[4], Ethene
1,1,2,2-TCA	Ethane, HCl[#]	Chloroethane[3], Ethene*
1,2-DCA	Ethane, HCl[#]	Chloroethane[5], Ethene*
Chloroethane	Ethane, HCl[#]	Ethene**

[1] Observed between 50°C–75°C, [2,3,4] Observed up to 100°C, [5]Observed up to 250°C, *Observed above 250°C, **Observed above 200°C, [#] more likely products, only identified.

1,1-DCE and cis-1,2-DCE: Between temperatures 50°C and 100°C ethane was the major detected product, chloroethane (<2%), ethene and vinyl chloride (<1%) were the major intermediates, indicating hydrogenolysis and hydrogenation as the reaction pathways. Between temperatures 100°C and 250°C, the observed product was ethane and no intermediate product was detected.

1,2-DCA, 1,1,2,2-TCA and chloroethane: During the reduction of 1,2-DCA, it was observed that at temperatures below 150°C, no significant conversion of 1,2-DCA occurred. However, at this temperature ethane was the main product and no ethene was present. At 200°C ethane was detected as end product and chloroethane was the intermediate product. Above 300°C no chloroethane was detected. The presence of ethane as the end product and chloroethane (<2%) as the intermediate product suggested that the hydrogenolysis was the main reaction pathway (>95%). Also the presence of ethene above 250°C, though in very small amount, demonstrated that either dihaloelimination or dehydrohalogenation reaction (~1-3%) also occurred along with the hydrogenolysis. Dihaloelimination or dehydrohalogenation reaction increased from ~1% to ~3% with increasing temperature from 300°C to 350°C.

During the degradation of 1,1,2,2-TCA, the observed intermediates were 1,1,2-TCA (<3% at 50°C, <2% at 100°C) and chloroethane up to 100°C and 1,2-DCA (<1%) up to 50°C. The end

product was ethane. Therefore, it can be suggested that the main reaction (>95%) was the stepwise hydrogenolysis and went through 1,1,2-TCA, then to 1,2-DCA and chloroethane and finally, to ethane. Above 250°C the presence of ethene indicated the dehydrohalogenation reaction (<3%) from intermediate step chloroethane.

During chloroethane reduction ethane was the main product that indicated hydrogenolysis as the main reaction pathway (>95%). Also, the presence of ethene (<2%) between 250°C and 450°C suggested a dehydrohalogenation reaction.

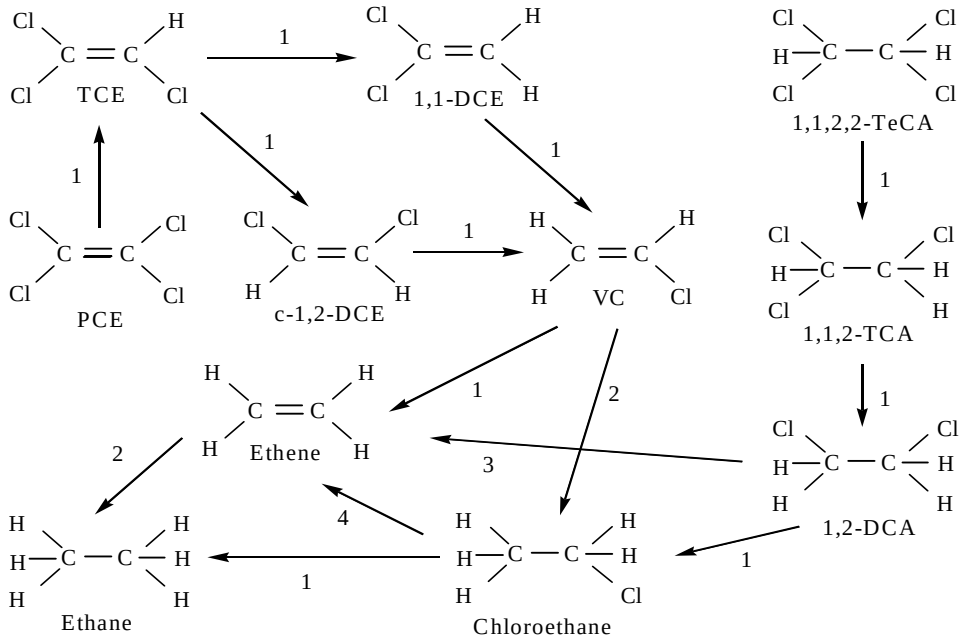

1. Hydrogenolysis 2. Hydrogenation 3. Dihaloelimination 4. Dehydrohalogenation

Fig. 5.5: Proposed reaction pathways for the reduction of gas phase PCE, TCE, cis-1,2-DCE, 1,1-DCE, 1,1,2,2-TCA, 1,2-DCA and chloroethane using palladium catalysts in the presence of hydrogen at elevated temperatures.

Chapter 6

Catalytic degradation of gas phase MTBE, ETBE, TAME and DIPE over palladium in the presence of hydrogen at elevated temperatures

6.1 Introduction

Ethers are widely used as oxygenates to improve the fuel combustion efficiency. Among the ethers methyl tert butly ether (MTBE) is used on the largest scale because of economic and technical reasons (Squillace et al., 1996; Shelly and Fouhy, 1994; Mormile, 1994). Approximately 20 million tons are consumed worldwide each year (60% in America and 15% in Europe). In Europe, over 78 000 tons are emitted annually, with approximately 92.4%, 4.4% and 3.2% being emitted into air, water and soil respectively (Arp and Schmidt, 2004, Eur 20417 EN 2002). MTBE is introduced into the environment both through point sources e.g., leaking underground storage tanks and diffuse sources e.g., evaporation and exhaust emissions from automobiles etc (Fayolle et al., 2003; Bradley et al., 1999; Kirchstetter et al., 1996; Fraser et al., 1998).

MTBE has a high water solubility and mobility, therefore, it is easily detectable in rainwater (Achten et al., 2001) as well as surface water (Achten and Püttmann, 2000; Achten et al., 2002) and groundwater (Squillace et al., 1996, Achten et al., 2002; Baehr et al., 1999; Klinger et al., 2002; Schmidt et al., 2004). Because of its carcinogenic potential (Squillace et al., 1996, Fayolle et al., 2003, Bradley et al., 1999, USEPA, 1999) the worldwide interest in the processes governing the fate of MTBE in the environment is rapidly increasing. The U.S. Environmental Protection Agency (USEPA) advised a concentration limit of 20-40 µg/L in ground water (USEPA, 1999). The California Department of Health Services has lowered this tolerable concentration range in groundwater to 5 µg/l (California Code regulation, 1999; Acero et al., 2001). Other oxygenates in use are ethyl tert butyl ether (ETBE) in France, Spain and Italy, and tert amyl methyl ether (TAME) in Finland. Recently, the European ETBE production is 1/8 of the MTBE production (Arp and Schmidt, 2004; Schmidt et al., 2002).

Ethers are generally considered as compounds being highly resistant to biological degradation (Fayolle et al., 2003, Prince, 2000; Fayolle et al., 2001; Deeb et al., 2000; Zwank et al., 2005). Moreover, the major product of biodegradation of MTBE in both oxic and anoxic conditions are tert-butyl alcohol (TBA) and tert-butyl formate (TBF) (Zwank et al., 2005; Arp et al., 2005; Wallington et al.,1991), those are even more toxic compounds. Furthermore, besides TBA and TBF, many other degradation products from MTBE oxidation in aqueous phase via conventional ozonation and the combination ozone/hydrogenperoxide are reported

(Acero et al., 2001). These products are acetone, formaldehyde, 2-methoxy-2methyl propionaldehyde, hydroxyisobutyraldehyde and methyl acetate. TBA and TBF are also the biodegradation products of ETBE (Arp et al., 2005; Wallington et al., 1991). During the hydrolysis of MTBE and ETBE in dilute aqueous acid, O'Reilly et al., 2001 also observed TBA as one of the products. However, for ethers other than MTBE, data in environmental samples are scarce, in particular in the peer-reviewed literature (Arp and Schmidt, 2004).

The objective of this work is to evaluate the degradability of gas phase methyl tert-butly ether (MTBE), ethyl tert-butyl ether (ETBE), tert-amyl methyl ether (TAME) and diisopropyl ether (DIPE), in the presence of noble metal catalyst (palladium) and hydrogen under different temperature and gas flow conditions. Palladium was chosen as the catalyst because of its broad reactivity for hydrogenation reactions (Rylander, 1979; Balko 1993; Schüth and Reinhard, 1998).

To figure out the relationships between the structure of the compounds and the degradation patterns, additionally the degradation of diethyl ether (DEE) and dimethyl ether (DME) were studied. DEE and DME are used as a common solvent, and their presence in the environment are not yet reported as toxic.

6.2 Materials and method

6.2.1 Materials

Catalytic degradation was studied using a total of 4 ether compounds – methyl tert butyl ether (MTBE-99.8%), ethyl tert butyl ether (ETBE-99%), tert amyl methyl ether (TAME-97%) and diisopropyl ether (DIPE-99%). All targeted compounds and ethanol were obtained from Sigma Aldrich GmbH, diethyl ether (DEE-98%), n-hexane, n-heptane, methanol and 2-propanol from Merck KgaA, isopentane (99%) and isopentene (99.5%) from Fluka. Gas standards for methane, ethane, ethene, acetylene, propane, propene, isobutane and isobutene were obtained from Messer Griesheim GmbH, carbon monoxide from Matheson Tri-Gas and dimethyl ether (DME-99.9%) from Sigma Aldrich GmbH. A spherical (3 mm) palladium on alumina catalyst with a palladium loading of 0.5% and a bulk density of 0.5 kg/l was used for all experiments.

To prepare contaminant solutions, respective contaminants were injected into deionized and degassed water stored in 20 liter Teflon© bags. The aqueous concentration was in general 10 mg/l, which corresponds to 113.45 µmol/l for MTBE, 97.87 µmol/l for ETBE, TAME and DIPE. Dimethyl ether is a very highly water soluble gaseous compound. Therefore, it was directly injected into the water. Cyclohexane, n-Hexane or n-Heptane was used as an internal standard depending on the retention time of the target compounds and the products. Air stripping with the help of a hollow fiber membrane module (Liqui-cel extra flow contactors-2.5″ x 8″) was used to transfer the contaminants from aqueous phase to the gaseous phase (Tarafder et al., 2007, McDermott et al., 2007).

6.2.2 Experimental setup and procedure

The experimental setup and procedure are illustrated in section 5.2.2 of chapter 5.

Water flow was varied from 0.05 to 0.055 l/min, gas flows were 1.0 l/min, 1.5 l/min, 2.0 l/min, 2.5 l/min and 3.0 l/min, which corresponds to the contact time of 0.15, 0.10, 0.075, 0.06 and 0.05 seconds respectively. The corresponding vacuum pressures to these gas flows were 0.125, 0.175, 0.225, 0.28 and 0.339 atm for a fixed instrument setting. Under these experimental conditions the removal of the contaminants from water to gas phase was above 90%. The measured gas phase concentrations for the water flow of 0.05-0.055 l/min were approximately 2.2-5 µmol/l for MTBE, 2.5-5.2 µmol/l for ETBE, 2-4.3 µmol/l for TAME and 2.5-4.4 µmol/l for DIPE.

The contaminated gas was allowed to pass through a catalytic column reactor. The column was made of stainless steel tubing (length 4.7 cm, diameter 1 cm) and was filled with 2.5 g of catalyst. It was placed inside a tube furnace having a 45 cm long and 3.5 cm diameter isothermal zone, (model: MTF 12/38/400) equipped with temperature controller type 201 and manufactured by Carbolite®. Moreover, a preheat coil was added inside the furnace just before the column in order to avoid the sudden cooling down of the catalytic bed by the sweep gas at the entrance of the catalytic column, especially during the experiment with high temperatures. From the vacuum pump to the outflow port, a stainless steel pipe was used to minimize the sorption of the contaminants and to protect itself form heat. Hydrogen gas (0.01 l/min) was added to the contaminated gas before entering into the furnace as well as the catalytic column. Both nitrogen and hydrogen flows were controlled by thermal gas mass-flow controllers (Bronkhorst©, F-201C).

6.2.3 Chemical analysis

Gas phase samples were collected from the ports located before and after the catalytic reactor using gas tight syringes. For the detection of the reactant and products, gas phase samples were injected in a Varian 3800 GC equipped with an Alltech AT-Q^{TM} capillary column (30 m x 0.53 mm i.d) and a FID and a Carlo Erba HR-GC (Model 5160) equipped with a CP-SIL-13CB capillary column and an electron capture detector (ECD) in series with a flame ionization detector (FID). For the detection of hydrogen and carbon monoxide, a Varian GC equipped with Agilent GS-Carbon PLOT (30 m x 0.32 i.d.) capilary column and thermal conductivity detector (TCD) were used. Products were identified initially by a GC (Hewlett Packard 6890) coupled with a MSD (Hewlett Packard 5972A) and a capillary column DB-624 (length 60 m, ID 0.25 mm, film 1.4 µm) based upon comparison of the full scan spectra with library spectra. For the GC ECD/FID analyses, standards were injected and identification and quantification of the educts and products was done.

6.2.4 Data analysis

The data analysis is discussed in the section 5.2.4 of chapter 5.

6.3. Results and discussions

6.3.1 Degradation of MTBE, ETBE, TAME and DIPE

The catalytic degradation experiments were conducted at temperatures generally ranging from 100°C to 250°C, for DIPE the temperature was increased up to 325°C. The temperatures were increased, in the most cases, with a cycle of 25°C. From the experiment, it was observed that catalytic degradation of the studied compounds MTBE, ETBE, TAME and DIPE at elevated temperatures were possible. The degradation of MTBE, ETBE and TAME at high temperatures is more or less similar. But, for DIPE relatively higher temperatures were needed. The reason for higher stability of DIPE might be the very symmetrical structure of the compound. Figure 6.2 shows the conversion of MTBE, ETBE, TAME and DIPE during the catalytic hydrogenation reaction at 225°C.

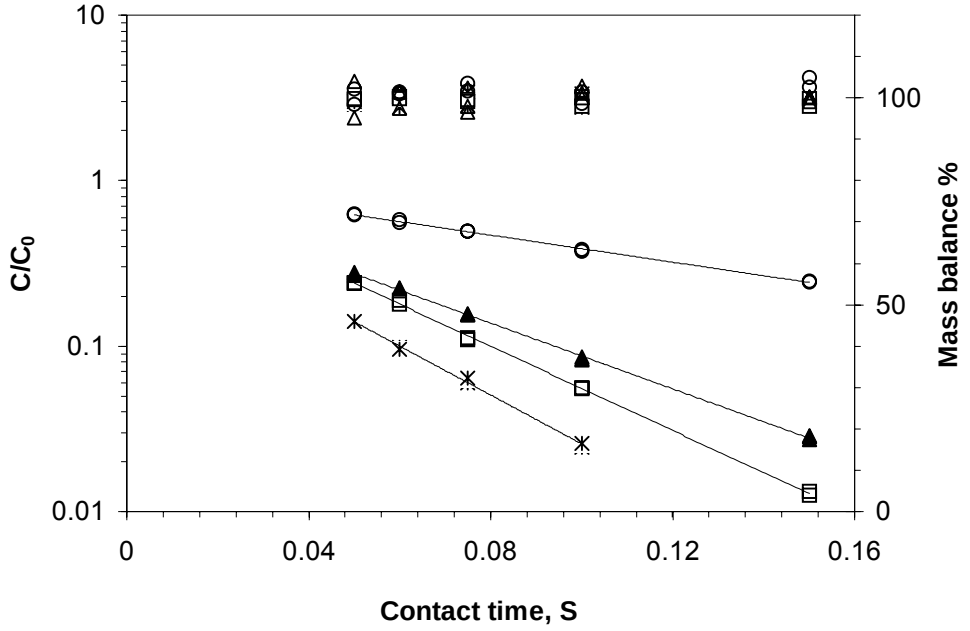

Fig. 6.2: Conversion for TAME (star marks), ETBE (open squares), MTBE (solid triangles) and DIPE (open circles) at 225°C temperature and fixed contact times over palladium catalysts. Mass balances are added on the top of the figure according to the right side scale. Error bars are too small to add.

At this temperature (250°C) and contact time of 0.05-0.15 second, the conversion of TAME varied between 85- >98%, that of ETBE varied between 75-98%, that of MTBE varied between 73-97% and that of DIPE varied between 36-75%.

Mass balances were made based on the products and are presented on the figure. At this particular temperature mass balances were between 97 -102% for TAME, 97-100% for ETBE, 96-104% for MTBE and 98 -105% for DIPE.

The hydrogenation reaction of those compounds can be explained by the pseudo-first order reaction kinetics as stated in equation 18 (Schüth and Reinhard, 1998; Kopinke et al., 2003). First order reaction rate constants were calculated using a log-linear plot of normalized concentration versus detention time. Figure 6.3 shows such an example of log linear plot for ETBE. Data for MTBE, TAME and DIPE are used to calculate the reaction rate constants (Appendix 3.1 and 3.2). The rate constants are presented in the Table 6.1. A temperature dependent increase of the rate constants were observed, which can be expected, because the increasing temperature gives rise to increasing number of collisions and more likely combinations among the molecules.

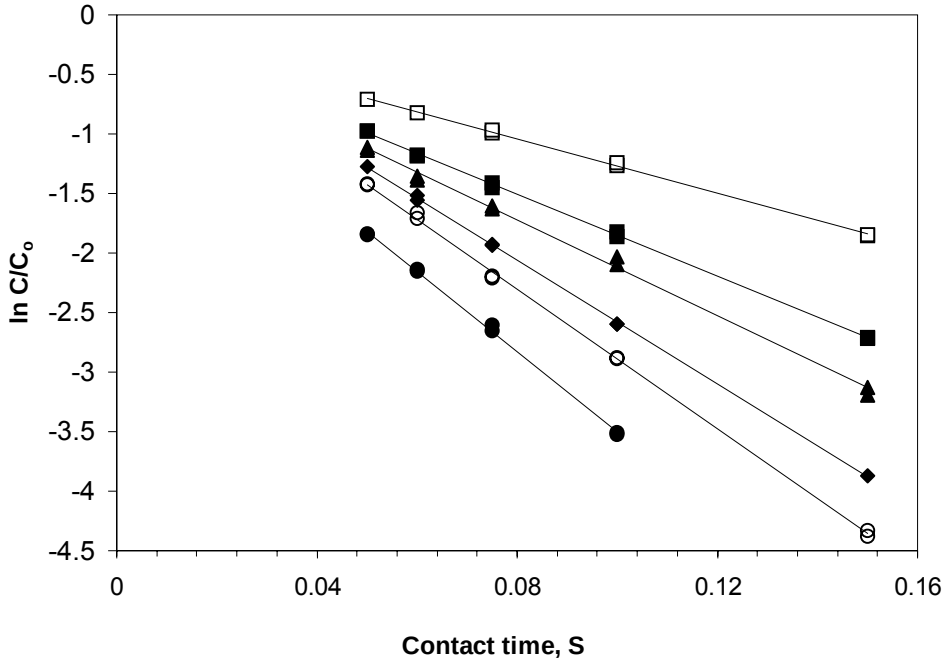

Fig. 6.3: Lines of best fit to the log-transformed normalized concentration versus time (linear regression analysis) were used to estimate k_r values for ETBE (Table 6.1). Temperature 100°C (open squares), temperature 150°C (solid squares), temperature 175°C (solid triangles), temperature 200°C (solid diamonds), temperature 225°C (open circles), temperature 250°C (solid circles). Error bars are too small to add.

Table 6.1: Rate constants for different compounds at different temperatures

	Rate constant, Sec^{-1}			
Tempera-ture, ^oC	TAME	ETBE	MTBE	DIPE
100	14.29±0.09	11.44±0.09	n.a.	n.a.
150	20.63±0.03	17.19±0.16	10.02±0.13	n.a.
175	24.31±0.32	20.05±0.43	13.03±0.12	n.a.
200	28.52±0.35	26.02±0.17	17.25±0.16	7.03±0.07
225	34.00±0.,64	29.31±.28	22.88±0.22	9.40±0.09
250	n.a.	33.63±.56	28.40±0.29	11.57±0.14
275	n.a.	n.a.	n.a.	15.06±0.18
300	n.a.	n.a.	n.a.	18.29±0.37
325	n.a.	n.a.	n.a.	23.43±0.30

n.a.: not analyzed

Because the rate constants are temperature dependent, the influence of temperature on the rate of gas phase hydrogenation reaction can be interpreted using the Arrhenius equation as stated in the equations 43 and 44 (Ebbing and Gammon, 2003-2004). Figure 6.4 shows a log-linear plot of reaction rate constant (ln k_r) versus 1/*T* and from that the reaction activation energy was calculated (Table 6.3).

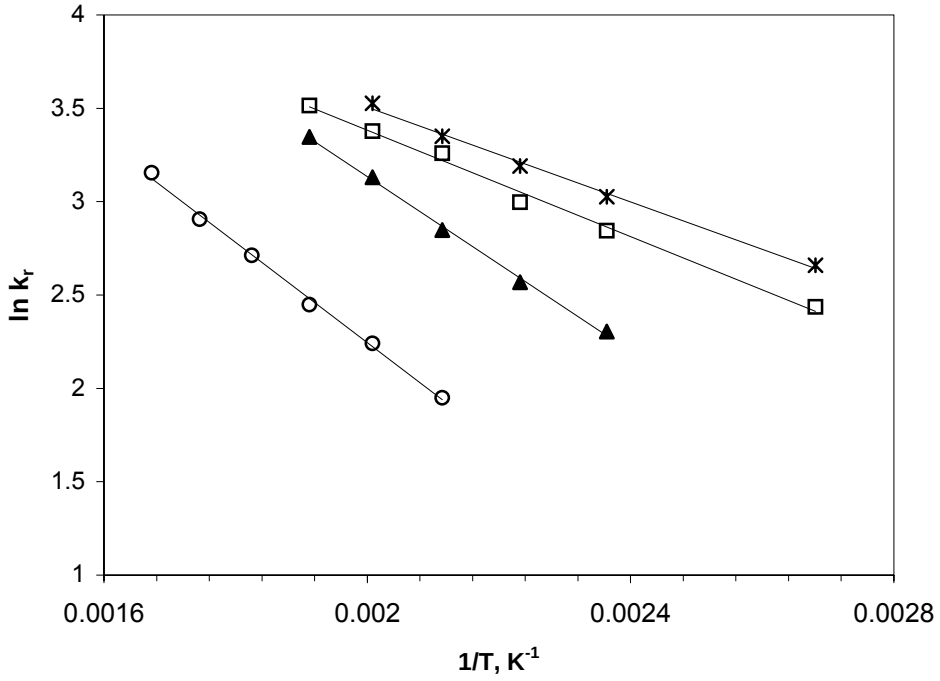

Fig. 6.4: Arrhenius plot. Dependence of first order rate constants (k_r) for TAME (star marks), ETBE (open squares), MTBE (solid triangles) and DIPE (open circles) reductions on temperatures during catalytic hydrogenation. Error bars are too small to add.

Table 6.2: Activation energy (E_a) calculated using Arrhenius equation.

Compound name	Activation energy, kj/mole	R^2
TAME	10.55±0.42	0.995
ETBE	11.84±0.49	0.993
MTBE	19.45±0.54	0.998
DIPE	22.25±0.60	0.997

From the Table 6.2, it can be seen that the reactivity of ether compounds decreased towards TAME > ETBE > MTBE > DIPE. To analyze that phenomenon, experiments were conducted using the more symmetrical and less branched ether compounds diethyl ether ($C_2H_5 – O – C_2H_5$) and the shortest symmetrical ether dimethyl ether ($CH_3 – O – CH_3$) to evaluate the reaction activation energies.

The experiments were conducted at three different temperatures – 300^{o}C, 350^{o}C and 400^{o}C and similar contact time like other experiments of this paper. The reaction rate constants at these respective temperatures were 9.26±0.10 (s^{-1}), 14.16±0.21 (s^{-1}) and 21.15±0.51 (s^{-1}) for DEE and 4.19±0.13 (s^{-1}), 7.37±0.25 (s^{-1}) and 12.03±0.10 (s^{-1}) for DME. The degradation products for DEE were methane, carbon monoxide, hydrogen and ethane and for DME were methane, methanol, carbon monoxide and hydrogen. From the reaction rate constant the calculated activation energies were 26.43±0.18 kJ/mole and 33.80±0.78 kJ/mole for DEE and DME respectively.

So, it can be speculated that the structure of the compound might be responsible for having different activation energies for different ether compounds to degrade. And the more symmetrical and less branched the structure of the compound was, the more activation energy was required. It is important to mention here that during the hydrolysis of MTBE, ETBE and TAME on acidic ion-exchange resins, O'Reilly et al. (2001) also observed the similar reaction trend like in the present work, that was the hydrolysis of TAME and ETBE were relatively faster than that of MTBE (O'Reilly et al., 2001).

The catalyst activity for the gas phase reaction in the fixed bed reactor at different temperatures and gas flows was calculated after Kopinke et al. (2003) as stated in equation 45. The catalyst activities vs temperatures for the target compounds are plotted on the figure 6.5. Only a fixed flow of 2 l/min was chosen here as no changes in the catalyst activities with gas flows were observed. As expected, from the figure 6.5 the temperature dependent increase of catalyst activities can be seen.

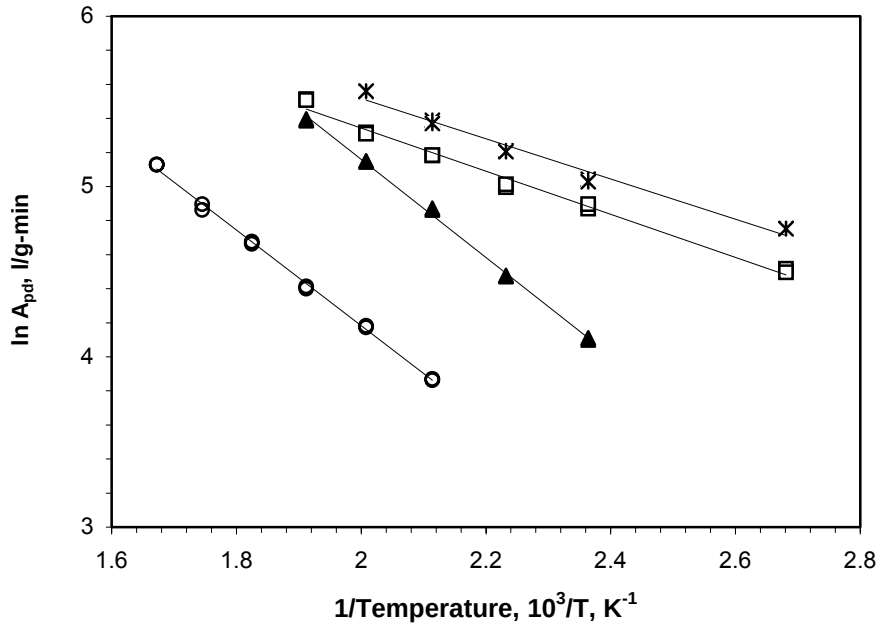

Fig. 6.5: Temperature dependencies on the catalyst activity, A_{pd} (l/g-min) in the gas phase hydrogenation reaction of TAME (star marks), ETBE (open squares), MTBE (solid triangles) and DIPE (open circles) using palladium catalyst.

6.3.2 Reaction products and pathways

Two reaction pathways were observed for all the studied compounds. One of them was hydrogenation and it was the dominating reaction pathway. The second one was the thermal cracking and rearrangement of the compound, which might happen because of the high temperatures in the presence of catalysts.

The second reaction pathway that can occur in the absence of hydrogen was separately analyzed for all target compounds, by running the experiments without the addition of hydrogen to the gas phase. However, although degradation products could be analyzed, a large data scatter was observed with lower reactivities at later times in the experiments. The reason might be that catalyst deactivation occurred due to the absence of hydrogen.

The reaction products of catalytic hydrogenation of MTBE, ETBE, TAME and DIPE are listed in the Table 6.3.

Table 6.3: List of products formed during the catalytic hydrogenation reaction.

Compound	Products
MTBE	Isobutane, methanol, isobutene[1], propane[2], carbon monoxide
ETBE	Isobutane, ethanol, isobutene[2], propane[2], methane, carbon monoxide
TAME	Isopentane, methanol, isopentene[1], n-butane[3], methane[3], carbon monoxide
DIPE	Propane, acetone, propene[2], ethene[4], ethane[4], methane[4]

[1]Observed above 175°C, [2]Observed above 200°C, [3]Observed above 225°C, [4]Observed between 300°C - 325°C.

6.3.2.1 MTBE

Experiments were conducted between temperatures 150°C to 250°C. At temperature 150°C, isobutane and methanol were identified as primary end products and the reaction occurred through scheme 1(a). Above 150°C, scheme 1(b) started and the selectivity of that scheme at 175°C was about (~) 6%, at 200°C (10%, at 225°C (22% of the total reaction occurred during the experiment. Scheme 1(b) is not unlikely as it is known that generally MTBE is synthesized commercially in the gas phase reaction of isobutene and methanol over acidic ion-exchange resins (O'Reilly et al., 2001; Nikolopoulos et al., 1996).

Scheme 1 (Methyl Tert Butyl Ether)

(a)

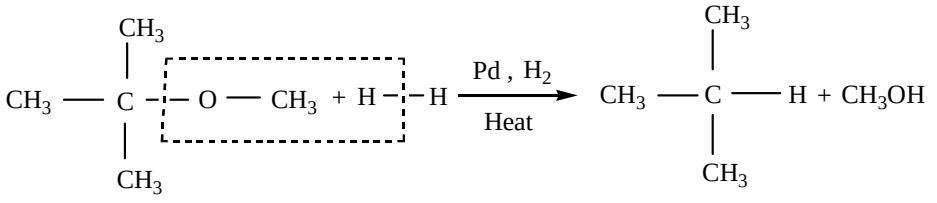

(b)

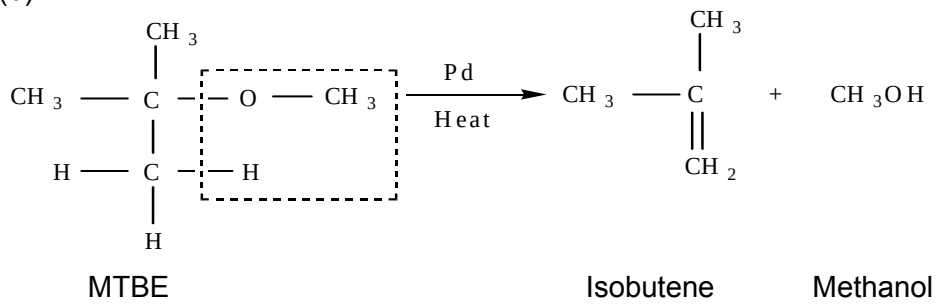

Fig. 6.6: Reaction pathways for the catalytic hydrogenation of gas phase MTBE

During the experiment, only circa 5% of the methanol was detected, which was much lower than the expected amount. To find out the reason, separate experiments with methanol were conducted. The experiments were done in the presence and absence of hydrogen. Degradation of methanol was observed in both cases. The degradation products were

carbonmonoxide and hydrogen. However, hydrogen was detected only in the experiments without hydrogen. Detailed study on the degradation of methanol was not of the interest as it was well studied by other authors (Shekhar and Barteau, 1995; Iwasa et al., 1993; Liu et al., 2000; Lee and Boudart, 1991).

At 225^{o}C and 250^{o}C, C3 hydrocarbon (propane) was detected (< 3% & <5% respectively) that might be considered as coupling products. Such coupling products were observed by other authors during the catalytic reduction of chlorinated hydrocarbon compounds (O'Loughlin et al., 1999; Liu et al., 2005).

Mass balances were done based on isobutane and isobutene and not with methanol as it was further degraded. Mass balances were between 95 to 104% with an average of 99.18%.

6.3.2.2 ETBE

Experiments were conducted between temperatures 100^{o}C and 250^{o}C. Up to 200^{o}C, the reaction occurred as shown in scheme 2(a) and the primary products were isobutane and ethanol. During the experiment, only trace amount of ethanol was detected. However, they should be produced stoichiometrically. To analyze the phenomenon, experiments were conducted using ethanol in the presence and absence of hydrogen. In both the cases, ethanol was further decomposed, even at 50^{o}C temperature. The identified products for the experiment in absence of hydrogen were carbon monoxide, methane and hydrogen, but for the experiment with hydrogen, carbonmonoxide and methane were detected, as hydrogen was already present in the system. However, the quantification of the products of ethanol degradation was not of interest as the catalytic degradation of ethanol under similar experimental condition was extensively studied by Cordi et al. (Cordi and Falconer, 1996).

At 225^{o}C and 250^{o}C the presence of isobutene suggested that the reaction scheme 2(b) was also present simultaneously and the selectivity for isobutene at temperature 225^{o}C was 15-18% and at 250^{o}C was 22-25% of the total reactions occurred. At this temperature range C3 hydrocarbon, propane (3-5%) was also formed, that might result due to the coupling caused at the high temperature.

Mass balances were done with isobutane and isobutene and were found to be between 96-102% with an average of 98.48%.

Scheme 2 (Ethyl Tert Butyl Ether)

(a)

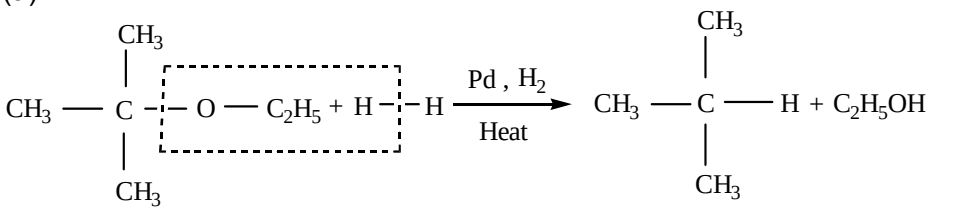

(b)

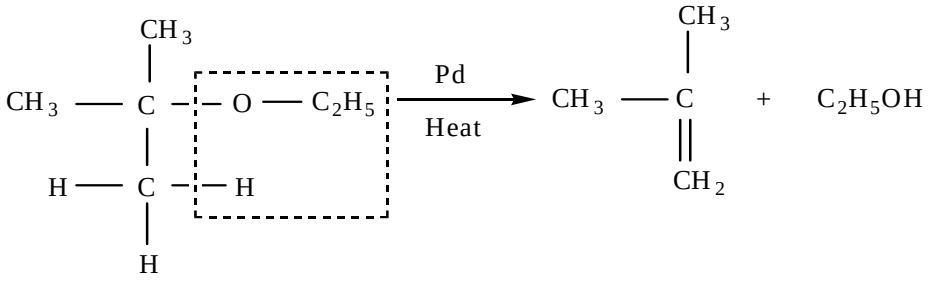

Fig. 6.7: Reaction pathways for the catalytic hydrogenation of gas phase ETBE.

6.3.2.3 TAME

The experiments were conducted between temperatures of 100°C and 225°C. Up to 150°C only reaction scheme 3(a) was observed and throughout the experimental range it was the dominating pathway. Above 150°C, scheme 3(b) was observed that indicates the thermal cracking and rearrangement of the compound. At 175°C scheme 3b takes over <4%, at 200°C 4-5%, and at 225°C 8-11% of the total reaction. At 225°C, n-butane (<3%) and methane (<3%) were also detected that might be anticipated as coupling products. Mass balances were done based on isopentane and isopentene, and were between 95-103%, with an average of 98.87%.

Scheme 3 (Tert Amyl Methyl Ether)

(a)

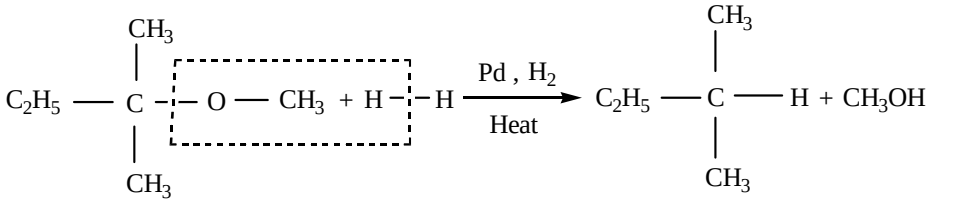

(b)

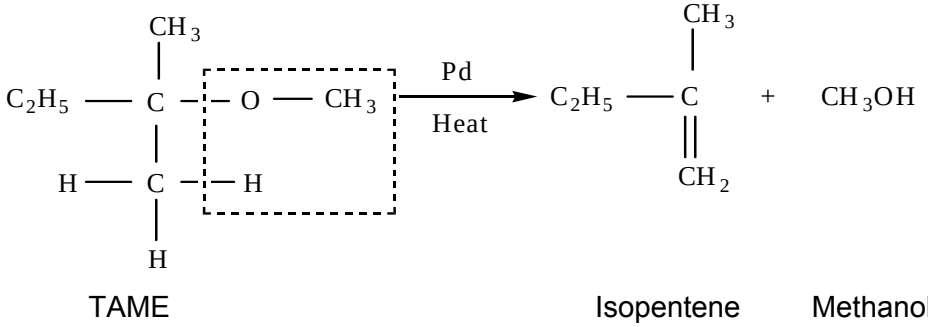

Fig. 6.8: Reaction pathways for the catalytic hydrogenation of gas phase TAME.

6.3.2.4 DIPE

The experiments were conducted between temperatures 200°C to 325°C. At this temperature range the main reaction went through scheme 4(a) and propane and acetone were detected as the products. If propane is produced, like other ether compounds in this paper 2-propanol should be produced as another product with propane. To analyze this observation, an experiment was conducted using 2-propanol and it was observed that 2-propanol was totally decomposed to acetone (scheme 4(c)). Such dehydrogenation of 2-propanol are well discussed by other authors (Shekhar and Barteau, 1995; Murthy and Awamy, 1994; Pepe et al., 1992; Katona et al., 1990). At 200°C, scheme 4(b) was also observed that means thermal cracking and rearrangement of the compound happened along with hydrogenation reaction. At temperature 225°C, less than 3% of the total reactions happened through scheme 4(b) that increased up to approximately 45% observed at 325°C.

Between 300°C and 325°C, ethene (<1%), ethane (~4-10%) and methane (~ 5-10%) were also detected as the products, which might results from sequential scission of the C – C bonds of 2-propanol as also observed by Shekbar and Barteau (1995). Mass balances were done based on the products listed on the table 6.3 and varied between 96 to 105% with an average of 100.99%.

Scheme 4 (Diisopropyl Ether)

(a)

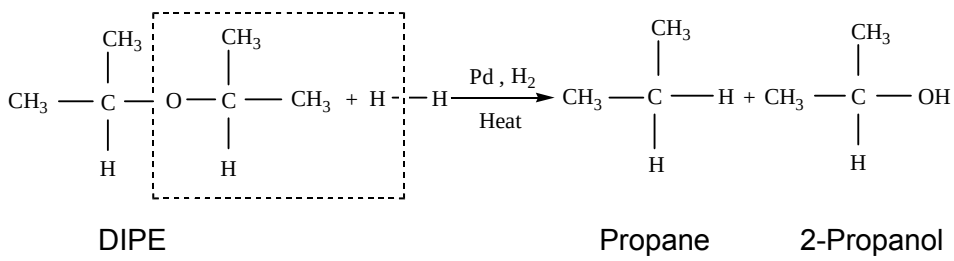

(b)

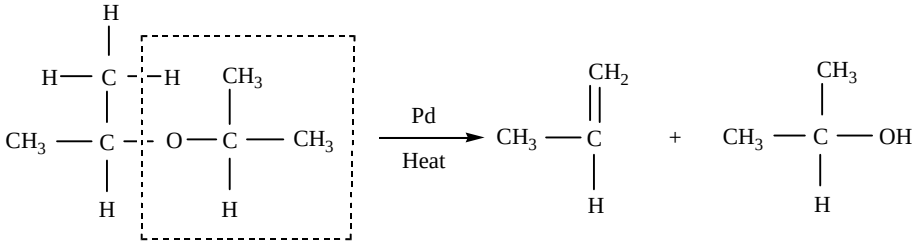

DIPE Propene 2-Propanol

(c)

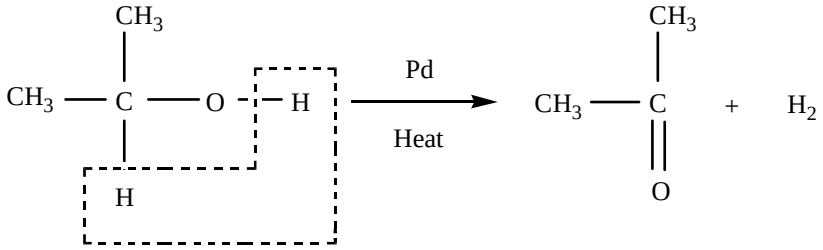

2-Propanol Acetone Hydrogen

Fig. 6.9: Reaction pathways for the catalytic hydrogenation of gas phase DIPE.

6.4 Conclusion:

In the present study, the results of the catalytic conversion of gas phase MTBE, ETBE, TAME and DIPE at elevated temperatures demonstrate that comparatively non-toxic and less toxic compounds are produced during the catalytic hydrogenation of the studied compounds. Gas phase reactions followed first order kinetics and were significantly fast having very short half lives of a second or fraction of a second. Compound dependant variations in the reaction activation energies were detected. The structures of the compounds were found to be responsible for the differences in the reaction activation energies.

Chapter 7

Catalytic oxidation and decomposition of gas phase MTBE, ETBE TAME and DIPE: reaction products, kinetics and thermodynamics

7.1 Introduction

Ethers are widely used as fuel oxygenates and therefore are detected everywhere in the environment. For instance, the MTBE was detected in rainwater (Achten et al., 2001) surface water (Achten and Puttmann 2000; Achten et al., 2002) and groundwater (Squillace et al., 1996; Achten et al., 2002; Schmidt et al., 2004; Klinger et al., 2002; Baehr et al.,1999). Several studies have been conducted by others on the degradation of ether compounds, such as biodegradation, aqueous phase oxidation via conventional ozonation and the combination ozone/hydrogenperoxide, hydrolysis in dilute aqueous acid. Most of the cases the identified products were similar toxic or more toxic compounds e.g., tertiary butyl alcohol (TBA) (Zwank et al., 2005; Arp et al., 2005; Wallington et al., 1991, Acero et al., 2001, O,Reilly et al., 2001). In the previous chapter (chapter 6), the catalytic hydrogenation of some ether compounds was successfully studied where the products were non-toxic C1 to C5 hydrocarbon gases. In this chapter another attempt to degrade the gas phase MTBE, ETBE, TAME and DIPE in the presence of oxygen and palladium at elevated temperatures was taken. The present study demonstrates that like catalytic hydrogenation catalytic oxidation is also effective for the decomposition of ether compounds. The decomposition of the ether compounds in the presence of oxygen and palladium catalyst at elevated temperatures can be expressed as:

Ether compounds + $O_2 \rightarrow CO_2 + H_2O$

7.2 Material and methods

7.2.1 Materials

The compounds of interest are the same as discussed in chapter 6. Because of the differences of reaction and products from the earlier chapter here additionally carbondioxide standard of Air Liquid and acetaldehyde of Fluka were used.

7.2.2 Experimental set up and procedure

The experimental set up is illustrated in figure 6.1. During the experiment, contaminated water was pumped through the shell side of the membrane module using an Ismatec© BVP-Z gear pump, whereas the sweep gas nitrogen was flowed in counter flow through the lumen

side where a Vaccubrand© MD4 VARIO diaphragm pump with vacuum controller were added to enhance the strip efficiencies. Water flow was varied from 0.05 to 0.055 l/min, gas flows were 1.0 l/min, 1.5 l/min, 2.0 l/min, 2.5 l/min and 3.0 l/min, which corresponds to the contact time of 0.15, 0.10, 0.075, 0.06 and 0.05 seconds respectively. The corresponding vacuum pressures to these gas flows were 0.125, 0.175, 0.225, 0.28 and 0.339 atm. for a fixed instrument setting. Under these experimental conditions the removal of the contaminants from water to gas phase was above 90%. The measured gas phase concentrations for the water flow of 0.05-0.055 l/min were approximately 2.2-5 µmol/l for MTBE, 2.5-5.2 µmol/l for ETBE, 2-4.3 µmol/l for TAME and 2.5-4.4 µmol/l for DIPE.

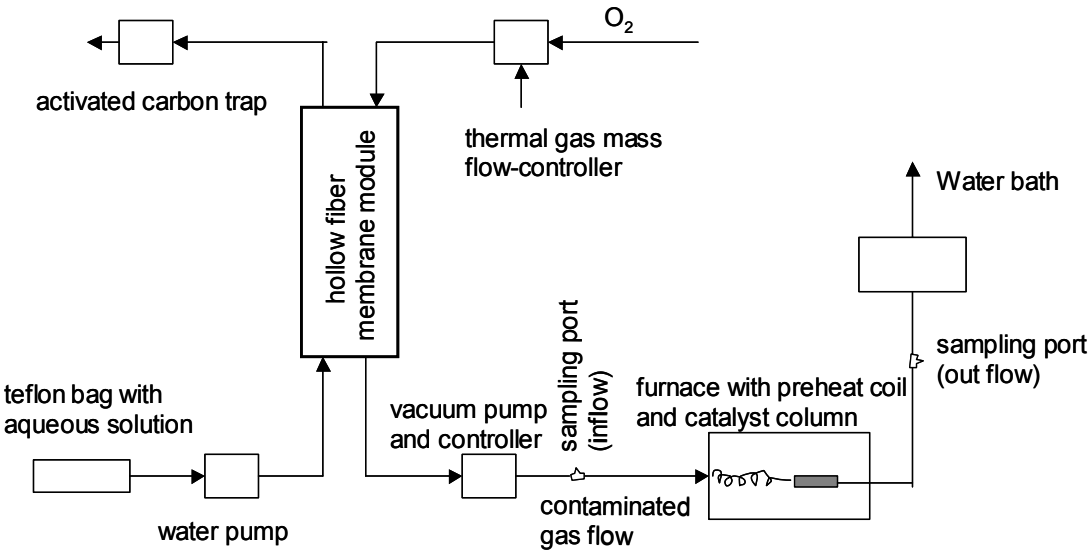

Fig. 7.1: Experimental set up.

The converted contaminants carried by the sweep gas nitrogen were allowed to pass through a catalytic column reactor. The column was made of stainless steel tubing (length 4.7 cm, diameter 1 cm) and was filled with 2.5 g of catalyst. It was placed inside a tube furnace having 45 cm long and 3.5 cm diameter isothermal zone, (model: MTF 12/38/400) equipped with temperature controller type 201 and manufactured by Carbolite®. Moreover, a preheat coil was added inside the furnace just before the column in order to avoid the sudden cooling down of catalytic bed by the sweep gas at the entrance of the catalytic column, especially during the experiment with high temperatures. From the vacuum pump to the outflow port, a stainless steal pipe was used to minimize the sorption of the contaminants and to protect itself form heat. Hydrogen gas (0.01 l/min) was added to the contaminated gas before entering into the furnace as well as the catalytic column. Both nitrogen and hydrogen flows were controlled by thermal gas mass-flow controllers (Bronkhorst©, F-201C).

7.2.3 Chemical analysis

Gas phase samples were collected from the ports located before and after the catalytic reactor using gas tight syringes. For the detection of the reactant and products, gas phase samples were injected into a Varian 3800 GC equipped with an Alltech AT-Q^{TM} capillary column (30 m x 0.53 mm i.d.) and a FID and a Carlo Erba HR-GC (Model 5160) equipped with a CP-SIL-13CB capillary column and an electron capture detector (ECD) in series with flame ionization detector (FID). For the detection of carbondioxide, a Varian 3800 GC equipped with an Agilent GS-Carbon PLOT (30 m x 0.32 i.d.) capillary column and thermal conductivity detector (TCD) was used. Products were identified initially by a GC (Hewlett Packard 6890) coupled with a MSD (Hewlett Packard 5972A) and a capillary column DB-624 (length 60 m, ID 0.25 mm, film 1.4 µm) based upon comparison of the full scan spectra with library spectra. For the GC ECD/FID analyses, standards were injected and identification and quantification of the educts and products was done.

7.2.4 Data analysis

The data analysis is discussed in the section 5.2.4 of chapter 5

7.3 Results and discussion

The catalytic oxidation experiments were conducted between temperatures ranged from 100^{o}C to 350^{o}C, and the temperatures were chosen depending on the degradability of the compound. The temperatures were increased, in the most cases, with an increment of 25^{o}C. From the experiment it was observed, that the total or partial oxidation and decomposition at elevated temperatures of the studied compounds MTBE, ETBE, TAME and DIPE were possible. For the same temperature, the degradation of ETBE was the highest and that of DIPE was the lowest among the four studied ether compounds.

Figure 7.2 shows the conversion of MTBE, ETBE, TAME and DIPE during the catalytic decomposition via oxidation at 225°C. At this temperature and contact times of 0.05-0.15 second, the conversion of ETBE varied between 92.7-99.9%, that of TAME varied between 85.4-99.6%, that of MTBE varied between 79.1-98.8%, and that of DIPE varied between 61.0-91.0%. Mass balances were made based on the products and are presented in the figure. At this particular temperature mass balances were between 94-112% for ETBE, 95-109% for TAME, 96-112 % for MTBE and 97-106% for DIPE.

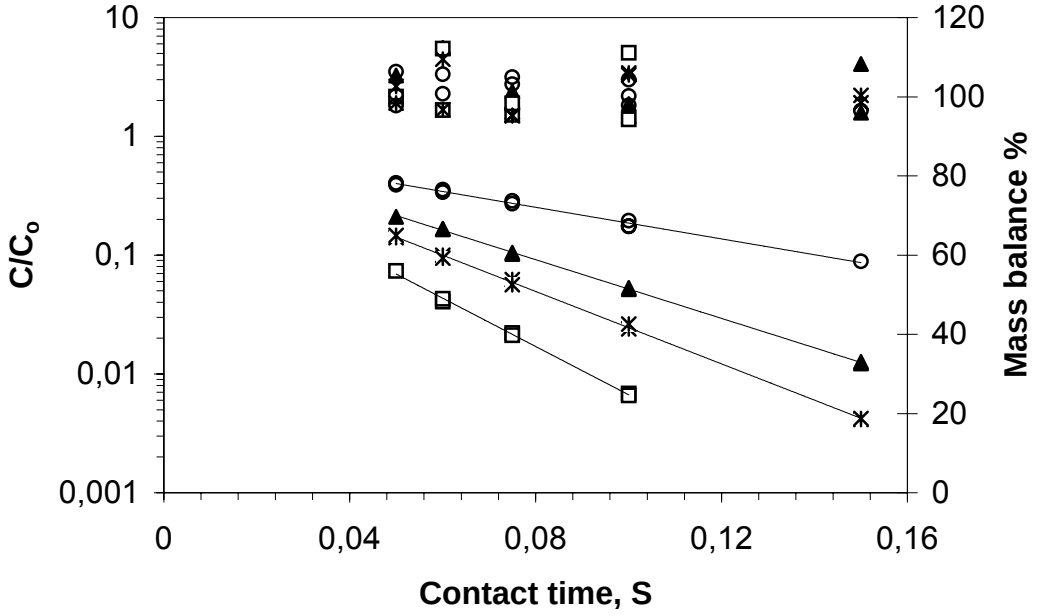

Fig. 7.2: Conversion for ETBE (open squares), TAME (star marks), MTBE (solid triangles) and DIPE (open circles) at 225°C and fixed contact times over palladium catalysts. Mass balances are added on the top of the diagram according to the right side scale. Error bars are too small to add.

Table 7.1: List of the intermediates and products formed during the catalytic oxidation reaction of ether compounds

Compound	Intermediate products	Products
MTBE	Isobutene[1], methanol[1]	Carbondioxide
ETBE	Isobutene[1], ethanol[2], acetaldehyde[1]	Carbondioxide
TAME	Isopentene[3], methanol[1]	Carbondioxide
DIPE	Propene[4], acetone[4]	Carbondioxide

[1] persists up to 300°C, [2] persists up to 200°C, [3] persists up to 325°C, [4] persists up to 350°C

For all the studied compounds, the final products were carbondioxide and water. However, only carbondioxide was detected and quantified, and not the water. But, water is also a more likely product as per the oxidation reaction. During the degradation of MTBE isobutene and methanol was found to be the intermediate products. At temperature 175°C, about <5% isobutene or methanol was observed which decreased to <2% at 225°C. Isobutene and

methanol were also observed as intermediate products by Mitani et al. (2001) during the catalytic oxidation of MTBE. Above 300^{o}C, no intermediate product was detected. Mass balances were done based on the products and varied between 91.09% and 112.32% with an average of 100.76%.

For ETBE, the intermediate products of degradation were isobutene, ethanol and acetaldehyde. At 175^{o}C, about <9% acetaldehyde, <5% isobutene and <3% ethanol was detected. However, no ethanol was seen above 200^{o}C, and it was same for isobutene and acetaldehyde above 300^{o}C. Mass balances for the experiments with four temperature conditions (Table 7.2) were done based on the products and were found to be 94.31% to 112.15% having an average of 104.13%.

During the degradation of TAME the detected intermediate products were isopentene and Methanol. At 175^{o}C, <5% isopentene and methanol were detected, which decreased to <2% at 225^{o}C. Above 325^{o}C, no intermediate product was noticed. Mass balances were done and varied between 95.25% and 111.84% having an average of 101.83%.

The intermediate products of DIPE were propene and acetone. At 200^{o}C, <2% propene and <40% acetone were detected which decreased to <1% and <5% respectively at 300^{o}C. Above 350^{o}C no intermediate products were seen. Mass balances were varied between 95.33% and 110.45% with an average of 102.11%.

Pseudo-first order reaction kinetics can be used to describe the oxidation reaction of those compounds as stated in eq. 40 (Schüth and Reinhard, 1998; Kopinke et al., 2003). First order reaction rate constants were calculated using a log-linear plot of normalized concentration versus detention time. Figure 7.3 shows such an example of log linear plot for ETBE. Data for MTBE, TAME, and DIPE were used to calculate the reaction rate constants (Appendix 4.1 & 4.2). The rate constants are presented in the Table 7.2. Temperature dependent increase of the rate constant was observed. As expected, the increasing temperature gives rise to increasing number of collisions and more likely combinations among the molecules.

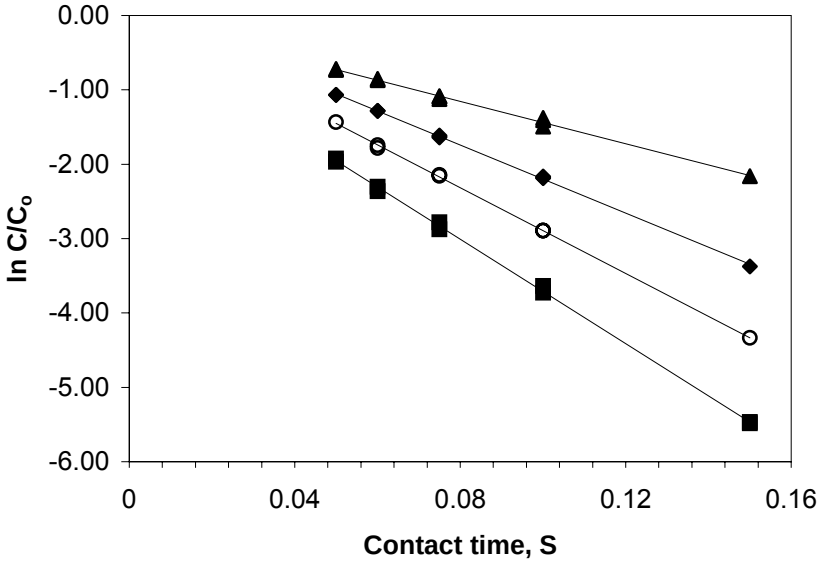

Fig. 7.3: Lines of best fit to the log-transformed normalized concentration versus time (linear regression analysis) were used to estimate k_r values for TAME (see Table 7.2). Temperature 175^{o}C (solid triangles), temperature 200^{o}C (solid diamonds), temperature 215^{o}C (open circles), temperature 225^{o}C (solid squares). Error bars are too small to add.

Table 7.2: Reaction rate constants for studied ether compounds at different temperatures during catalytic oxidation

Rate constant, Sec^{-1}

Tempera-ture, ^{o}C	ETBE	TAME	MTBE	DIPE
150	12.32±0.49			n.a.
175	20.82±0.47	14.25±0.35	11.03±0.07	n.a.
200	30.86±0.36	22.90±0.19	18.09±0.25	8.59±0.32
215	n.a.	28.84±0.26	23.14±0.16	n.a.
225	46.78±0.92	35.10±0.38	28.46±0.22	15.32±0.47
250	n.a.	n.a.	n.a.	23.13±0.18
275	n.a.	n.a.	n.a.	34.29±0.35

n.a.: not analyzed

Figure 7.3 shows a log-linear plot of reaction rate constant (ln k_r) versus 1/T and from that the reaction activation energy was calculated (Table 7.3).

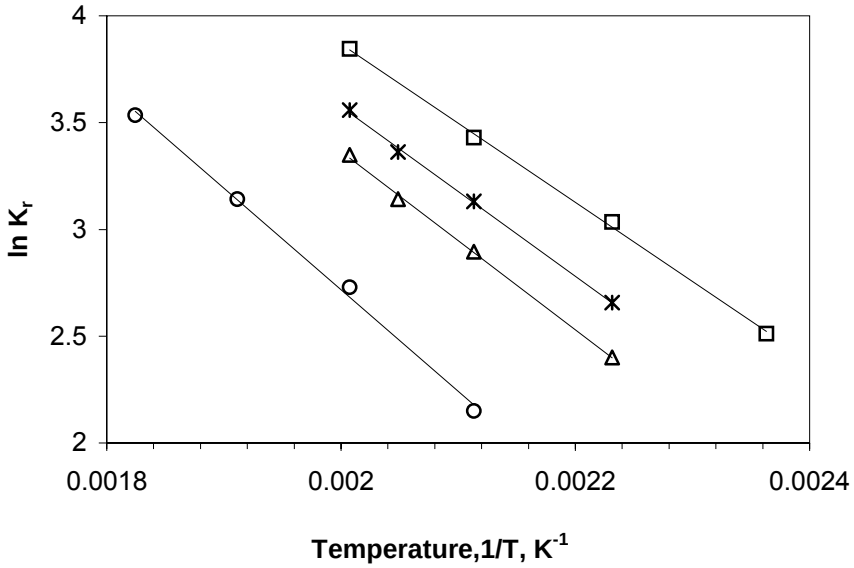

Fig. 7.3: Arrhenius plot. Dependence of first order rate constants (k_r) on temperatures for ETBE (open squares), TAME (star marks), MTBE (solid triangles) and DIPE (open circles) during catalytic oxidation and decomposition. Error bars are too small to add.

Table 7.3: Activation energy (E_a) calculated using Arrhenius equation.

Compound name	Activation energy, kJ/mole	R^2
ETBE	30.85±0.42	0.998
TAME	32.99±0.49	0.998
MTBE	34.71±0.54	0.998
DIPE	39.50±0.60	0.997

From the Table 7.2 and 7.3, it can be seen that the reactivity of the studied ether compounds decreased towards ETBE > TAME > MTBE > DIPE. The reason is not that clear, but the structure of the compound and the reaction products might have the effect on reaction activation energies. The DIPE possessed the most symmetrical and less branched structure and that have the highest activation energy. Böhm et al. (2000) observed a faster ETBE oxidation compared to MTBE and TAME. According to them the existence of a $–OC_2H_5$ group in the ETBE molecule leads to the formation of acetaldehyde, which further produces peracetic acid by abstraction of H followed by O_2 and H addition. The presence of peracetic acid accelerates the reaction rate due to degenerate branching. Similarly, in the present study, the presence of acetaldehyde might cause the faster oxidation of ETBE than other ether compounds.

Following Kopinke et al. (2003) the catalyst activity for the gas phase oxidation reaction in the fixed bed reactor at different temperatures and gas flows was calculated as stated in equation 45. The calculated catalyst activities at different gas flows (1 l/min – 3 l/min) vs temperatures for the target compounds are plotted on the figure 7.4. As expected, from the

figure 7.4 it can be seen that the catalyst activity is independent of gas flow. However, the temperature dependent increase of catalyst activities is observed.

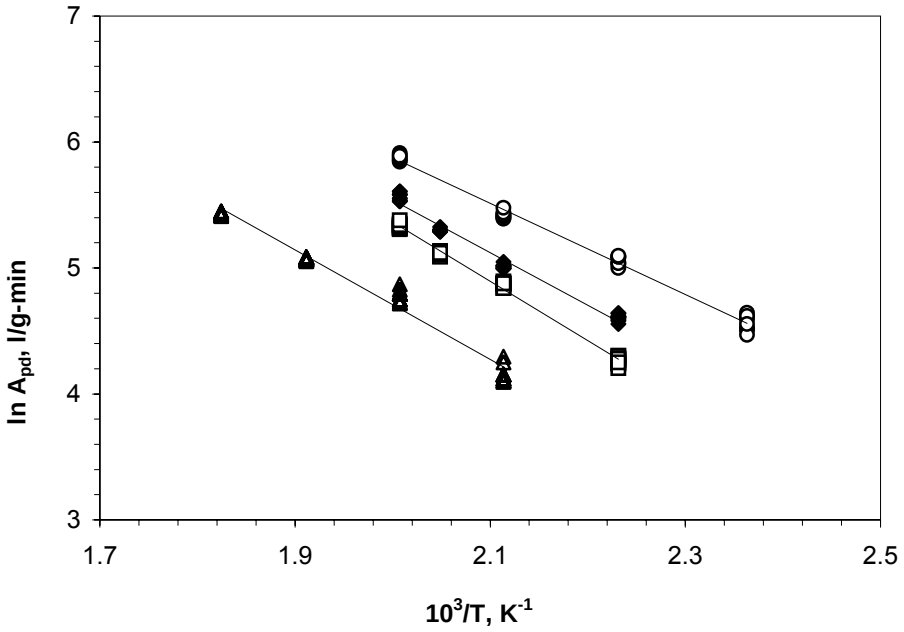

Fig. 7.4: Temperature and gas flow dependencies of the catalyst activity, A_{pd} (l/g-min) in the gas phase oxidation reaction of ETBE (open circles), TAME (solid diamond), MTBE (open squares) and DIPE (open triangles). Single line represents catalyst activities at different gas flows between 1 l/min to 3 l/min for a particular compound.

In conclusion, it could be shown that the catalytic oxidation is an effective way to destroy the ether compounds in gaseous stream. The final oxidation products are carbondioxide and water. However, It was observed that the temperature from 150^{o}C to higher for ETBE, MTBE and TAME and from 200^{o}C to higher for DIPE was suitable in order to get an efficient and stable degradation of the compounds studied in the present research.

Chapter 8

Summary
In this study, the performance of a two step treatment method for the remediation of waters contaminated with volatile to semi-volatile organic contaminants was analyzed and optimized.

The first treatment step involves the transfer of the contaminants form the aqueous phase to the gaseous phase using a microporous polypropylene hollow fiber membrane (HFM) module. With a very small footprint, HFM modules provide a large surface area for mass transfer and enable an independent control of gas and liquid flow rates without the risk of flooding. In addition, a vacuum can be applied to enhance stripping efficiencies.

To test the performance of the HFM module, six aliphatic, five aromatic and one ether compound were selected covering a large range of Henry's law constants. The main findings of the experiments can be summarized as follows:

- The removal efficiency for a compound is solely dependent on its Henry's law constant. Compared to the Henry constant, the molecular structure (aromatic or aliphatic) and the polarity of the molecule seem to not significantly influence the efficiency. This indicates that the membrane has no selectivity and has no impact on the partition coefficients.

- There are no significant differences in removal efficiencies regardless of whether the water is contaminated with a single compound or mixtures of several compounds.

- If the strip gas flow rate and the pressure are held constant, a decrease in the water flow rate leads to better removal efficiencies as the residence time of the water in the HFM module increases.

- Vacuum can be either used to increase removal efficiencies, or to decrease the amount of strip gas that has to be treated without sacrificing efficiency. In the latter case, contaminant concentrations in the gas phase will be much higher compared to ambient pressure conditions, however, the contaminant fluxes will be the same.

- The results indicate, that for the low strip gas to water ratios used in this study, a substantial mass transfer limitation exists on the gas side.

While modeling the data, the conventional resistance in series model failed to predict removal efficiencies, i.e. mass transfer coefficients. This is attributed to the fact that the

model assumes a domination of the liquid side mass transfer resistance on the overall resistance, even for the operation conditions chosen in this study. Therefore, a process based hybrid numerical analytical modeling approach was developed, in cooperation with the geohydraulics group at the University of Tübingen. Input parameters for the model are the geometry of the HFM module, the diffusion coefficients of the stripped compounds in air and water dependent on temperature and pressure, the tabulated Henry's law coefficients, and the operation conditions.

The model was validated against 177 experimental results, reflecting the 12 compounds used and a wide range of operation conditions, and simulated the experimental data very well. With this, the model can potentially be used to efficiently design HFM filtration systems and to optimize stripping schemes.

After transferal of the stripped compounds to the gas phase, treatment of the gas phase is required. The second treatment step therefore involves the reductive or oxidative catalytic conversion of the contaminants to harmless products with palladium as the catalyst. The experiments were conducted at temperatures ranging from 50°C up to 450°C, depending on the conversion rates of the organic compounds. For reductive degradation, hydrogen gas was used as the reductant, for oxidative degradation, ambient air was used as the oxygen source.

The gas phase catalytic degradation of a total of seven saturated and unsaturated chlorinated aliphatic compounds and six ether compounds (fuel oxygenates) were studied. For the chlorinated aliphatic compounds reductive conditions were applied. Degradation of the ether compounds was studied under reductive as well as oxidative conditions. The main findings of the gas phase degradation experiments were:

- Unsaturated aliphatic chlorinated compounds were dehalogenated with much faster rates compared to saturated aliphatic compounds.
- For the unsaturated aliphatic compounds, temperatures well below 100°C are sufficient for high degradation rates.
- Saturated aliphatic compounds, that cannot be degraded with palladium catalysts in the water phase (i.e. 1,2-DCA and 1,1,2,2-TCA) react with sufficient rates in the gas phase at elevated temperatures (> 150°C).
- For catalytic reduction of the ether compounds, the degradation products were carbon monoxide and non-toxic C1 to C5 hydrocarbons.

- For catalytic oxidation of the ether compounds, the products were carbondioxide and water.
- The reaction kinetics were always pseudo-first order with respect to the compounds concentrations.
- For all compounds, half lives on the order of seconds to milliseconds could be achieved, depending on the compounds and temperature conditions.
- For reductive conditions, activation energies were between 10 and 35 kJ/mole. For the oxidation of the ether compounds, activation energies in general were higher at 30 to 40 kJ/mole.
- No catalyst fouling was observed during the experiments.

The results for the two individual treatment steps indicate, that this two step treatment concept has a high potential to be used as a water treatment option. Pilot scale testing is necessary to show the applicability of the concept under real treatment conditions.

References

Acero, J. L., Haderlein, S. B., Schmidt, T. C., Gunten, U. V. (2001): MTBE oxidation by conventional ozonation and the combination ozone/hydrogen peroxide: efficiency of the processes and bromate formation, Environ. Sci. Technol. 35 (21), 4252-4259.

Achten, C., Kolb, A., Puttmann, W. (2001): Methyl tert-butyl ether (MTBE) in urban and rural precipitation in Germany, Atmos. Environ. 35 (36), 6337-6345.

Achten, C., Kolb, A., Puttmann, W. (2002): Occurrence of methyl tert-butyl ether in riverbank filtered water and drinking water produced by riverbank filtration. 2, Environ. Sci. Technol. 36 (17), 3662-3670.

Achten, C., Kolb, A., Puttmann, W., Seel, P., Gihr, R. (2002): Methyl tert-butyl ether in river and wastewater in Germany. 1. Environ. Sci. Technol. 36 (17), 3652-3661.

Achten, C., Puttmann, W. (2000): Determination of methyl tert butyl ether in surface water by use of solid-phase microextraction, Environ, Sci. Technol. 34 (7), 1359-1364.

Aptel, P. Semmens, M.J. (1996): Multiphase membrane processes, in: J. Mallavialle, P.E. Odendaal, M.R. Wiesner (Eds.), Water treatment: membrane processes, McGraw Hill, New York.

Arnold, W., Roberts, A.L. (2000): Pathways and kinetics of chlorinated ethylene and chlorinated acetylene reaction with Fe (0) particles, Environ. Sci. Technol. 34 (9), 1794-1805.

Arp, H. P.H., Fenner, K., Schmidt, T. C. (2005): Predicting methyl tert-butyl ether, tert-butyl formate, and tert-butyl alcohole levels in the environment using the fugacity approach, Environ. Sci. technol. 39 (9), 3237-3244.

Arp, H. P.H., Schmidt, T. C. (2004): Air-water transfer of MTBE, its degradation products, and alternative fuel oxygenates: the role of temperature, Environ. Sci. technol. 38 (20), 5405-5412.

Baehr, A.L., Stackelberg, P.E., Baker, R.J. (1999): Evaluation of the atmosphere as a source of volatile organic compound in shallow groundwater, Water Resour. Res. 35 (1), 127-136.

Balko, E.N., Przybylski, E., Trentini, F.V. (1993): Exhaustive liquid-phase catalytic hydrodehalogenation of chlorobenzenes, Appl. Catal. B 2 (1), 1-8.

Baudot, A., Floury, J., Smorenburg, H.E. (2001): Liquid-liquid extraction of aroma compounds with hollow fiber contactor, AIChE J., 32(11), 1780-1793.

Bhowmick, M. (1992): A novel closed loop air stripping process, Ph.D. thesis, University of Minnesota.

Bhowmick, M., Semmens, M.J. (1994): Batch studies on a closed loop air stripping process, Water Res., 28 (9), 2011-2019.

Bodnariuk, P., Coq, B., Ferrat, G., Figueras, F. (1989): Carbon-chlorine hydrogenolysis over PdRh and PdSn bimetallic catalysts, Jour. Catal. 116 (2), 459-466.

Böhm, H., Baronnet, F., Kadi, B.E. (2000): Comparative modelling study on the inhabiing effect of TAME, ETBE and MTBE at low temperature Phys. Chem. Chem. Phys. 2 1929-1933.

Bradley, P. M., Landmeyer, J. E., Chapelle, F. H. (1999): Aerobic mineralization of MTBE and tert-butyl alcohol by stream-bed sediment microorganisms, Environ. Sci. Technol. 33 (11), 1877-1879.

Brewer, J. (1991): Literature reviews and research scoping study on the treatment of volatile organic carbon compounds in the off-gas from contaminated groundwater and soil remedial technologies, National Groundwater and soil Remediation Program, Environment Canada, Ottawa.

California Code regulation, (1999): Title 22, section 64449, January 07.

Carslaw, H.S., Jaeger, J.C. (1959): Conduction of heat in solids, Oxford University Press 1959.

Choi, H.C., Choi, S.H., Yang, O.B., Lee, J.S., Lee, K.H., Kim, Y.G. (1996): Hydrodechlorination of carbon tetrachloride over Pt/MgO, Jour. Catal. 161 (2), 790-797.

Clark, R.M., Eilers, R.G., Goodrich, J.A. (1984): VOCs in drinking water, Ibid (6), 1146-1162.

Coq, B., Ferrat, G., Figueras, F. (1986): Conversion of chlorobenzene over palladium and rhodium catalysts of widely varying dispersion, Jour. Catal. 101 (2), 434-445.

Cordi, E.M., Falconer, J.L. (1996): Decomposition and oxidation of $CH_3{}^{13}CH_2OH$ on Al_2O_3, Pd/Al_2O_3, and PdO/Al_2O_3 catalysts, Catal. Lett. 38, 45-51.

Crittenden, J.C., Cortright, R.D., Rick, B., Tang, S.R. Perram, D. (1988): Using GAC to remove VOCs from air stripper off-gas, J. Am. Water Works Assoc. 80 (5), 73-84.

Deeb, R. A., Scow, K.M., Alvarez-Cohen, L. (2000): Aerobic MTBE biodegradation: an examination of past studies, current cahllenges and future research directions, Biodegradation 11 (2-3), 171-186.

Early, K., Kovalchuk, V.I., Lonyi, F., Deshmukh, S., D'Itri, J.L. (1999): Hydrodechlorination of 1,1-dichlorotetrafluoroethane and dichlorodifluoromethane catalyzed by Pd on fluorinated aluminas: the role of support material, Jour. Catal. 182 (1), 219-227.

Ebbing, D.D., Gammon, S.D. (2003-2004): General chemistry, Houghton Mifflin Company, Boston, New York.

Eur 20417 EN (2002): European Union risk assessment report on tert-butyl methyl ether; Hansen, B.G., Munn, S.J., Pakalin, S., Musset, C., Luotamo, M., de Bruijin, J., Berthault, F., Vegro. S., Pellegrini, G., Allanou, R., Scheer, S. Eds., office for official publications of the European Communities: Luxembourg, Vol. 19.

Evans, R.B., Watson, G.M., Mason, E.A. (1961): Gaseous diffusion in porous media at uniform pressure, J. Chem. Phys., 35 (6), 2076- 2083.

Fayolle, F., Francois, A., Garnier, L., Godefroy, D., Mathis, H., Piveteau, P., Monot, F. (2003): Limitations in MTBE biodegradation, Oil & Gas Sci. & Technol. 58 (4), 497-504.

Fayolle, F., Vandecasteele, J.-P., Monot, F. (2001): Microbial degradation and fate in the environment of methyl tert-butyl ether and related fuel oxygenates, Appl. Microbiol. Biotechnol. 56 (3-4), 339-349.

Fetter, C.W. (1993): Contaminant hydrogeology, Prentice-Hall International.

Fraser, M. P., Cass, G. R., Simoneit, R. T. (1998) : Gas-phase and particle-phase organic compounds emitted from motor vehicle traffic in a Los Angeles roadway tunnel, Environ. Sci. Technol. 32 (14), 2051-2060.

Freeze, R.A., Cherry, J.A. (1979): Groundwater, Prentice Hall, Englewood Cliffs, NJ 07632.

Fuller, E.N., Schettler, P.D., Giddings, J.C. (1966): A new method for prediction of binary gas-phase diffusion coefficients, Ind. Eng. Chem. 58 (2), 19- 27.

Fung, S.C., Sinfelt, J.H. (2004): Hydrogenolysis of methyl chloride on metals, Jour. Catal. 103 (1), 220-223.

Gabelman, A., Hwang, S.T. (1999): Hollow fiber membrane contactors, J. Membr. Sci., 159, 61-106.

Grathwohl, P. (1998): Diffusion in natural porous media: contaminant transport, sorption / desorption and dissolution kinetics, Kluwer Academic Publishers.

Greenwood, N.N., Earnshaw, A. (1984): Chemistry of elements, Pergamon Press, New York, NY.

Hayduk, W. Laudie, H. (1974): Prediction of diffusion coefficients for nonelectrolytes in dilute aqueous solutions, AIChE J. 20, 611-615.

Helmig, R. (1997): Multiphase flow and transport processes in the subsurface: a contribution to the modeling of hydrosystems, Springer, Berlin.

Helmig, R., Huber, R. (1998): Comparison of Galerkin-type discretization techniques for two-phase flow in heterogeneous porous media, Adv. in Water Resour. 21, 697-711.

Helmig, R., Zielke, W. (1996): Finite-element simulation of multiphase flows in fractured rock, Deutsche Geowasserkundliche Mitteilungen 40, 26-36.

Hughes, R. (1984): Deactivation of Catalysts, Academic Press, London.

Istok, J. (1989): Groundwater Modeling by the Finite Element Method, American Geophysical Union.

Iwasa, N., Kudo, S., Takahashi, H., Masuda, S., Takezawa, N. (1993): Highly selective supported Pd catalysts for steam reforming of methanol, Catal. Lett. 19, 211-216.

Karpinski, Z., Early, K., d'Itri, J.L. (1996): Catalytic hydrodechlorination of 1,1-dichlorotetrafluoroethane by Pd/Al_2O_3, Jour. Catal.164 (2), 378-386.

Katona, T., Hegedüs Z., Kopasz, Cs., Molnár, Á., Bartók, M. (1990): Effects of dehydrogenation of 2-propanol on the structure and catalytic activity of an amorphous copper-zirconium alloy sample, Catal. Lett. 5, 361-368.

Keller, A.A., Bierwagen, B.G. (2001): Hydrophobic hollow fiber membrane for treating MTBE-contaminated water, Environ. Sci. Technol. 35 (9), 1875-1879.

Kirchstetter, T.W., Singer, B.C., Harley, R.A., Kendall, G.R., Chan, W. (1996): Impact of oxygenated gasoline use on California light-duty vehicle emissions, Environ. Sci. Technol. 30 (2), 661-670.

Kleineidam, S., Schüth, C., Grathwohl, P. (2002): Solubility-normalized combined pore-filling-partitioning sorption isotherms for organic pollutants, Environ. Sci. Technol. 36 (2002) 4689-4697.

Klinger, J., Stieler, C., Sacher, F., Brauch, H.J. (2002): MTBE (methyl tert-butyl ether) in groundwaters: Monitoring results from Germany, J. Environ. Monit. 4 (2), 276-279.

Kolditz, O. (2002): Computational Methods in Environmental Fluid Mechanics, Springer-Verlag, Berlin Heidelberg New York.

Kolditz, O., Beinhorn, M., Xie, M., Kalbacher, T., Bauer, S., Wang, W., McDermott, C.I., Chen, C., Beyer, B., Gronewold, J., Kemmler, D., Walsh, R., Du, Y., Park, C.-H., Hess, M., Bürger, C. and Delfs, J.-O. (2006): GeoSys/RokFlow – Version 4.3.2.1 (WW), Open source software design proposal, Zentrum für Angewandte Geowissenschaften, Lehrstuhl für GeoSystemForschung, Universität Tübingen, 74.

Kopinke, F.-D., Mackenzie, K., Köhler, R. (2003): Catalytic hydrogenation of groundwater contaminants in water and in the gas phase using Pd/γ-Al_2O_3, Appl. Catal. B 44 (1), 15-24.

Kovenklioglu, S. Cao, Z., Shah, D., Farrauto, R.J., Balko, E.N. (1992): direct catalytic hydrodechlorination of toxic organics in wastewater, AIChE J. 38 (7), 1003-1012.

Kreith, F. Black, W.Z. (1980): Basic Heat Transfer, Harper & Row, New York.

Lee, J.S., Boudart, M. (1991): Reactivity of tungsten carbides I. Catalytic and temperature-programmed reactions of methanol, Catal. Lett. 8, 107-114.

Lèvèque, J.A. (1928) : Les Lois de la transmission de chaleur par convection, Annales de Mines 13, 201- 299.

Liu, Y., Majetich, S.A., Tilton, R.D., Sholl, D.S., Lowry, G.V. (2005): TCE dechlorination rates, pathways, and efficiency of nanoscale iron particles with different properties, Environ. Sci. Technol. 39 (5), 1338-1345.

Liu, Y., Suzuki, K., Hamakawa, S., Hayakawa, T., Murata, K., Ishii, T., Kumagai, M. (2000): Highly active methanol decomposition catalyst derived from Pd-hydrotalcite dispersed on mesoporous silica, Catal. Lett. 66, 205-213.

Mahmud, H., Kumar, A., Narbaitz, R.M., Matsuura, T. (1998): Membrane air stripping: a process for removal of organics from aqueous solutions, Jour. Separ. Sci. and Technol., 33 (14), 2241-2255.

Mahmud, H., Kumar, A., Narbaitz, R.M., Matsuura, T. (2000): A study of mass transfer in the membrane air-stripping process using microporous polypropylene hollow fibers, J. Membr. Sci. 179, 29-41.

Mahmud, H., Kumar, A., Narbaitz, R.M., Matsuura, T. (2002): Mass transport in the membrane air-stripping process using microporous polypropylene hollow fibers: effect of toluene in aqueous feed, J. Membr. Sci. 209, 207-219.

Mahmud, H., Kumar, A., Narbaitz, R.M., Matsuura, T. (2004): The air-phase mass transfer resistance in the lumen of a hollow fiber at low air flow, Chem. Eng. J. 97, 69-75.

Malek, A., Li, K., Teo, W.K. (1997): Modeling of microporous hollow fiber membrane modules operated under partially wetted conditions, Ind. Eng. Chem. Res. 36, 784-793.

McDermott, C., Tarafder, S.A., Kolditz, O., Schüth, C. (2007): Removal of volatile to semi volatile organic contaminants from water using hollow fiber membrane contactors II: A hybrid numerical-analytical modeling approach, J. Membr. Sci. 292, 17-28.

McNab Jr., W.W., Ruiz, R. (1998): Palladium-catalyzed reductive dehalogenation of dissolved chlorinated aliphatics using electrolytically-generated hydrogen, Chemosphere 37 (5), 925-936.

Miller, C.T., Christakos, G., Imhoff, P.T., McBride, J.F.Pedit, J.A., Trangenstein, J.A. (1998): Multiphase flow and transport modeling in heterogeneous porous media: challenges and approaches, Adv. in Water Resour. 21, 77-120.

Mitani, M.M., Keller, A.A., Golden, S.J., Hatfield, R., Cheetham, A.K. (2001): Low temperature catalytic decomposition and oxidation of MTBE, Appl. Catal. B: Environ. 34,87-95.

Moon, D.J., Chung, M.J., Park, K.Y., Hong, I. (1998): Deactivation of Pd catalysts in the hydrodechlorination of chloropentafluoroethane, Appl. Catal. A 168 (1), 159-170.

Mormile, M. R., Liu, S., Suflita, J. M. (1994): Anaerobic biodegradation of gasoline oxygenates: extrapolation of information to multiple sites and redox conditions, Environ, Sci. Technol. 28 (9), 1727-1732.

Murthy, I.A.P.S., Awamy, C.S. (1994): Catalytic decomposition of 2-propanol on $Co_{1+x}Al_{2-x}O_4$ spinel system, Catal. Lett. 27, 103-112.

Nikolopoulos, A.A., Kogelbauer, A., Goodwin Jr., J.G., Marcelin, G. (1996): Gas phase synthesis of MTBE on fluoride-modified zeolites, Catal. Lett. 39, 171-178.

O'Loughin, E.J., Burris, D.R. (2004): Reduction of halogenated ethanes by green rust, Environ. Toxico. And Chem. 23 (1), 41-48.

O'Loughlin, E.J., Burris, D.R., Delcomyn, C.A. (1999): Reductive dechlorination of trichloroethene mediated by humic metal complexes, Environ. Sci. Technol. 33 (7), 1145-1147.

O'Reilly, K.T., Moir, M.E., Taylor, C.D., Smith, C.A., Hyman, M.R. (2001): Hydrolysis of tert-butyl methyl ether (MTBE) in dilute aqueous acid, Environ. Sci. Technol. 35 (19), 3954-3961.

Ordóñez, S., Sastre, H., Díez, F.V. (2000): Hydrodechlorination of aliphatic organochlorinated compounds over commercial hydrogenation catalysts, Appl. Catal. B 25 (1), 49-58.

Pepe, F., Polini, R., Stoppa, L. (1992): Role of the support and of the preparation method for copper-based catalysts in the 2-propanol decomposition, Catal. Lett. 14, 15-25.

Pirkanniemi, K., Sillanpää, M. (2002): Heterogeneous water phase catalysis as an environmental application: a review, Chemosphere 48 (10), 1047-1060.

Polland, W.G., Present, R. D. (1948): On gaseous self-diffusion on long capillary tubes, Phys. Rev. 73 (7), 762- 774.

Prince, R. C. (2000): Biodegradation of methyl tertiary-butyl ether (MTBE) and other fuel oxygenates, Crit. Rev. Microbiol. 26 (3), 163-178.

Qi, Z., Cussler, E.L. (1985): Bromine recovery with hollow fiber gas membranes, J. Membr. Sci., 24, 43-57.

Qi, Z., Cussler, E.L. (1985): Microporous hollow fiber for gas absorption. II. Mass transfer across the membrane, J. Membr. Sci. 23, 333-345.

Reed, B.W., Semmens, M.J., Cussler, E.L. (1995): Membrane contactors, in R. D. Noble, S.A. Stern (Eds.), Membrane separation technology, principles and applications, Elsevier, New York, 239- 268.

Ribeiro, F.H., Gerken, C.A., Rupprechter, G., Somorjai, G.A., Kellner, C.S., Coulston, G.W., Manzer, L.E., Abrams, L. (1998): Structure insensitivity and effect of sulfur in the reaction of hydrodechlorination of 1,1-Dichlorotetrafluoroethane (CF_3-$CFCl_2$) over Pd catalysts, Jour. Catal. 176 (2), 352-357.

Ribeiro, F.H., Gerken, C.A., Somorjai, G.A., Kellner, C.S., Coulston, G.W., Manzer, L.E., Abrams, L. (1997): Turnover rate and kinetic mechanism for the reaction of hydrodechlorination of 1,1-dichlorotetrafluoroethane (CF_3-$CFCl_2$) over polycrystalline Pd foil, Catal. Lett. 45 (3-4), 149-153.

Rupprechter, G., Somorjai, G.A. (1997): Palladium-catalyzed hydrogenation without hydrogen: the hydrodechlorination of chlorofluorocarbons with solid state hydrogen over the palladium (111) crystal surface and its implications, Catal. Lett. 48 (1-2), 17-20.

Rutqvist, J., Wu, Y.S., Tsang, C.F., Bodvarsson, G. (2002): A modeling approach for analysis of coupled multiphase fluid flow, heat transfer, and deformation in fractured porous rock, Inter. Jour. of Rock Mech. and Mining Sci. 39, 429-442.

Rylander, P. (1979): Catalytic Hydrogenation in organic Synthesis, Academic Press, New York, 1979.

Satterfield, C.N. (1970): Mass transfer in heterogeneous catalysis, Cambridge MA., MIT Press.

Schlimm, C., Heitz, E. (1996): A wastewater treatment process: reductive dehalogenation of chlorinated hydrocarbons by metal, Environ. Prog. 15, 38-47.

Schmidt, T.C., Morgenroth, E., Schirmer, M.; Effenberger, M., Haderlein, S.B., In Diaz, A.F., Drogos, D.L. (Eds.) (2002): Oxygenates in Gasoline: Environmental Aspects. ACS, Washington, 58-79.

Schmidt, T.C., Schirmer, M., Weiss, H., Haderlein, S.B. (2004): Microbial degradation of methyl tert-butyl ether and tert-butyl alcohol in the subsurface, J. Contam. Hydrol. 70 (3-4), 173-203.

Schöner, P., Plucinski, P., Nitsch, W., Daiminger, U. (1998): Mass transfer in the shell side of cross flow hollow fiber modules, Chem. Eng. Sci., 53, 2319-2326.

Schreier, C.G., Reinhard, M. (1995): Catalytic hydrodehalogenation of chlorinated ethylenes using palladium and hydrogen for the treatment of contaminated water, Chemosphere 31 (6), 3475-3487.

Schüth, C. (2003): Organic contaminants in groundwater-innovative remediation approaches and stable isotope techniques, Habilitationsschrift, Geowissenschaften Fakultät, Universität Tübingen.

Schüth, C. Disser, S., Schüth, F.; Reinhard, M. (2000): Tailoring catalysts for hydro-dechlorinating chlorinated hydrocarbon contaminants in groundwater. Appl. Catal. B: Environ. 28 (3-4), 147-152.

Schüth, C., Kummer, N.-A., Weidenthaler, C., Schad, H. (2004): Field application of a tailored catalyst for hydrodechlorinating chlorinated hydrocarbon contaminants in groundwater, Appl. Catal. B 52, 197-203.

Schüth, C., Reinhard, M. (1998): Hydrodechlorination and hydrogenation of aromatic compounds over palladium on alumina in hydrogen-saturated water, Appl. Catal. B 18 (3-4) 215-221.

Schwarzenbach, R.P., Gschwend, P.M., Imboden, D.M. (2003): Environmental organic chemistry, 2nd edition, Wiley, USA.

Semmens, M.J., Qin, R. Zander, A. (1989): Using a microporous hollow-fiber membrane to separate VOCs from water, J. Am. Water Works Assoc., 81(4), 162- 167.

Shah, J.J., Singh, H.B. (1988): Distribution of volatile organic chemicals in outdoor and indoor air, Environ. Sci. Technol., 22, 1381-1388.

Shekhar, R., Barteau, M.A. (1995): Structure sensitivity of alcohol reactions on (110) and (111) palladium surfaces, Catal. Lett. 31, 1995, 221-237.

Shelly, S., Fouhy, K. (1994): The drive for cleaner burning fuel, Chem. Eng. 101 (1), 61-63.

Shen, T.T., Sewell, G.H. (1988): Control of VOC emissions from waste management facilities, J. Environ. Eng. 114, 1392.

Singh, H. B., Salas, L., Smith, A.J., Shigeishi, H. (1981): Measuremnets of some potentially hazardous organic chemicals in urban environments, Atmos. Environ., 15 (4), 601-612.

Souchon, I., Pierre, F.X., Samblat, S., Bes, M., Marin, M. (2002): Recovery of aroma compounds from tomato industry effluent using membrane based solvent extraction, J. Desalination, 148, 87-92.

Squillace, P.J., Zogorski, J.S., Wilber, W.G., Price, C.V. (1996): Preliminary assessment of the occurrence and possible sources of MTBE in groundwater in the United States, 1993-1994, Environ. Sci. Technol. 30 (5), 1721-1730.

Staudinger, J., Roberts, P.V. (2001): A critical compilation of Henry's law constant temperature dependence relations for organic compounds in dilute aqueous solutions, Chemosphere 44, 561-576.

Tarafder, S.A. (2003): M.Sc. Thesis, Center for applied Geoscience, University of Tübingen.

Tarafder, S.A. McDermott, C., Schüth, C. (2007): Vacuum assisted removal of volatile to semi volatile organic contaminants from water using hollow fiber membrane contactors. I: Experimental results, J. Membr. Sci. 292, 9-16.

USEPA (1991): Toxic release inventory, public data release, office of pollution prevention and toxics, Washington, DC.

USEPA, EPA A420-R-99-021 (1999): The report of the blue ribbon panel on oxygenates in gasoline, US Government Printing Office, Washington DC.

Wallington, T. J., Japar, S. M. (1991): Atmospheric chemistry of diethyl ether and ethyl tert-butyl ether, Environ. Sci. technol., 25 (3), 410-415.

Wang, D. Teo, W.K., Li, K. (2002): Removal of H_2S to ultra concentrations using an asymmetric hollow fiber membrane module, J. Separ. Purific. Technol., 27, 33-40.

Wickramasinghe, S.R., Semmens, M.J., Cussler, E.L. (1991): Mass transfer in various hollow fiber geometries, J. Membr. Sci. 69, 235-250.

Wiersma, A., Sandt, E.J.A.X. v. d., Hollander, M.A.d., Bekkum, H.v., Makkee, M., Moulijn, J.A. (1998): Comparison of the performance of activated carbon-supported noble metal catalysts in the hydrogenolysis of CCl_2F_2, Jour. Catal. 177 (1), 29-39.

Wilke, C.R., Chang, P. (1955): Correlation of diffusion coefficients in dilute solutions, AIChE J. 1, 264-270.

Yang, M.C., Cussler, E.L. (1986): Designing hollow-fiber contactors, AIChE J. 32 (11), 1910-1916.

Zander, A.K., Semmens, M.J., Narbaitz, R.M. (1989): Removing VOCs by membrane stripping, J. Am. Water Works Assoc. 81 (11), 76-81.

Zwank, L., Berg, M. E., Schmidt, T. C., Schwarzenbach, R. P., Haderlein, S. B. (2005): New evaluation scheme for two-dimensional isotope analysis to deciper biodegradation processes: application to groundwater contamination by MTBE, Environ. Sci. Technol. 39 (4), 1018-1029.

Appendices

Appendix 1.1: Dependency of removal efficiencies on the Henry's law constants and water flow rates. Experimental data - open symbols, modeling results - solid symbols. Strip gas flow 5x water flow, pressure 0.2 atm.

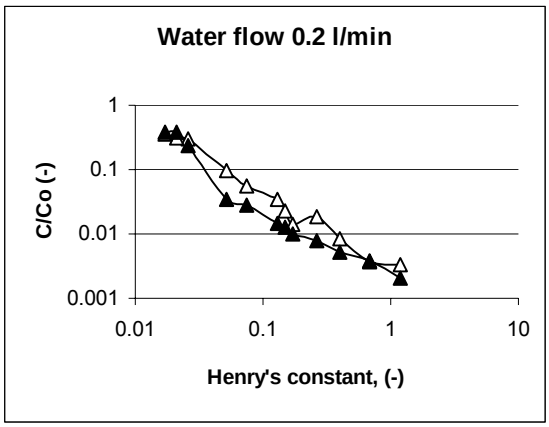

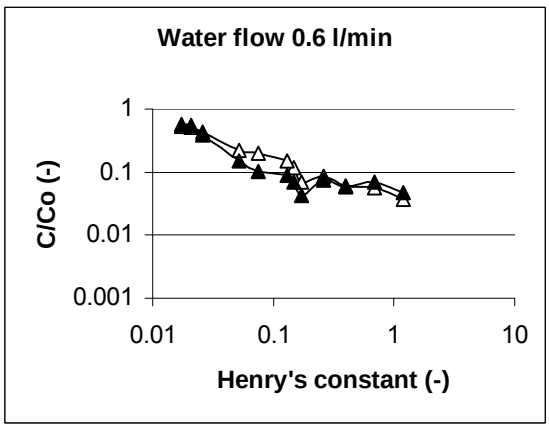

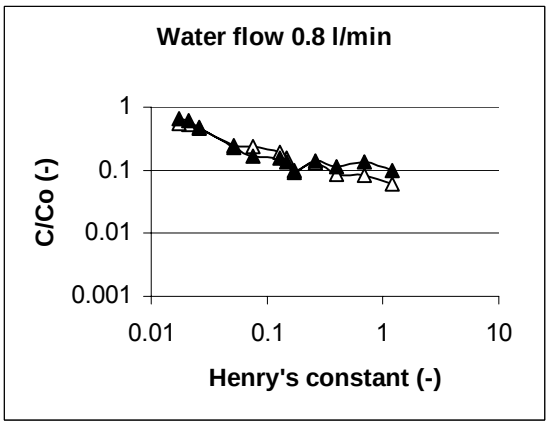

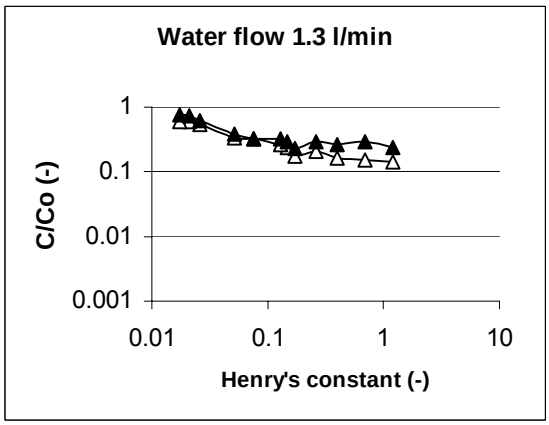

Appendix 1.2 (a): Dependency of removal efficiencies on the strip gas to water ratio ($R_{(a/w)}$). Experimental data - open symbols, modeling results - solid symbols. Water flow and gas flow constant at 0.5 l/min. Pressures were decreased from ambient pressure to 0.035 atm.

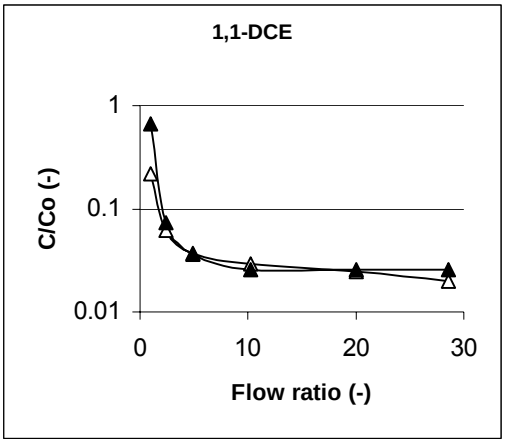

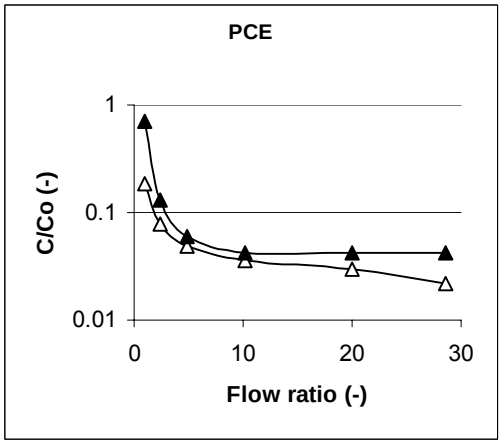

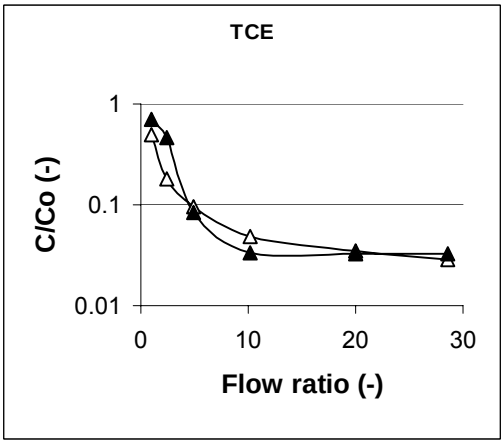

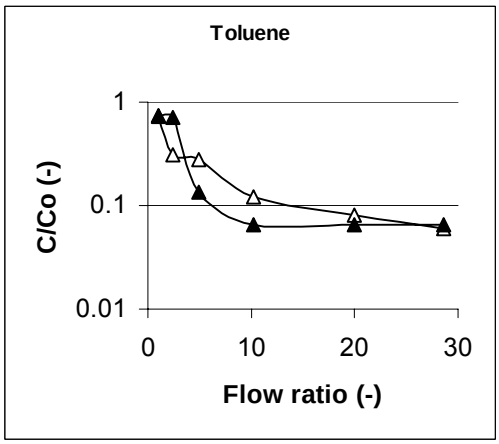

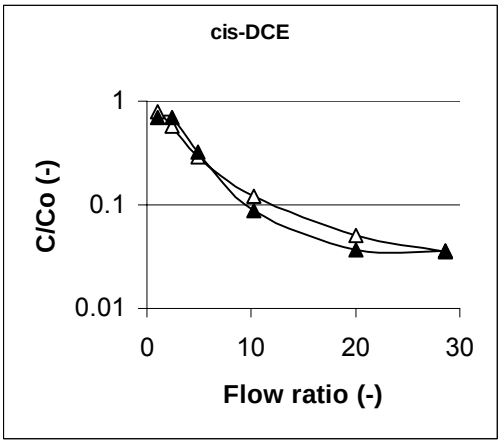

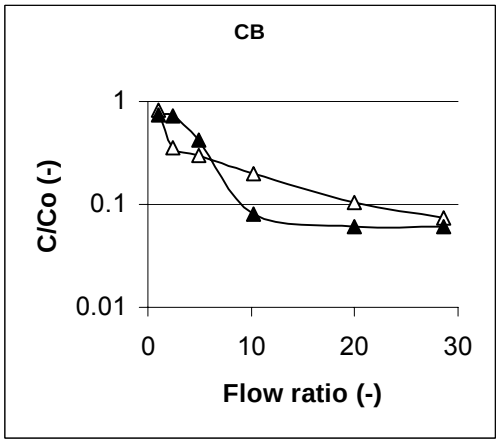

Appendix 1.2 (b): Dependency of removal efficiencies on the strip gas to water ratio ($R_{(a/w)}$). Experimental data - open symbols, modeling results - solid symbols. Water flow and gas flow constant at 0.5 l/min. Pressures were decreased from ambient pressure to 0.035 atm.

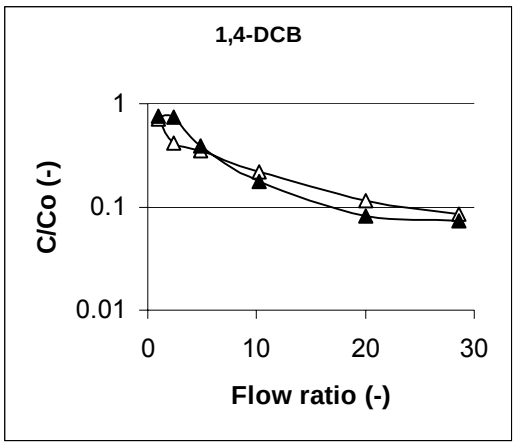

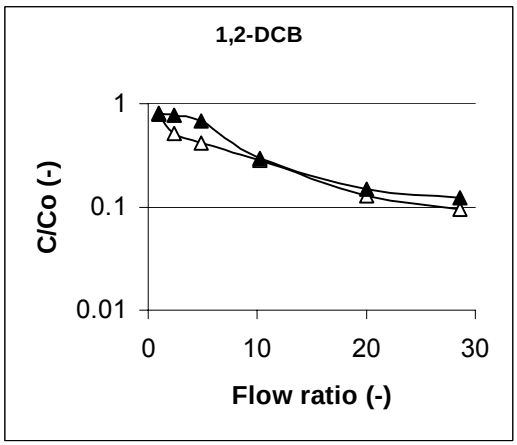

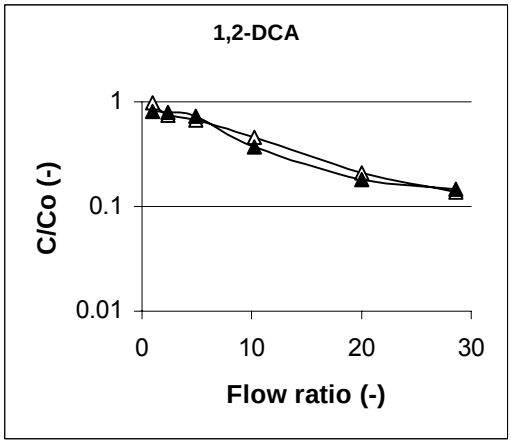

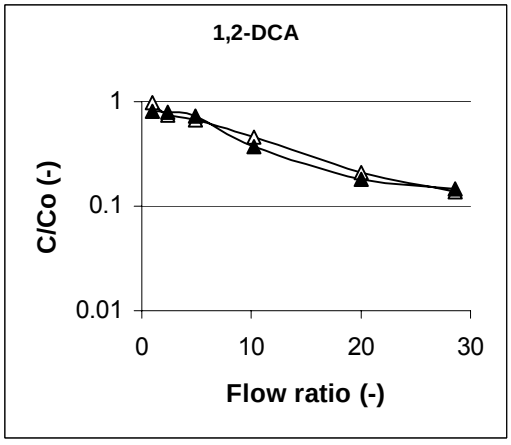

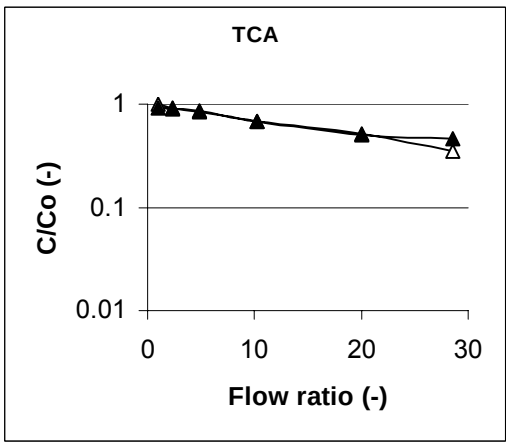

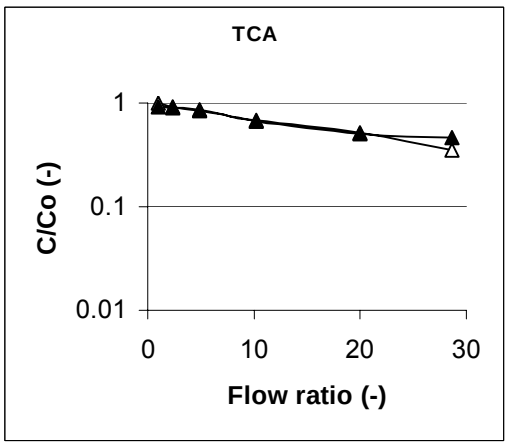

Appendix 2.1 : Lines of best fit to the log-transformed normalized concentration versus time (linear regression analysis) were used to estimate reaction rate constants (*K*) for 1,1-DCE (upper) and cis-1,2-DCE (lower). Temperature 50°C (open circles), temperature 75°C (solid circles), temperature 100°C (open triangles), temperature 150°C (solid triangles). Error bars are too small to be added.

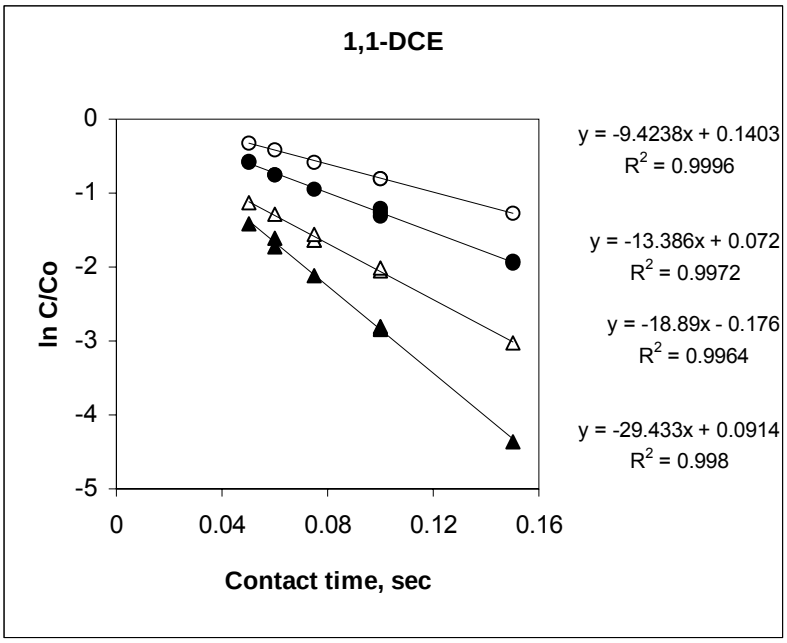

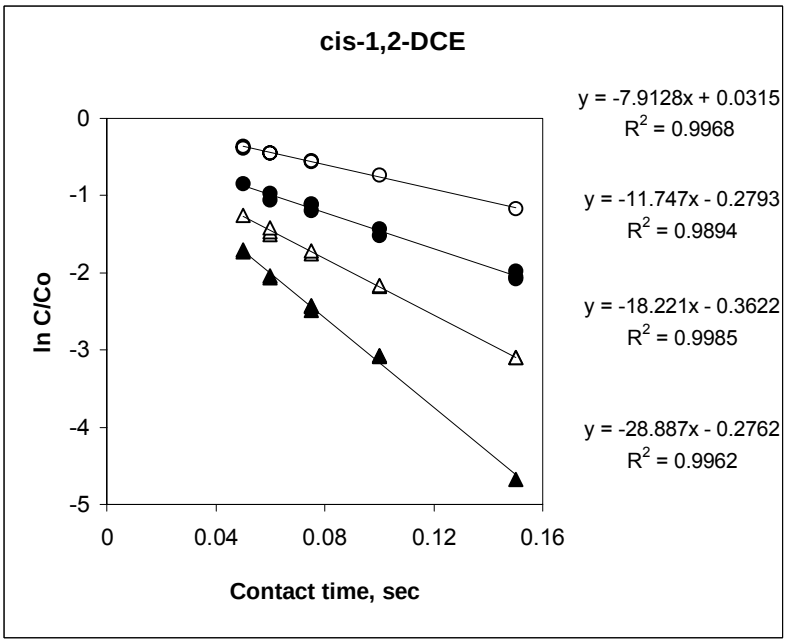

Appendix 2.2: Lines of best fit to the log-transformed normalized concentration versus time (linear regression analysis) were used to estimate reaction rate constants (*K*) for PCE (upper) and 1,2-DCA (lower). Temperature 50°C (open circles), temperature 75°C (solid circles), temperature 100°C (open triangles), temperature 150°C (solid triangles), temperature 200°C (open squares), temperature 250°C (solid squares), temperature 300°C (star marks), temperature 350°C (cross marks). Error bars are too small to be added.

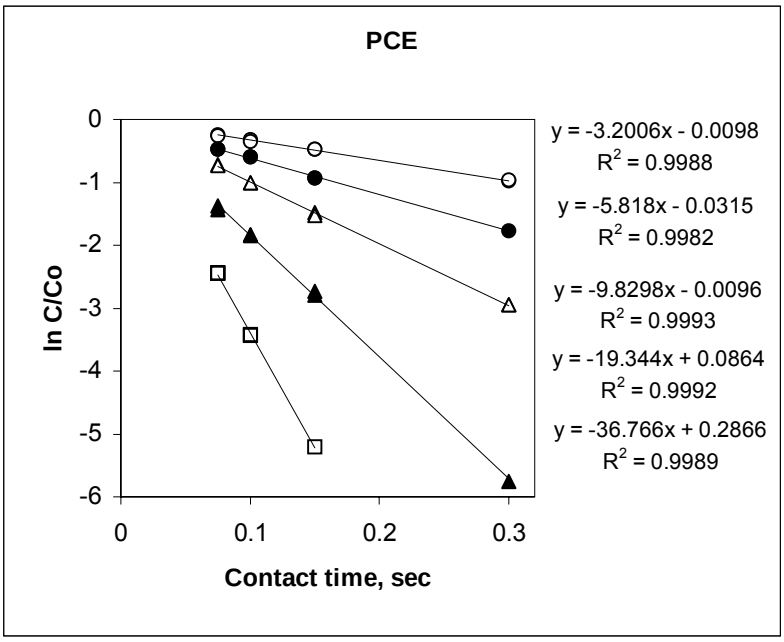

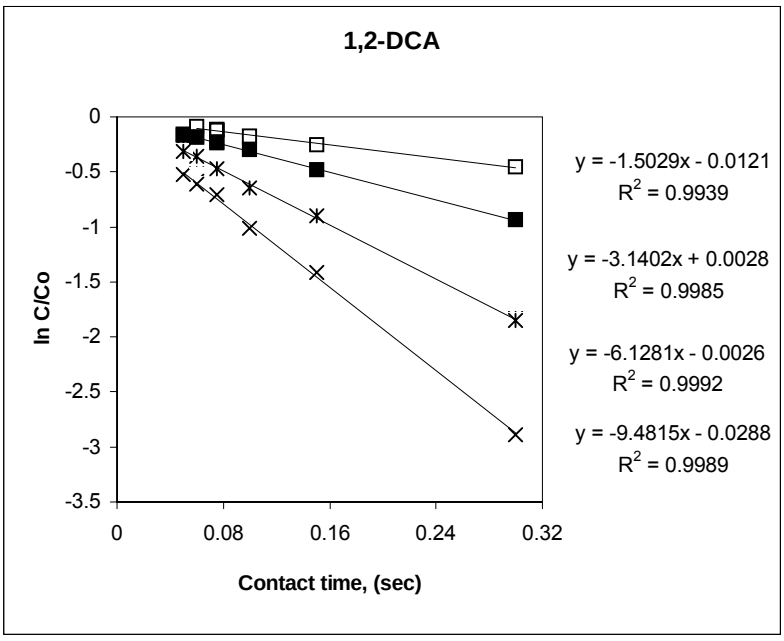

Appendix 3.1: Lines of best fit to the log-transformed normalized concentration versus time (linear regression analysis) were used to estimate reaction rate constants (*K*) for MTBE, TAME. Temperature 150°C (solid squares), temperature 175°C (solid triangles), temperature 200°C (solid diamonds), temperature 225°C (open circles), temperature 250°C (solid circles). Error bars are too small to add.

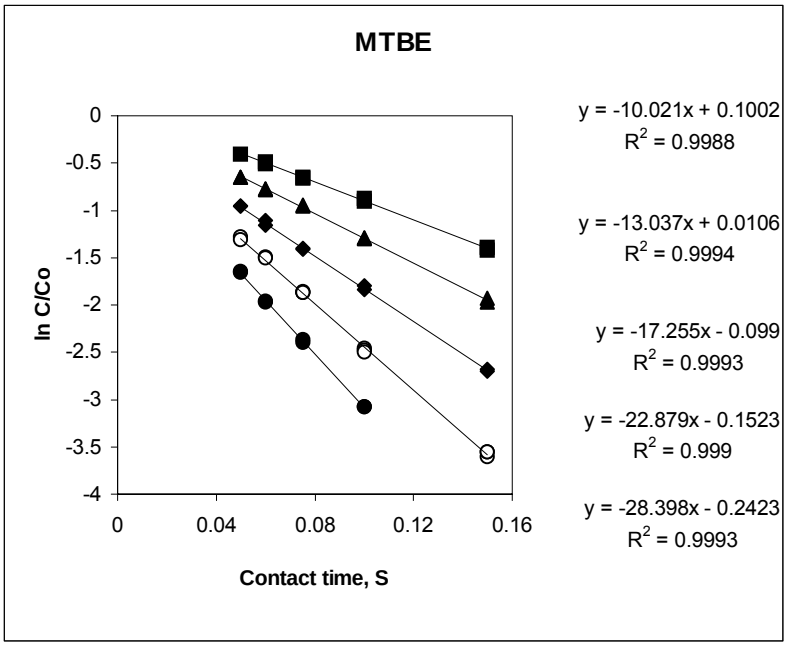

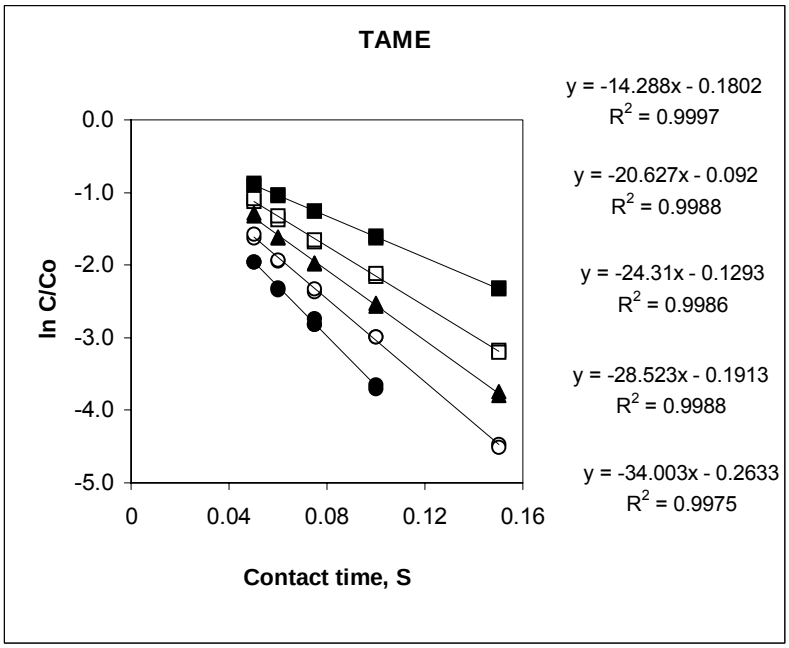

Appendix 3.2: Lines of best fit to the log-transformed normalized concentration versus time (linear regression analysis) were used to estimate reaction rate constants (k) for DIPE. Temperature 200°C (solid diamonds), temperature 225°C (open circles), temperature 250°C (solid circles), temperature 275°C (star marks), temperature 300oC (open triangles) and temperature 325°c (solid triangles). Error bars are too small to add.

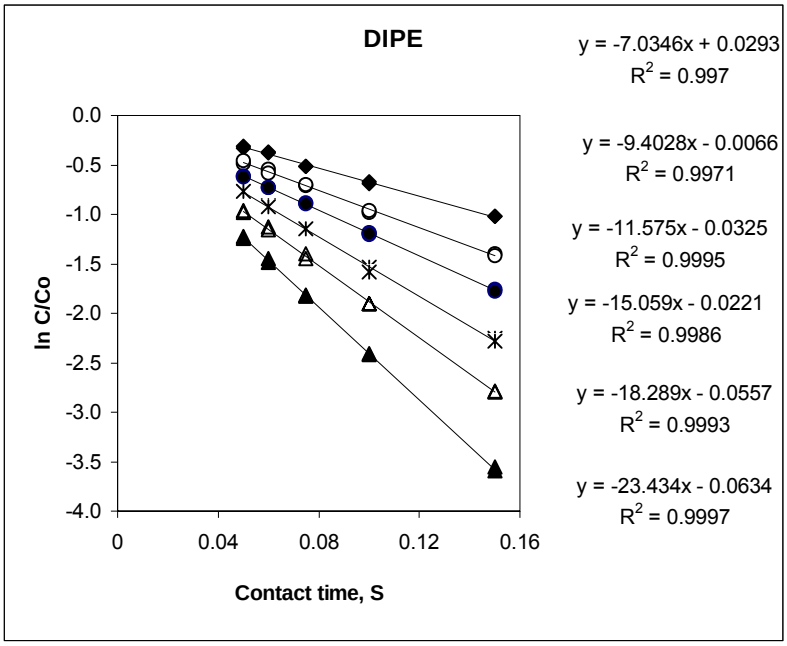

Appendix 4.1: Data for catalytic oxidation of ether compounds. Lines of best fit to the log-transformed normalized concentration versus time (linear regression analysis) were used to estimate reaction rate constants (k) for DIPE. Temperature 150°C (open triangles), temperature 175°C (solid triangles), temperature 200°C (solid diamonds), temperature 215°C (open circles), temperature 225°C (solid squares). Error bars are too small to add.

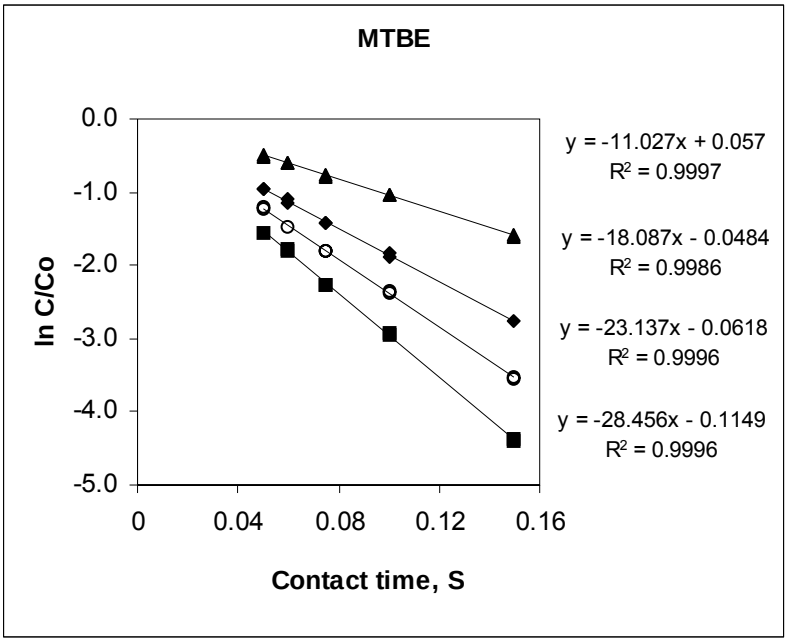

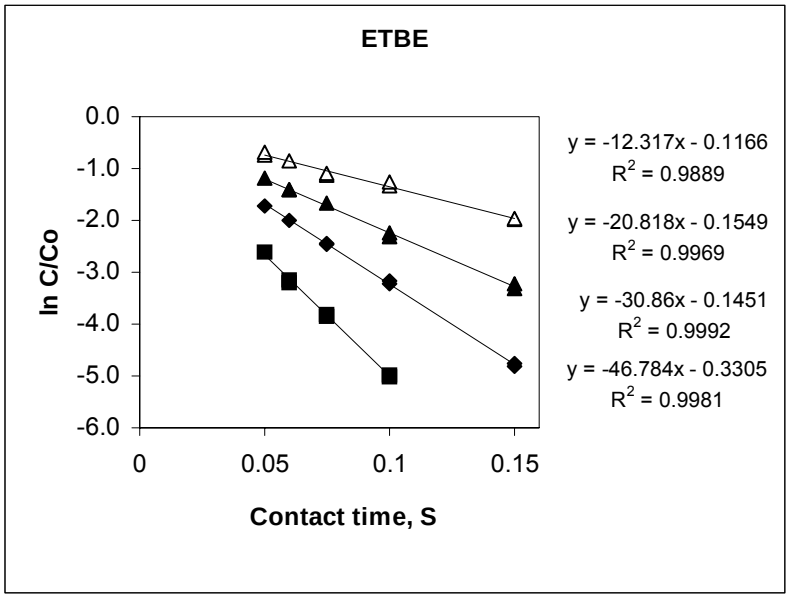

Appendix 4.2: Data for catalytic oxidation of ether compounds. Lines of best fit to the log-transformed normalized concentration versus time (linear regression analysis) were used to estimate reaction rate constants (k) for DIPE. Temperature 200°C (solid triangles), temperature 225°C (open squares), temperature 250°C (solid circles), temperature 275°C (star marks), Error bars are too small to add.